UNIVERSITÉ DU QUÉBEC

MÉMOIRE

PRÉSENTÉ À

L'UNIVERSITÉ DU QUÉBEC À CHICOUTIMI

COMME EXIGENCE PARTIELLE

DE LA MAÎTRISE EN SCIENCES DE LA TERRE

PAR

DAPHNE SILVA PINO

B.A.A.

STRUCTURAL HYDROGEOLOGY IN THE KENOGAMI UPLANDS, QUEBEC, CANADA

AOÛT 2012

"Those were the stories that stayed with you, that meant something. (...) Folk in those stories had lots of chances of turning back, only they didn't. They kept going, because they were holding on to something."

J. R. R. Tolkien

(*The Lord of the rings – The two towers*)

To my parents, Francisco and Marina,

my sister, Ingrid, and my best friend, Vitor.

For always giving me something to hold on to.

ABSTRACT

Characterizing the joint system is a very significant component of investigations on fractured rock aquifers, as the secondary porosity controls the groundwater flow. It is also important to analyze the types of interactions between the joints, e.g., the types of termination and the dominancy of a certain joint set, since such information helps to understand the tectonic events that were responsible for the generation of the joint systems in the aquifer. Moreover, the current stress field is usually the most significant in controlling joint aperture, which plays a major role in groundwater flow.

The main objective of this work is to characterize an aquifer in fractured crystalline rocks with a fairly homogeneous lithology, defining a hydrogeological model of the study area, through structural surveys at different scales and hydrogeologic data analyses. This study was carried out in the Kenogami uplands, within the Saguenay graben, Quebec. It aimed to answer the following questions: (1) is there a structured joint system in the bedrock, that is, is it possible to identify preferential joint orientations and structural domains? (2) Can joint systems be defined at different scales, e.g. regional and local scales? If yes, are there any relationships between the systems observed at different scales? (3) Can any correlation between the joint system(s) and the past and present stress fields be identified? (4) Is there a relationship between the hydrogeological properties obtained from boreholes and the joint system(s)?

The structural survey involved three main phases. First, a characterization at the regional scale of the joint system is derived from air photo interpretation, lineament analysis, and a general field survey at selected sites. The latter involves the investigation

of the spatial distribution of the main joint sets, and the study of the relative ages of joint sets and past stress field components conducted on horizontal outcrops. Second, a detailed structural survey of selected road cuts was carried out to define and characterize the main joint sets that compose the joint system in the study area. Third, the realization of geophysical borehole logging provided valuable information at depth, especially regarding subhorizontal joint sets. These steps allowed to answer the questions proposed in the beginning of this research.

This project allowed the characterization of an aquifer in fractured crystalline rocks, regarding the following aspects: joint systems at different scales, past stress fields, hydraulic properties and the possible relationships between these parameters. The methodology adopted may be applied to other studies on fractured rock aquifers.

Finally, a conceptual model was developed for the fractured rock aquifer in the Kenogami uplands, using the unit block approach. This model may be extrapolated to a regional scale, and it reflects the predominance of the subvertical joints in the study area. Other contributions from this work include the introduction of procedures for applying Terzaghi's correction on computers without using specialized softwares and for analyzing the orientation of the main horizontal component of past stress fields on horizontal outcrops. Moreover, it highlighted the value of characterizing a fractured media with the unit block, through a discussion of its association to hydraulic properties and their incorporation into numerical models.

RÉSUMÉ

La caractérisation du système de joints est un élément très important lors de la réalisation de levés sur les aquifères fracturés, puisque la porosité secondaire contrôle l'écoulement des eaux souterraines. Il est également important d'analyser les types d'interactions entre les joints. Par exemple, les types de terminaison des joints ainsi que la prédominance de certaines familles de joints représentent des informations qui permettant de comprendre les événements tectoniques responsables de la génération des systèmes de joints dans l'aquifère. En outre, le champ de contrainte actuel est habituellement le paramètre le plus important dans le contrôle de l'ouverture des joints, laquelle joue un rôle majeur dans l'écoulement des eaux souterraines.

L'objectif principal de ce travail est de caractériser un aquifère dans des roches cristallines fracturées avec une lithologie relativement homogène, en définissant un modèle hydrogéologique de la zone d'étude. Ce modèle a été construit à l'aide de levés structuraux à différentes échelles et des analyses de données hydrogéologiques. Cette étude a été réalisée sur le seuil de Kénogami, dans le graben du Saguenay, au Québec. Elle visait à répondre aux questions suivantes: (1) est-ce que le système de joints dans le socle rocheux est structuré, c'est à dire, est-il possible d'identifier des orientations préférentielles de joints et des domaines structuraux? (2) Les systèmes de joints peuvent-ils être définis à différentes échelles, par exemples aux échelles régionale et locale? Si oui, y a-t-il des relations entre les systèmes observés à différentes échelles? (3) Est-il possible d'identifier des corrélations entre le(s) système(s) de joints et les champs de

contraintes passés et actuel? (4) Y a-t-il une relation entre les propriétés hydrogéologiques obtenues à partir de forages et le(s) système(s) de joints?

Le levé structural a comporté trois phases principales. Premièrement, une caractérisation à l'échelle régionale du système de joints a été effectuée à partir de l'interprétation de photos aériennes, de l'analyse des linéaments, et d'un levé général de terrain sur des sites sélectionnés. Ce dernier type de levé implique l'étude de la distribution spatiale des principales familles de joints, et l'étude des âges relatifs des familles de joints et des champs de contrainte passés, menée sur des affleurements horizontaux. Deuxièmement, un levé détaillé sur des coupes de routes sélectionnées a été réalisé afin d'identifier et caractériser les familles de joints qui composent la fracturation dans la zone d'étude. Enfin, la réalisation de diagraphies géophysiques dans des forages a fourni des informations sur les joints en profondeur, notamment les familles de joints subhorizontaux. Ces étapes ont permis de répondre à la problématique proposée au début de cette recherche.

Ce projet a permis la caractérisation d'un aquifère dans des roches cristallines fracturées, selon les aspects suivants: les systèmes de joints à différentes échelles, les champs de contraintes passés, les propriétés hydrauliques et les relations possibles entre ces paramètres. La méthodologie adoptée pourra être appliquée à d'autres études sur les aquifères rocheux fracturés.

Enfin, un modèle conceptuel a été développé pour l'aquifère fracturé dans le seuil de Kénogami, en utilisant l'approche du bloc unitaire. Ce modèle peut être extrapolé à l'échelle régionale et il reflète la prédominance des joints subverticaux dans la zone d'étude. Les autres contributions de ce travail comprennent la mise en place de procédures : (1) pour appliquer la correction de Terzaghi sur ordinateur sans utilisation de logiciels spécialisés, et (2) pour l'analyse de l'orientation de la composante horizontale principale des champs de contraintes passés sur les affleurements horizontaux. Aussi, ce travail a mis en valeur l'intérêt de la caractérisation d'un milieu fracturé avec l'approche du bloc unitaire, par une discussion de sa relation avec les propriétés hydrauliques, suivie de leur incorporation dans les modèles numériques.

ACKNOWLEDGEMENTS

I thank everyone who has been on this road with me, and that contributed at an academical, technical and/or emotional level with my project and, hopefully, with some personal growth on my part. Those are stories that shall surely stay with me.

First, I'd like to thank my advisor, Prof. Dr. Alain Rouleau, for the invitation to participate on the projects *Analyse des réservoirs aquifères en socle rocheux fracturé* and the *Programme d'acquisition de connaissances sur les eaux souterraines du Québec* in the Saguenay-Lac-Saint-Jean area (PACES-SLSJ). Thank you for the confidence placed in me, and for all the teachings and discussions on Structural Hydrogeology. Thank you for making me feel welcome since my first day in Canada.

Second, I'd like to thank my co-advisor Prof. Dr. Denis W. Roy, for the many ideas brought to the project, and for the countless and extensive talks on the Grenville Province geology and on our dear unit block.

Third, I'd like to thank the two other members of my committee, Dr. Amélia J. Fernandes, particularly for the suggestions and discussions on structural Geology and fieldwork approaches, and Prof. Dr. Romain Chesnaux, for participating in fieldwork and for the audacious projects during Hydrogeology courses which ended up contributing a lot to my experience. I'd also like to thank Prof. Dr. Réal Daigneault, for the discussions on Structural Geology and help during fieldwork, and my advisor during my BSc in Brazil, Prof. Dr. Ricardo Hirata, for putting me in touch with my MSc advisor in the first place.

I also thank the funders of this project: *Fonds québécois de recherche sur la nature et les technologies* (FRQNT), the *Fondation de l'UQAC* (FUQAC) and the *Programme d'acquisition de connaissances sur les eaux souterraines du Québec* (PACES), with contribution by the *Ministère du Développement durable, de l'Environnement et des Parcs*, UQAC, *Ville de Saguenay* and the four *Municipalités régionales de comté* of the SLSJ region.

I'd like to thank the PACES-SLSJ members, for their assistance and for taking me as part of the team. I'd also like to thank the USGS team, Dr. Roger H. Morin and Mrs. Barbara Corland, and Mr. Jean Roy for the help with geophysical loggings and insights on their interpretations.

I also have many friends to thank in Canada, many of whom were not directly involved with my research but who affected my life at some point during my studies. I'd like particularly to thank Sandra Richard, who has been with me at almost every phase of my work and who has encouraged me outside it as well.

I'd like to thank my friends in Brazil, who always supported me, and who make me feel like I haven't been gone a single day whenever I come back home. I'd like to specially thank Vitor Y. Taga, for always staying by my side these last years, even though we were so far. *Doumo* for keeping fighting with me and never letting us give up. *Aishiteru ne*!

Finally, I thank my family: my parents, Francisco and Marina, and my sister, Ingrid. Thank you for your daily support, for always believing in me, for giving me confidence, and, mostly, for all your love that keeps me going. I'd also like to thank my grandmothers, Dinah and Nair (both always asked me when am I coming back home), my aunts, Cleide and Yara, and my great-aunt, Edith. I love you all.

SUMMARY

List of Figures

LIST OF TABLES

1

INTRODUCTION

Fractured bedrock aquifers have been described as "*complex hydrogeological systems that are essential for water resources*" (Gleeson & Novakowski 2009). Igneous and metamorphic rocks in particular often show negligible matrix permeability, although featuring a great variability of their hydraulic properties due to their joint system (Gustafson & Krásný 1994, Lachassagne *et al.* 2001). Characterizing the joint system that cuts these aquifers is fundamental to a good understanding of the dynamics of the groundwater that flows through them.

Joints are an important object of study in several Geology fields; they influence mineral deposition by guiding ore-forming fluids and provide fracture permeability for water, magma, geothermal fluids, oil and gas (Pollard & Aydin 1988). The present study focuses on joints as a possible path for groundwater flow. The term "joints" is here considered as fractures that show no discernible relative displacements; a concept presented by several authors (Hodgson 1961; Price 1966; Hancock 1985; Dunne & Hancock 1987; Ramsay & Huber 1987). Joints are considered as the most common result of brittle deformation (Pollard & Aydin 1988). The term "fault" is reserved to cases when kinematic indicators allow the determination of movement in the discontinuity surface. Thus, following the nomenclature adopted in this work, "fracture" would be the general term, that is, it could refer either to a joint or a fault; however, its use is restrained in this text in order to avoid misunderstandings regarding the discontinuities types. Additional useful definitions are found on Appendix 1.

This project was conducted in relation with a regional groundwater mapping program in the Saguenay – Lac-Saint-Jean (SLSJ) region, as part of the *Programme d'acquisition de connaissances sur les eaux souterraines du Québec* (PACES). PACES projects require the development of tools and approaches that allow a proper characterization of different aquifer types in Quebec, including the ones constituted by fractured rock units. Although Canada has only 0.5% of the world's population (23.6% are in Quebec Province), its lands comprise about 7% of the world's renewable water supply, and 3% are in Quebec alone (MDDEP 2000; Statistics Canada 2011; Environment Canada 2012).

The present work consists in a structural survey and the characterization of a fractured crystalline rock aquifer in the Kenogami uplands, within the SLSJ region (Fig. 1.1). In the SLSJ area, 27,9% of the population relies on aquifers for water supply, of which around 32% is obtained by private wells (MDDEP 2000).

The Kenogami uplands area (Fig. 1.1) forms a relative transverse topographic highground within the Phanerozoic Saguenay graben, in meridional Quebec, and are considered one recharge area for groundwater that flows toward the lowlands. The uplands correspond to a surface area of approximately 1,300km². Its crystalline rocks are relatively homogeneous, composed mainly of anorthosite, and also constitute a potential crystalline fractured rock aquifer. Two other points in favor of the selected area are: (1) the considerably large number of outcrops, especially in the southern part, and many of them located in roadcuts and quarries; and (2) the little number of studies of fractured crystalline rock aquifers in Quebec, even though many important water supply reservoirs in the world are located in fractured media (Masoud & Koike 2006).

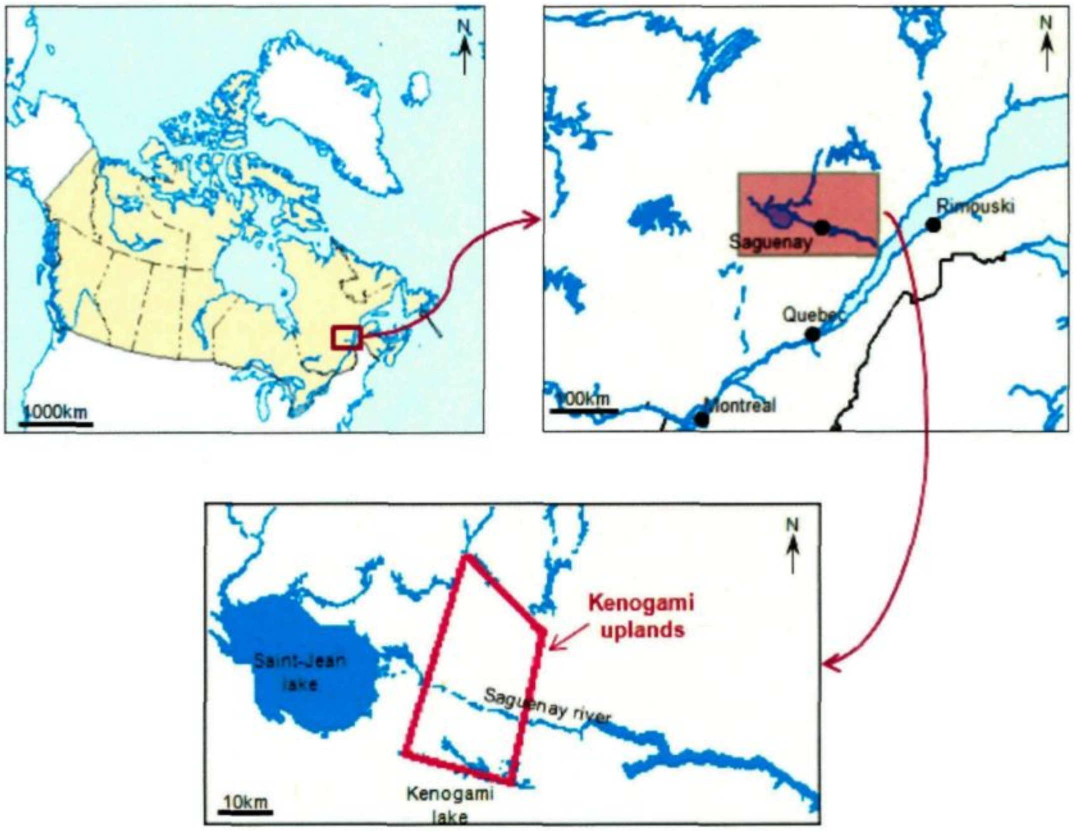

Fig. 1.1 The Kenogami uplands (bottom) are located within the Saguenay-Lac-Saint-Jean region (top right). The study area is located within Quebec Province, Canada (top left). Top left image: adapted from Natural Ressources Canada (1999); top right and bottom images: adapted from Walter et al. (2010).

1.1 Objectives

The aim of the present work was to answer the following questions regarding the Kenogami uplands region:

1) Is there a structured joint system in the bedrock, that is, is it possible to identify preferential joint orientations and structural domains?

2) Can joint systems be defined at different scales, e.g. regional and local ones? If yes, are there any relationships between the systems observed at different scales?

3) Can any correlation between the joint system(s) and the past and present stress fields be identified?

4) Is there a relationship between the hydrogeological properties obtained from boreholes and the joint system(s)?

Once the questions above were answered, the objective was to develop a conceptual hydrogeological model of the bedrock aquifer in the Kenogami uplands, based on structural and hydrogeological data, coupling them with information of the present stress field, that is, its influence over the hydrogeological properties.

The importance of this kind of study relies on its utility on water resource management, a clearly important issue in Quebec (MDDEP 2000; Environment Canada 2012). Once the dynamic of the aquifer is well characterized, it allows a better development of plans of use and preservation of the water resource, preventing its overexploitation. Moreover, in the case of an anthropogenic contamination, knowing how the aquifer behaves contributes to predict the migration of the contaminant, e.g. to determine the wells or discharge points that will be affected by the contamination and at what time.

The bibliographic synthesis presented in chapter 2 covers a great range of possible approaches for studying fractured aquifers. The present project aimed to combine strong points of the methodologies described (e. g. lineament analysis, geophysical logging, detailed structural surveys, analysis of the relative ages of tectonic events) and to characterize a fractured crystalline rock aquifer on the basis of a unit block, which represents the true joint distribution in the fractured media, as opposed to the observed one. A tectonic study was also carried on, where some of the stress fields responsible for generating the joint systems that constitute the Kenogami uplands were deduced by the study of the interactions between the joints. This kind of information is important because the tectonic events control the joint characteristics (connectivity, aperture, density, orientation), which control groundwater flow. The methods chosen shall provide greater precision and reliability to the conceptual model developed.

Publications related to the development of this work are: Pino *et al.* (2010; 2011a, b; 2012a, b) and Roy *et al.* (2011).

2

REVIEW OF PREVIOUS WORKS ON FRACTURED AQUIFERS

A discussion on the application of structural data for modeling fractured aquifers is presented in this chapter. The idea of using structural geology information for groundwater studies was already present in the 1980's work, though it only became a more common practice in the late 1990's. The survey approaches presented in this chapter do not intend to be exhaustive. Instead, selected previous works at various scales of observation are discussed, with special attention to the following aspects: the tectonic history and structural domains, the current stress field, and the relationship between hydrogeological properties and the structural domains. Finally, some categories of numerical modeling of fractured rock aquifers are presented.

2.1 Structural and hydrogeological surveys

The relevance of structural geology studies in hydrogeology relies on the importance of fractured rock aquifers to water supply; understanding the dynamics of groundwater flow in such systems highly depends on a good characterization of its joint systems and of the effects of faulting and folding events on them. The present work focuses on the effects of brittle deformation on fractured crystalline rock aquifers.

2.1.1 Scale of observation of the discontinuity systems

Different observation scales may influence the development of models of water flow through a fractured media, as different hydraulic properties might be estimated for the same system. Additionally, features that do not show up in a local scale may be of importance at a regional scale, or *vice-versa*. Structural observations made at different scales must be correlated in order to obtain a coherent model.

A suggested procedure to improve structural data collection, particularly with geophysical method, is the "*top down*" approach (Robinson *et al.* 2008), in which the survey begins with the smaller scale (e. g. airborne surveys for dominant structures) and goes to local logging. This is a commonly adopted methodology in regional hydrogeological studies.

The occurrence of scale effects of hydraulic properties of fractured rock aquifers has already been attributed to inhomogeneities of the rock (Gustafson & Krásný 1994). The variability of properties within the aquifer is supposed to be smaller for smaller scales; so that at a regional scale, a fractured aquifer might be considered approximately uniform (Gustafson & Krásný 1994; Nastev *et al.* 2004) (see section 2.2 for the equivalent porous media approach).

The absolute value of certain aquifer properties, e. g. hydraulic conductivity, was also demonstrated to be affected by the scale of measurement (Rouleau *et al.* 1996, Nastev *et al.* 2004). Hydraulic tests in fractured orthoquartzites have shown that hydraulic conductivity increases with the size of investigated volume, indicating a good connectivity of the discontinuities responsible for flow in the scales considered (Rouleau *et al.* 1996). When considering heterogeneous rock aquifers characterized by intermittent densely and sparsely fractured zones, large scale measurements tended to yield lower hydraulic conductivities than small scale hydraulic tests (Nastev *et al.* 2004). This effect was attributed to the fact that small scale tests measure hydraulic conductivities over larger aquifer volumes, hence being more likely to encounter highly interconnected fractured zones and preferential flow paths (Nastev *et al.* 2004). It has also been considered that the scale effect may be a result of the aquifer heterogeneity and the spatial distribution of measurements (Nastev *et al.* 2004). These findings emphasize the importance of characterizing an aquifer in different scales, for a better appreciation of fracture-matrix interactions and of flow and transport processes.

Another interesting observation regarding well specific capacities in boreholes and scale effects is that wells located in lineaments parallel to extensional joints are usually more productive, though such interpretation may vary with the scale of the lineaments (Fernandes *et al.* 2007; Fernandes 2008).

2.1.2 Detection of structures by remote sensing

Remote sensing allows the identification of surface features, such as lineaments and potential outcrops for fieldwork, as it will be discussed in section 4.1 below.

Stereo aerial photographs may be used for structural analysis and for creating an inventory of hydrogeological features in a study area (Kresic 1995). The analysis of surface features often reveals the existence of structural discontinuities, which may influence groundwater flow. Likewise, satellite imagery may be used to detect lineaments and other major structures (Masoud & Koike 2006). These methods may be applied to different geological settings, e.g. karstic environments (Kresic 1995), fractured basalts (Fernandes & Rudolph 2001) and sedimentary aquifers in compression zones (Odeh *et al.* 2009). Remote sensing and geographic information systems are particularly useful for correlating structural data with information on hydraulic properties distribution (Masoud & Koike 2006; Fernandes 2008), groundwater flow and chemistry (Odeh *et al.* 2009).

Overall, the importance of studying joints and well defined lineaments relies not only on the fact that they are indispensable elements of regional and local tectonic analyses, but also they provide insights into various fields, such as environmental geology and natural resource exploitation.

2.1.3 Geophysical surveys

Geophysical surveys provide valuable subsurface data, which should be combined with the surface data acquired on outcrops, allowing a 3D description of fractured aquifers. Not only these surveys may be useful to identify trends and recurrent patterns in physical characteristics, but also some of them yield direct information on the joint system or on its role within the aquifer.

The hydrogeological characterization of a fractured aquifer has been qualified a "*challenging task*" (Morin *et al.* 2007), as underlined by many examples in this chapter. The frequently suggested helpful methodologies for determining hydrogeologic properties of fractured aquifers include: geophysical loggings, geological mapping, rock core descriptions and pumping tests, with particular interest for geophysical logging for identifying trends in the hydrogeological characteristics of the aquifer (Morin *et al.* 2007; Robinson *et al.* 2008; Francese *et al.* 2009).

In geophysical loggings in boreholes, many probes may be used; some of the most recurrent are: fluid temperature and conductance, flowmeter, caliper, acoustic televiewer (ATV), natural gamma, rock resistivity and electrical resistivity (Morin *et al.* 1997, 2007) (see section 4.2.2 for information these probes provide to structural and hydrogeological studies). In the case of fractured aquifers, the ATV is particularly interesting, as it provides information of joint orientation and dip at depth. Discussions regarding this method began in the late 1980's (Lau *et al.* 1987, 1988; Cruden 1988). Although the technology was relatively new at that time, it has been proved to be significantly efficient, as shown by later works (Morin *et al.* 1988, 1997, 2007).

Surface-geophysical survey methods are also useful for locating and determining the orientation of fractured zones in the bedrock (Degnan *et al.* 2004). An example is the coupling of geophysical (e.g. ground penetrating radar and resistivity profile) and surface structural analyses with the monitoring of water level to characterize the joint system of an aquifer and its water flow (Degnan *et al.* 2004). Other geophysical methods that improve the identification of subsurface structures – and, thus, of potential water flow paths – are the electric, magnetic and gravity (Grauch *et al.* 1999; Robinson *et al.* 2008). However, some regional scale methods, such as the airborne surveys (Grauch *et al.* 1999; Robinson *et al.* 2008), are usually part of larger and governmental projects due to their high cost, not always related to geological surveys, although they may be used in the studies such as the ones discussed here.

Successful examples of geophysical methods applied to study fractured rock aquifers may be found in many locations, such as: in Nevada, USA (Morin *et al.* 1988), in New Jersey, USA (Morin *et al.* 1997), near the frontier between Canada and United States (Morin *et al.* 2007), and in the Apennines, Italy (Francese *et al.* 2009).

In Nevada, USA, the combination of data obtained with ATV and fluid injection in boreholes allowed to quantitatively estimate the hydraulic conductivity across discrete intervals in the aquifer (Morin *et al.* 1988).

In an aquifer in central New Jersey, USA, two principal joint sets were identified in an apparently complex and heterogeneous fractured media (Morin *et al.* 1997). Likewise, the most transmissive joints in the population were distinguished using different geophysical logs: fluid temperature and conductance, flowmeter, caliper, ATV, natural gamma, rock resistivity and electrical resistivity (see also section 4.2.2).

In the Quebec portion of the Châteauguay River Basin, there was a general agreement between joint data from the geophysical logs and the observations in outcrops and quarries, as well as for the elastic properties and stress models associated (Morin *et al.* 2007). The probes used during the loggings were: caliper, natural gamma activity, sonic profile, ATV and flowmeter; pumping tests were also performed (Morin *et al.* 2007).

The local aquifers in the Apennines, Italy, are generally constituted by thinly-fractured reservoirs, often within low permeability formations (Francese *et al.* 2009). They were studied through an integrated multiscale approach, focusing on the definition of the geometry of brittle structures (Francese *et al.* 2009). The data analyzed included surface geology, with particular interest to joints and faults geometry, well productivity and surface geophysical surveys (ground penetrating radar and earth resistivity tomography) that allow the identification of geological structures in the subsurface. It is relevant to notice that there was a general good agreement between geological and geophysical data (Francese *et al.* 2009), which indicates that such merging of information is effective to define a good structural model of a study area.

2.1.4 Joint connectivity

The quantity of groundwater flow through low permeability rocks depends on the density, connectivity and aperture of the existing joints (Domenico & Schwartz 1990). A higher degree of joint connectivity characterizes a media where most of the joints intercept each other, creating many possible paths for fluid flow. The importance of joint connectivity is clear, and defining this parameter is a frequently mentioned step in the development of hydrogeological models (Francese *et al.* 2009; Singhal & Gupta 2010).

An *interconnectivity index* was proposed to describe the degree of interconnection between two fracture sets (Rouleau & Gale 1985), considering the values of: the mean trace length *l* and the average spacing *s* for each joint set; and the average angle γ between the joint sets (Fig. 2.1). This index was suggested during the structural and hydrogeological characterization studies in granitic rocks in Sweden.

The connectivity and density of joints has a clear effect on groundwater flow, influencing the values of hydraulic conductivity. These parameters will play an important role at different scales (Fernandes 2008, Francese *et al.* 2009).

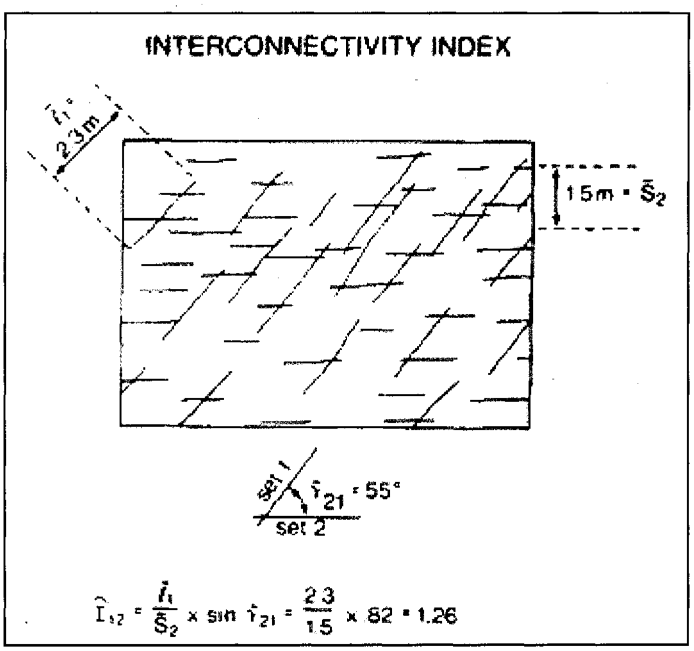

Fig. 2.1 Calculating the joint interconnectivity index. Source: Rouleau & Gale (1985).

2.1.5 Tectonic history and structural domains

One or more tectonic events can be responsible for generating a joint system in a given area. The occurrence of one or more systems, as well as their possible groupings, allows the definition of one or more structural domains, each of which is characterized by a common tectonic history. A structural domain would tend to present its own hydraulic properties as well, due exactly to the distinct joint systems and history that formed them. Structural domains will clearly influence the groundwater flow, and therefore it is essential to characterize them properly during the study of a fractured rock aquifer. Nonetheless, a proper characterization of a structural domain requires a good understanding of the relationships among its joint sets and other existing structures.

When analyzing structural populations on joint pole density diagrams, the identification of patterns may be challenging. A statistical method was proposed in order to evaluate the presence of patterns, taking into account a contingency table analysis based on the frequencies of joint poles observed in corresponding parts of stereoplots being compared (Miller 1983). This allows the grouping of homogeneous structural domains. It is important to define correctly the structural domains during hydrogeological studies, as the corresponding hydrologic properties may vary from one domain to another (Miller 1983).

Studying various cases of joint interactions (Fig. 2.2) and their relationships with the stress field that generated them help to define a structural domain and its tectonic history (Pollard & Aydin 1988). Intersections are an essential element of the interpretation of joint patterns, as well as joint continuity, sequence of development and propagation direction at intersections (Pollard & Aydin 1988). This type of data is of extreme relevance for retracing the tectonic events responsible for the joint sets in a region, since they provide information

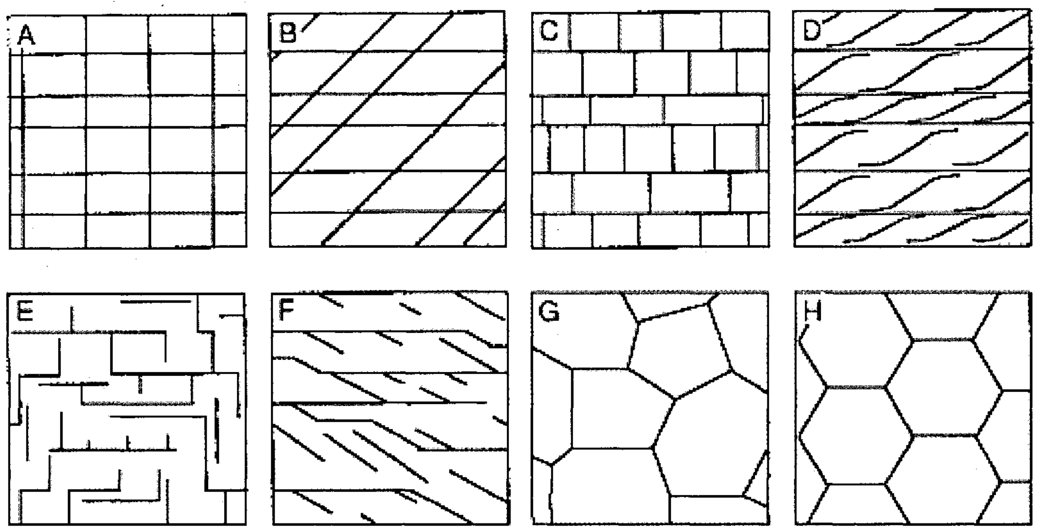

Fig. 2.2 Sketch of joint patterns. (A) Orthogonal and continuous. (B) Conjugate and continuous (type X). (C) Orthogonal, one continuous and other discontinuous (type T). (D) Conjugate, one continuous and other discontinuous. (E) Orthogonal, both discontinuous. (F) Conjugate, both sets discontinuous. (G) Triple intersections with all sets discontinuous at several angles. (H) Triple intersections at angles of 120°. Image source: Pollard & Aydin (1988). Classification on type of joint based on Dunne & Hancock (1994).

regarding relative ages and conjugate pairs of joints (Stearns 1969), as well as past stress field orientation. Joints are thought to be commonly initiated at material inhomogeneities (e. g. fossils, grains, clasts, pores, sole marks, microcracks), which concentrate local tensile stresses due to the compression of the rock mass (Pollard & Aydin 1988). Finally, by determining the relative ages of joints and other structures (such as faults, veins and dykes), it is possible to identify different phases of brittle deformation during the geologic time (Pollard & Aydin 1988).

In the case of orthogonal joints (Rives *et al.* 1994), it is suggested that a less continuous joint set might be the result of: (1) a stress change due to the development of the first set, (2) tectonic stress reversals, (3) post-tectonic relaxation effects or (4) a new stress event. The case of mutual abutments in an orthogonal network of joint sets may be due to the presence of a tensile stress in the late stage of joint development or to successive reversals between the medium and the minimal stress field components (σ_2 and σ_3, respectively) (Rives *et al.* 1994).

Slikensides (Appendix 1) are another feature that may provide interesting information on regional structural characterization surveys and help to reconstruct the tectonic history of the study area, as they are parallel to the movement along faults (Tjia 1964; Angelier 1979). They are commonly associated to steps on the fault wall (Appendix 1), being strongly oblique to them, which help to infer the sense of movement on the wall. When no infilling or mineral growth is observed on the wall, the motion is contrary to the steps; if there is infilling or mineral growth on the fault wall, the motion is on the same sense as the step. Tjia (1964) uses the position of the mineral grain on the slickensides to prove the latter relationship (Appendix 1).

Another important observation regarding the tectonic history of a region is that the most recent events would have the most significant influence on the aperture of the joints in the system and, therefore, on the regional groundwater flow (Fernandes & Rudolph 2001; Zeeb *et al.* 2010). This remark is based on the role of *in situ* stress on joint aperture, which is important for rock hydraulic conductivity (Fernandes & Rudolph 2001) and should be considered within the joint system characteristics for fractured aquifer studies (Zeeb *et al.* 2010). Such consideration is fairly reasonable, as even a very small aperture, with less than 0.1mm, is of relevance for water flow. Moreover, hydraulic conductivity of a joint system in a rock mass is related to the cube of the joint aperture (Snow 1968, 1969) by the following equation:

$$K = \frac{(2b)^3}{W}\frac{\rho g}{12\mu} \quad \text{(Eq. 2.1)}$$

In Eq. 2.1, K is the hydraulic conductivity [m/s], *2b* is joint aperture [m], W is joint true spacing [m] (calculated after Terzaghi's correction; Terzaghi 1965), ρ is the fluid density [kg/m^3], *g* is gravity acceleration [m/s^2] and μ is the dynamic viscosity of the fluid [Pa.s]. When only one joint is considered, Eq. 2.1 may be rewritten as:

$$K = (2b)^2\frac{\rho g}{12\mu} \quad \text{(Eq. 2.2)}$$

2.1.6 Current stress field

As discussed above, the orientation of the past stress fields determines the orientation of the joint sets and major structures such as faults. The current stress field, by its turn, has great influence on the opening or closing of joints, according to the orientation of the stress field components regarding the orientations of pre-existing joints. Therefore, the present stress field plays an important role in determining the most transmissive joints.

Numerical models are an interesting approach to study the effects of the present stress field on the joint system of a fractured rock aquifer. Examples may include. a three dimensional finite element simulation of the stress field, considering the effect of the mean principal stress and the direct effect of the deviatoric stress tensor on joint planes (Gaudreault *et al.* 1994) or even quantifying the closure of joints with depth when the joint system is submitted to a given stress regime (Mortimer *et al.* 2011a, b). Another example of numerical method is the analysis of the present-day stress field and dilatation tendencies to estimate the probable orientations and relative transmissivities of conductive joints (Mattila & Tammisto 2012). A drawback to the latter method is that it requires the knowledge of the full stress field tensor and not simply a two-dimensional approximation of the stress components.

The orientation of a joint set with respect to the main components of the present stress field will affect its hydraulic properties (Gaudreault *et al.* 1994), as the orientation of the stress field controls the current opening or closing of joints, and hence, their transmissivity (Barton *et al.* 1995; Morin & Savage 2003; Fernandes 2008). The possible effects of the present stress field on a given joint set have been classified in three main cases (Gaudreault *et al.* 1994): (1) closure with σ_1 almost perpendicular to the discontinuity plane; (2) opening with σ_3 nearly perpendicular to the joint plane; (3) shearing with σ_1 at an intermediate angle (between 30° and 60°) with the discontinuity plane.

2.1.7 Relationships between hydrogeological properties and structural domains

Studying the role of major tectonic structures is valuable for well location, evaluating groundwater use, its management and contaminant control (Apaydin 2010). This section presents a discussion on the possible relationships between lineaments (which may be considered as a surface expression of a geological structure) and hydrogeological aspects (such as well productivity and rock permeability).

Well productivity

Analyzing lineaments is an indirect way of evaluating the influence of joints in well production (Fernandes & Rudolph 2001; Fernandes *et al.* 2007; among others). When correlating the production of wells and the factors that induce the groundwater flow, it is important to evaluate the influence of factors such as: tectonic history and current stress field of the region, proximity of the wells to lineaments, nature and thickness of the unconsolidated material, lithology, topography and depth of inflow into the well (Fernandes 2008). This, as a first approach, may provide important information for the understanding of the hydraulic properties of fractured aquifers (Fernandes 2008) and also homogeneous geologic blocks (Fernandes *et al.* 2007). It is then interesting to compare it with some lineament aspects, such as density, connectivity and structural trends, as well as to analyze the well productivity in relation with their proximity to lineaments (Fernandes & Rudolph 2001). Well productivity may be assessed by values of specific capacity, which indicates the aquifer potential more directly than the simple pumping rate, though the productivity might be influenced by well construction aspects (Fernandes *et al.* 2007). Although sometimes the most productive wells tend to be in the highly fractured domains (e.g. Sultan *et al.* 2008), some studies concluded the contrary, that is, the most productive wells are not in the areas with higer density of lineaments (e.g. Madrucci 2004). Therefore, a causal relationship between lineaments and most productive wells should not be automatically assumed, particularly because not all lineaments represent conduits for water flow, as discussed in the section below.

<u>Lineaments as flow barriers or conduits</u>

Faults, fracture zones and shear zones (all may appear as lineaments in a map) are usually considered as preferential conduits for groundwater flow; however, they may also act as barriers to groundwater, due to the configuration between fault core and damage zone at the fault zone (Francese *et al.* 2009; Gleeson & Novakowski 2009; Apaydin 2010). The fault core is the portion where most of the displacement is accommodated, while the associated damage zone is mechanically related to the growth of the fault zone (Caine *et al.* 1996). Assuming that lineaments are conduits for groundwater is overly simplistic, and characterizing the lineaments and/or the joint system is a very significant aspect of investigations on fractured aquifers (Gleeson & Novakowski 2009).

Evaluation schemes for permeability of fault-related structures, using field data, laboratory permeability measurements and numerical models of water flow near and within fault zones were developed in order to assess the role fault cores and fault damage zones play as barriers and conduits, respectively (Fig. 2.3; Caine *et al.* 1996). In crystalline rocks, the fault core (less permeable) and the associated damage zone (more permeable) tend to form an anisotropic structure that is a hydraulic conduit, a barrier or a conduit-barrier system, depending on their architecture and on the direction of the flow (Caine *et al.* 1996; Gleeson & Novakowski 2009). The behavior of the ensemble will be determined by the relative importance of fault core and damage zone structures, as well as by the lithology affected and its degree of weathering.

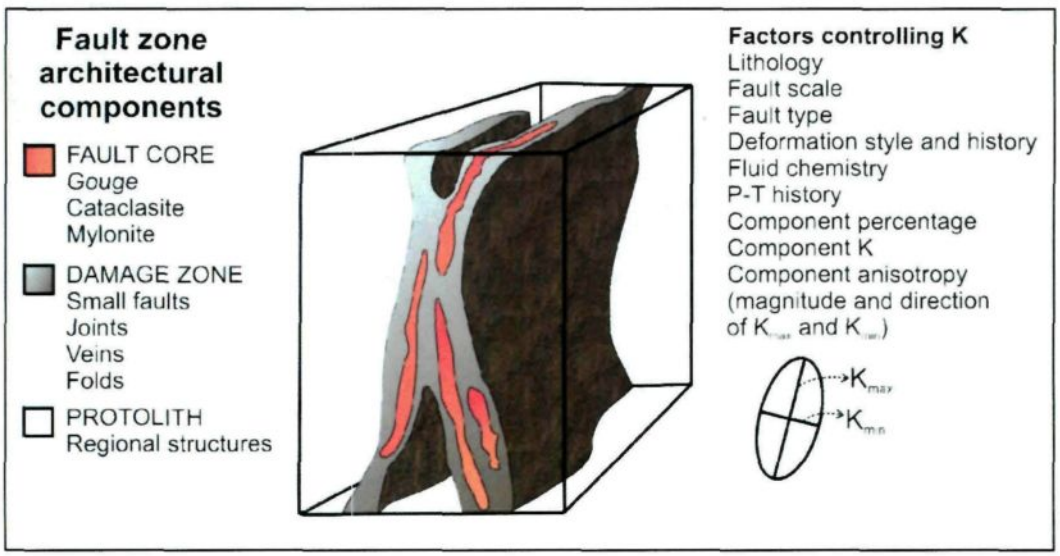

Fig. 2.3 Conceptual model of a fault zone. The relative magnitude and bulk two-dimensional permeability tensor that may be associated to the components of the fault zone are shown on bottom right. After: Caine *et al.* (1996).

The permeability of faults also depends on their stage of development (UNESCO 1984; Tirén 1991; Caine *et al.* 1996); fault core materials may not always act as a barrier, especially during deformation (Caine *et al.* 1996). Nonetheless, damage zones are usually better conduits as compared to the fault core and the protolith (Fig. 2.3; Caine *et al.* 1996): a damage zone may have permeability values that are three to four orders of magnitude higher than a fault core, while an undeformed fractured rock would present intermediate values (Evans *et al.* 1997).

2.2 Mathematical and numerical models of fractured aquifers

Some of the models of fractured aquifers proposed in the literature are grouped here according to porosity type. This criterion allows distinguishing models of fracture network with impermeable matrix, double porosity (discussed jointly with models based on unit blocks[1]) and equivalent porous media (discussed jointly with the permeability tensor approach). Finally, some possibilities of integrating the numerical models of fractured aquifers with data of an *in situ* stress field are presented. Regardless of the model that is considered, Neuman (2005) states that it is truly important to treat a fractured aquifer considering the *"highly erratic heterogeneity, directional dependence, dual or multicomponent nature and multiscale behavior of fractured rocks*".

2.2.1 Models of impermeable matrix and the discrete joint network approach

Most of the discrete joint network models consider the rock matrix as impermeable, that is, only the secondary porosity is taken into account (Neuman 2005). The discrete joint network model allows the estimation of the fluid flow velocity within the joints and might

---

[1] A unit block is a basic structural unit that defines a fractured rock mass. See section 4.3.4 for detailed definition of the unit block.

represent either small or relatively large networks. The small networks usually comprise one to ten joints, so the application of a deterministic method is feasible, in which the position of joints is known (e.g. Tezuka & Watanabe 2000; Selroos *et al.* 2002). In the case of larger networks, a hundred or more joints are considered, which may be generated using a stochastic approach (e.g. Schwartz *et al.* 1983; Rouleau 1984; Rouleau & Gale 1987; Neuman 2005; Mortimer *et al.* 2011a).

The development of both the discrete fracture network model and the unit block are based on true (corrected) joint data. They differ with respect to joint connectivity: in the discrete network model, the joints are not necessarily connected, while in the unit block, the joints are assumed to be always connected. Nonetheless, compilations of distribution of the length of visible joint traces (for each of the main joint sets) on an observation face and the number of the observed intersections between the joint sets might aid to achieve a more reliable model.

2.2.2 Double porosity approach and models based on unit blocks

The concept of unit block was largely developed in the oil industry, starting in the 1970's and the 1980's, because it is fairly important to characterize the fluid flow on both joints and matrix of a reservoir, in order to consider possible fluid exchanges between these two reservoir components (Kazemi *et al.* 1969; Ghez & Janot 1974, Kazemi *et al.* 1976, Streltsova 1976; Aguilera & Poollen 1977; Boulton & Streltsova 1977; Gilman & Kazemi 1983; Sonier *et al.* 1988). These models are based on the double porosity approach, first proposed by Barenblatt *et al.* (1960) and Warren & Root (1963). These models consider both primary and secondary porosities.

Barenblatt *et al.* (1960) proposed an equation of hydraulic diffusivity (ratio between hydraulic transmissivity and storavity) in fractured rocks, describing a fractured media composed of porous blocks separated by fractures of infinite extent. Warren & Root (1963), on the other hand, applied an analytic method and cubic blocks (Fig. 2.4) to represent a given joint system, assuming that the primary porosity contributes significantly to the pore volume, but that it is negligible to the flow capacity.

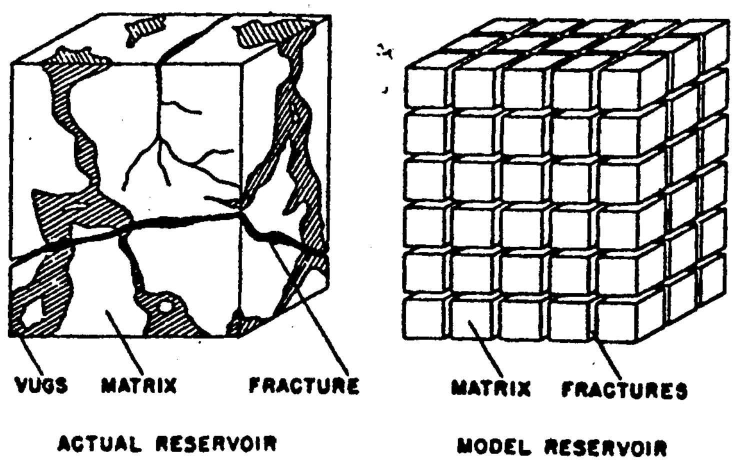

Fig. 2.4 Relatively simple fracture networks used to be considered for modeling. They were an idealization of the heterogeneous media. Nowadays, models with more complex networks are available, as discussed in the text. Source: Warren & Root (1963).

Major flaws of the double porosity approach are the assumption of uniform matrix properties throughout the system and of a uniform, cubic joint network. Some solutions were later proposed: the development of parallelepiped unit blocks (Barker 1985) and the model of two separate sets of matrix properties (Abdssah & Ershaghi 1986). As the double porosity approach continued to be used (Almeida & Oliveira 1990; Dutra & Aziz 1992; Lough *et al.* 1997) and more recent works also discussed the flow through the matrix-fracture interface (Zhang *et al.* 2006; Weatherill *et al.* 2008), the coupling of the unit block data with a double porosity model is here suggested as a possible way to integrate the structural data into a numerical model of fractured aquifers[2].

2.2.3 Equivalent porous media models and the permeability tensor

Models based on an "equivalent porous media" concept may be developed with the hydraulic conductivity tensor approach. In this case, it is possible to estimate the hydraulic conductivity tensor of the whole rock mass by summing the tensor calculated for each joint, using Eq. 2.2. The interesting point of this approach is that it takes into account the joint system characteristics, such as geometry and orientation. However, equivalent porous media models usually suppose that each joint is infinite, that is, each one crosses the entire analyzed zone, which is rarely realistic. Nonetheless, a case in British Columbia, Canada, has shown that equivalent porous media model may return valid results and be useful for characterizing and quantifying hydraulic properties of fractured rock aquifers at a regional scale (Surrete 2006). Structural domains were defined by using joint density data and modeling with a stochastic, discrete joint system of equivalent porous media (Fig. 2.5) (Surrete 2006). The results obtained are in accordance to data independently obtained in pumping tests in the same area (Surrete 2006). Other works that adopted the equivalent porous media approach include: Nastev *et al.* (2005), Chesnaux & Allen (2008) and Chesnaux *et al.* (2009), both in fractured sedimentary rocks. An interesting particularity of the latter two is that they use an impermeable matrix model with the discrete joint system approach to construct a hydraulic conductivity tensor that represents an equivalent porous

[2] The double porosity approach, however, is not advised for crystalline rock aquifers, given that their matrix permeability is much lower than the joint permeability, even though the matrix porosity is higher than joint porosity. A double porosity model is more interesting in the case of fractured sedimentary rock aquifers.

media. The authors also emphasize the contributions of modeling fractured rock aquifers to understand their behavior and to evaluate their exploitation.

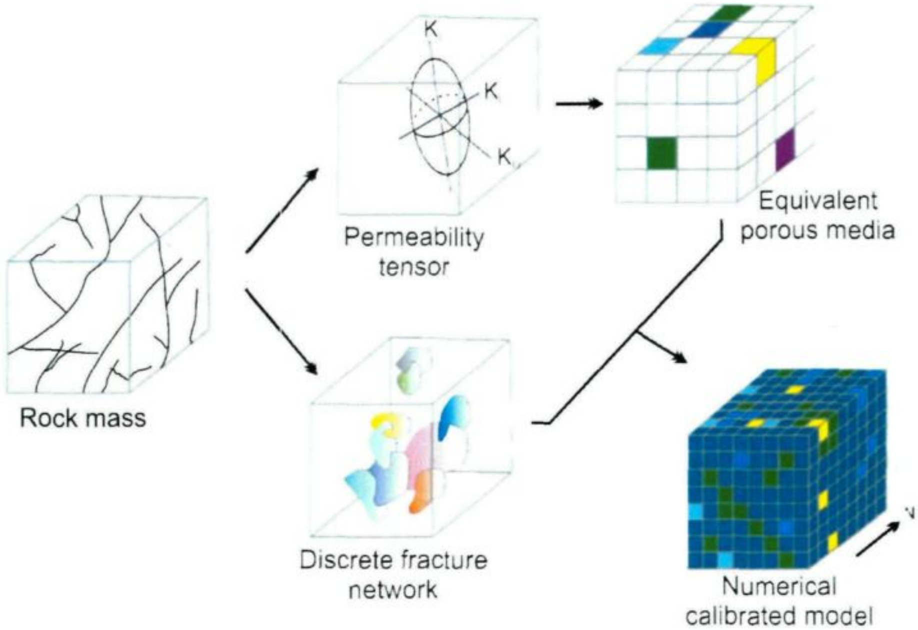

Fig. 2.5 Scheme based on the work of Surrete (2006) for generating a numerical model of a fractured aquifer by combining two different model approaches: equivalent porous media model and discrete fracture network. Adapted from: Surrete (2006).

The example from Fig. 2.5 uses a permeability tensor to develop the equivalent porous media model. This approach has long been discussed for homogeneous and anisotropic media (Bianchi & Snow 1968; Snow 1968, 1969, 1970; Rocha & Franciss 1977; Long *et al.* 1982; Oda 1985; Raven 1986). For illustration purposes, two of these studies of permeability tensors are further described.

Bianchi & Snow (1968) applied the theory proposed by Snow (1968) for analyzing the directional permeability of any fracture model, computing the permeability from fracture geometry (orientation and measured apertures). It is assumed that the contribution of all fractures measured at a sampling site is given by the sum of all individual contributions, and so the equivalent permeability of the medium may be given by the average of values obtained for several sites.

Next, Oda (1985) argues that a joint system cannot be replaced by an equivalent porous media unless there are a sufficient number of joints in the representative elementary volume; that is, this model is subjected to the scale effect and it is, thus, more recommended for regional studies. When that is the case, the fractured rock mass can be treated as an equivalent homogeneous and anisotropic porous media. Although this representation does not consider the high velocity of fluid flow in the joints, it might be better designed by introducing a symmetric tensor (the "joint tensor") which relies only on the geometry (aperture, size and orientation) of the related joints (Oda 1985). The permeability tensor is defined as a unique function of the joint tensor (Oda 1985), and it yields valuable information: the degree of anisotropy in hydraulic response of rock masses, the principal axes of the permeability tensor and a quantitative comparison between rock masses.

2.2.4 The effect of an in situ stress field

Considering the three modeling approaches discussed above, it is also interesting to add to the model the effect of an *in situ* stress field. As previously discussed in this chapter, the present-day stress field has great control on joint aperture, and, consequently, on groundwater flow. A number of existing software codes are capable of simulating the effects of stress field on fluid flow through joints, such as the Universal Distinct Element Code (UDEC; Itasca™), used by several researchers (Fernandes & Rouleau 2008; Noël 2009; Mortimer *et al.* 2011a, b). It allows to capture, for instance, the closure of joints with depth when the joint system is submitted to a given stress regime. Some works with UDEC models also tested the potential influence of a determined stress field on the permeability tensor of their model (Mortimer *et al.* 2011a, b). The deformed and undeformed models were compared through the estimation of two dimensional planar hydraulic conductivity ellipses at different depths, in order to also take into account the effect of decreasing joint densities. Studies on the effect of normal stresses to individual joint planes in a discrete joint network can also be found (e.g. Grégoire 1988).

2.3 Final considerations

In brief, all of these previous studies underline the importance of structural hydrogeology. Proper characterization of the structural discontinuities is essential for a good understanding of the aquifers in fractured media, either for academic purposes or for water management. The previous sections presented investigation methods that lead to the development of conceptual models of an aquifer, as well as different possibilities of numerical models for groundwater flow in a fractured media.

Some of the works that were reviewed discuss the effects of scale of observation on hydraulic properties. The present work shall analyze structural geology data at different scales in order to determine if they may really be compared. The hydraulic properties of the Kenogami uplands discussed in chapter 6 come from a regional study, which applied an analytic model of groundwater flow (Chesnaux [accepted]).

The use of remote sensing is widely accepted among researchers to identify regional structures, as previously seen. Given the data available, this project used aerial photographs to identify lineaments and major outcrops.

Regarding geophysical logging, some of the techniques proposed were adopted (e.g. the ones by Morin *et al.* 1997). Geophysical logging shall be used here as a complement to surface structural survey, and not as the main source of data, unlike many of the works described above.

Although the joint interconnectivity index was not quantified for the Kenogami uplands, the relationships among joints were studied in order to infer the orientation of the main component of past stress fields (much like Pollard & Aydin 1988). This approach helps to understand tectonic history of the region. The relations between joints were analyzed at the outcrop scale and data from the different observation sites were later combined. A detailed approach for this particular study is also described.

One of the objectives of identifying the past stress fields is to define the most recent one, and for that, it is important to know the tectonic history of the studied region. A compilation of the current regional stress field data both in the SLSJ area and surrounding areas in southeastern Canada is further presented.

Finally, in the present work, hydrogeological properties from the Kenogami uplands are related to the unit block, considered as the basic unit that characterizes a fractured media, as described in upcoming chapters.

3

GEOLOGY AND HYDROGEOLOGY OF THE STUDY AREA

The bedrock geology in Quebec is divided in three large regions: the Canadian Shield, the Saint-Lawrence Platform and the Appalachian Orogen (Fig. 3.1). The Canadian Shield is divided in four geological provinces, according to deformation style and age: Grenville, Superior, Rae and Nain (Fig. 3.1). As the study area is located in the Canadian Shield, in the Grenville Province, attention will be focused on this Province.

3.1 The Grenville Province

The Canadian Shield was formed between 2850 and 850Ma and covers 90% of the Quebec province (Hocq 1994). The Grenville Province is located in the southeastern part of the Shield, and is characterised by a generally high metamorphic degree and by a large quantity of magmatic rocks crystallized at high temperatures, such as mangerite and anorthosite (Tollo *et al.* 2004). Three lithotectonic zones subdivide the province (Rivers *et al.* 1989): Parautochthonous Belt, Allochthonous Polycyclic Belt and Allochthonous Monocyclic Belt (Fig. 3.2). The tectonic boundaries between them are (Rivers *et al.* 1989): Grenville Front, Allochthon Boundary Thrust and Monocyclic Belt Boundary Zone (Fig. 3.2).

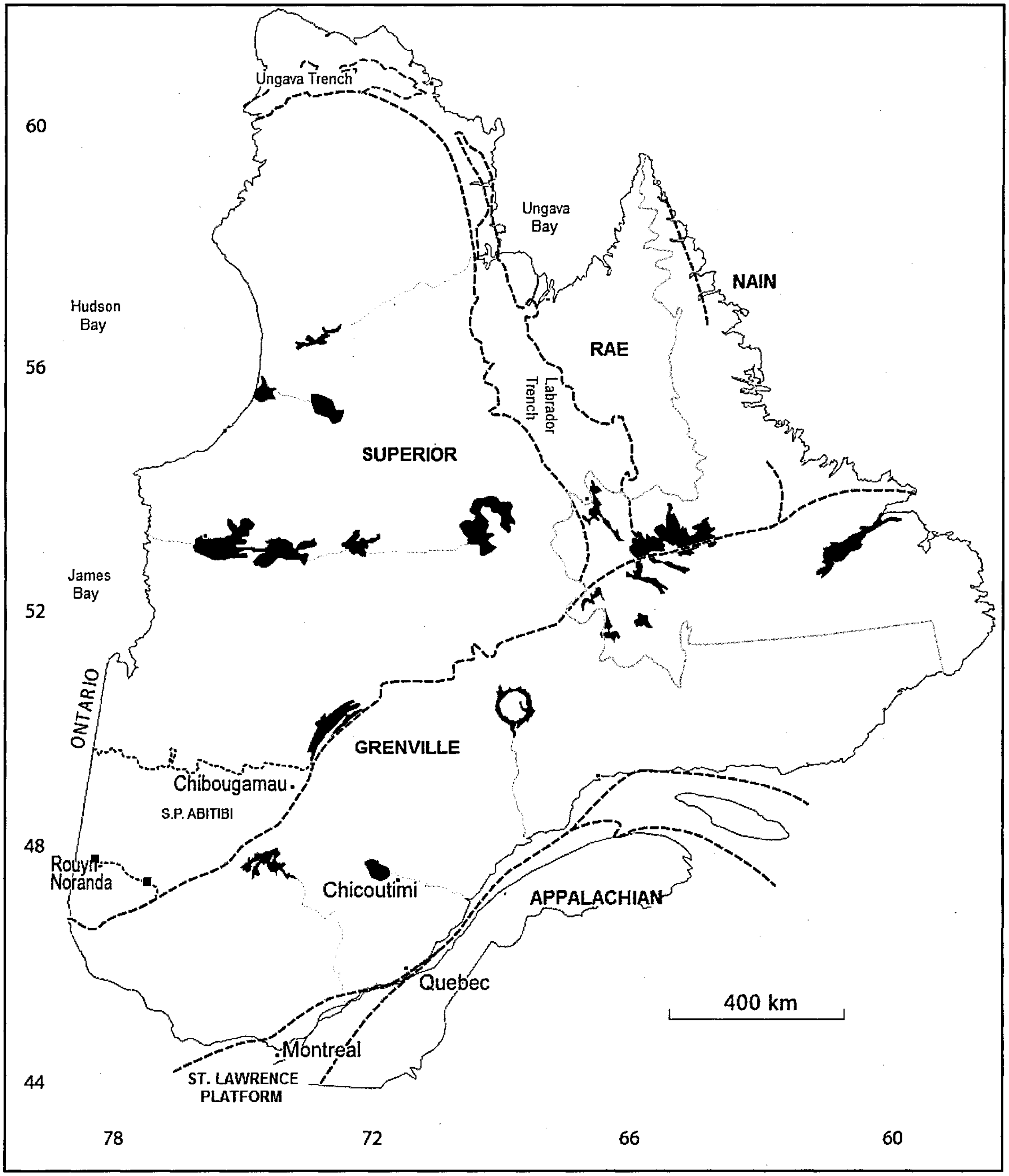

Fig. 3.1 Geological provinces in Quebec. The area of the present study is located in the Grenville Province, near Chicoutimi city. Adapted from: Roy *et al.* (2006).

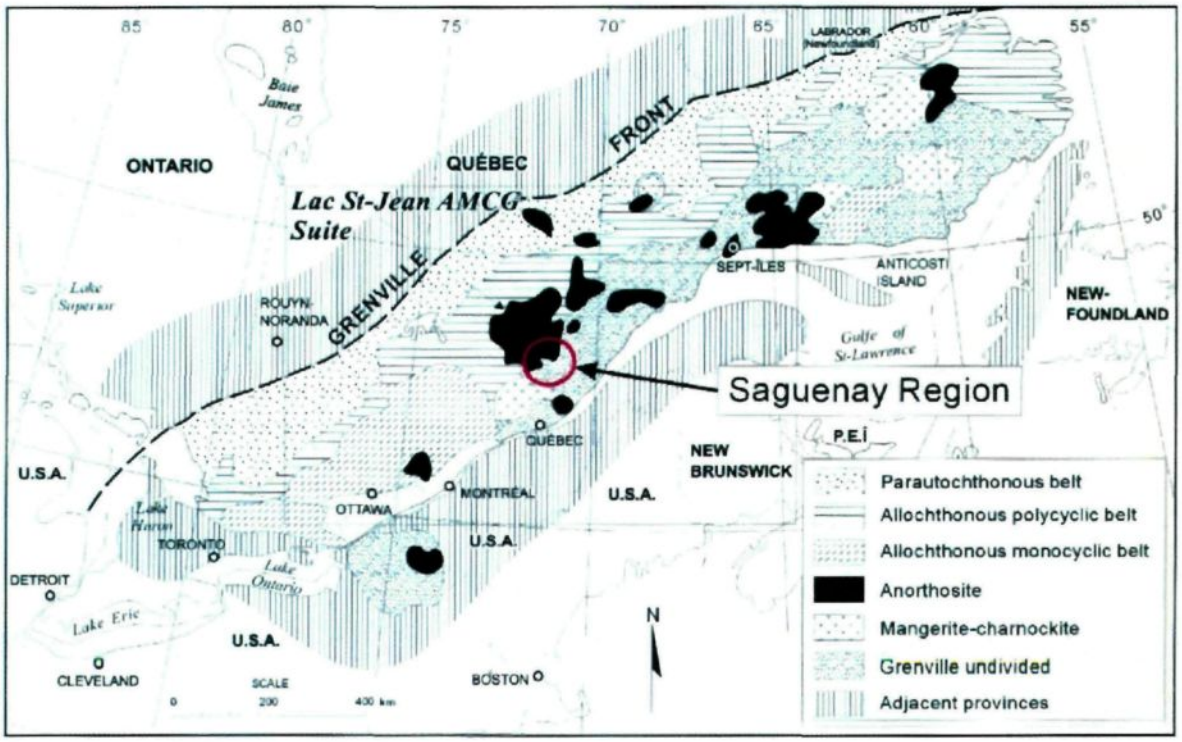

Fig. 3.2 Lithotectonic terrains in the Grenville Province. The Kenogami uplands are mostly constituted by rocks from the large anorthosite massif of the Saguenay region. Source: Hébert (2004).

The Grenville Province constitutes the youngest orogenic belt in the Canadian Shield (Tollo *et al.* 2004). Its multiple episodes of orogenesis were recognized in the 1970's (e.g. Wynne-Edwards 1972; Moore & Thompson 1980).

3.2 The Kenogami uplands

The Kenogami uplands, the area of the present study, are sometimes referred to as "Kenogami horst", a name probably first proposed by Blanchard (1953). However, a horst is defined as "*an elongate uplifted block bounded by faults on its long side*" (USGS 2010). Therefore, the expression "Kenogami horst" is a misuse of the term, since the discontinuities that delimitate these uplands on their "long side" (east and west sides) are major regional lineaments, with no faults being identified until the present day. Nonetheless, as these lands clearly constitute a subregional topographic high, they will be referred to as Kenogami uplands.

The Kenogami uplands are located in the center of the Saguenay graben (Fig 3.3). The southern and northern walls of the graben are parallel to the WNW-ESE trend of the end of the Grenvillian orogeny. This orientation is also reflected in other regional structures, such as the Ottawa graben (Kumarapeli 1981; Rimando & Benn 2005) and the transform faults in both Canada and United States (Kumarapeli 1970; Thomas 1991).

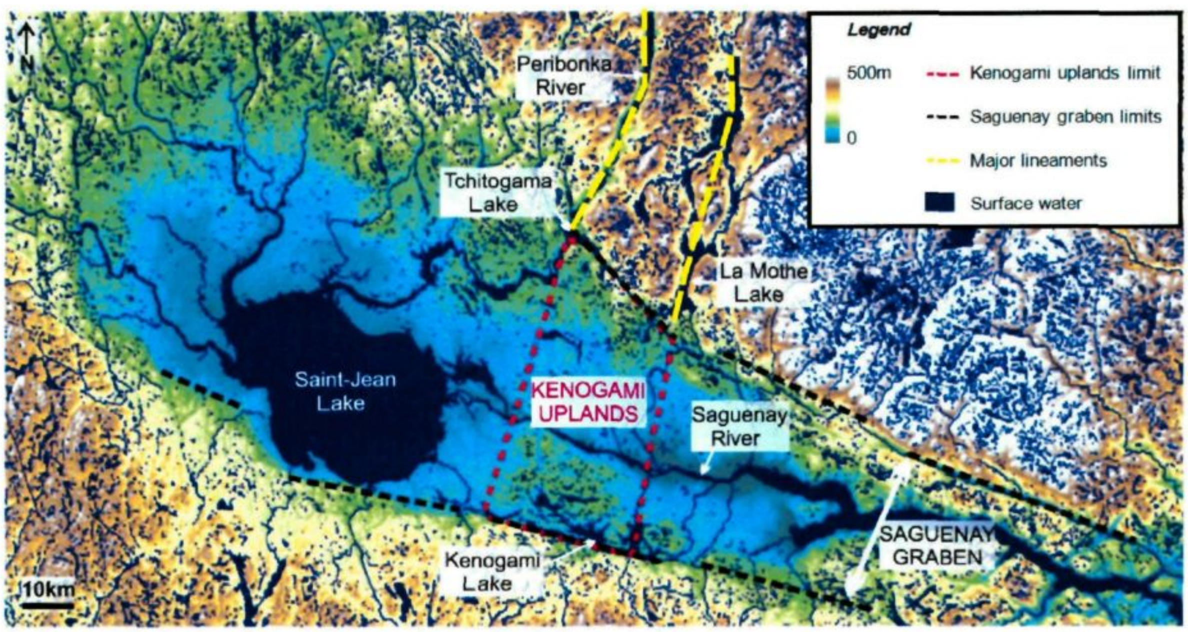

Fig. 3.3 Topography and approximate delimitation (red dashed line) of the Kenogami uplands. Adapted from: Walter *et al.* (2010).

The Kenogami uplands are limited to the south and to the north by the Kenogami and the Tchitogama Lakes, respectively (Fig. 3.3). Their western and eastern limits are not defined by known faults, but by major lineaments: the western side appears as a continuation of the lineament suggested by the trend of Peribonka River located to the north (Fig. 3.3); the eastern side could correspond to the lineament suggested by the Gélinas bay (in the Kenogami Lake) to the south, which is in line with the La Motte Lake to the north of the graben (Fig. 3.3). These regional linear structures were already identified in the maps presented by Lasalle & Tremblay (1978). It is also interesting to notice that Woussen *et al.* (1988) present a map from the SLSJ area with a shear zone oriented approximately N-S that is near the western limit of the Kenogami uplands considered in this work; those structures may be related, even though this shear zone was not identified in the field in the present study.

Other important regional brittle structures to the west of the Kenogami uplands are oriented NNW and NNE. Such structures are in continuation with the Hudson-Champlain lineament (in the USA), prolonged to Quebec by the Richelieu and Saint-Maurice Rivers axes (Kumarapeli & Saull 1966; Isachsen 1989). The main regional structures are completed by the ones oriented NE-SW, parallel to ductile shear zones and to the Saint-Lawrence and the Appalachian axes, and by some NW-SE structures. They also follow the Late Precambrian – Early Paleozoic trend of rift segments in the Iapetus Ocean described by Thomas (1991).

The study area is mainly composed of anorthosite (Fig. 3.4), from the large Lac-Saint-Jean Anorthosite massif (LSJ Anorthosite). Exposures of granitic rocks and of syenite, monzonite, granodiorite and diorite can also be found in the northwest and northeast

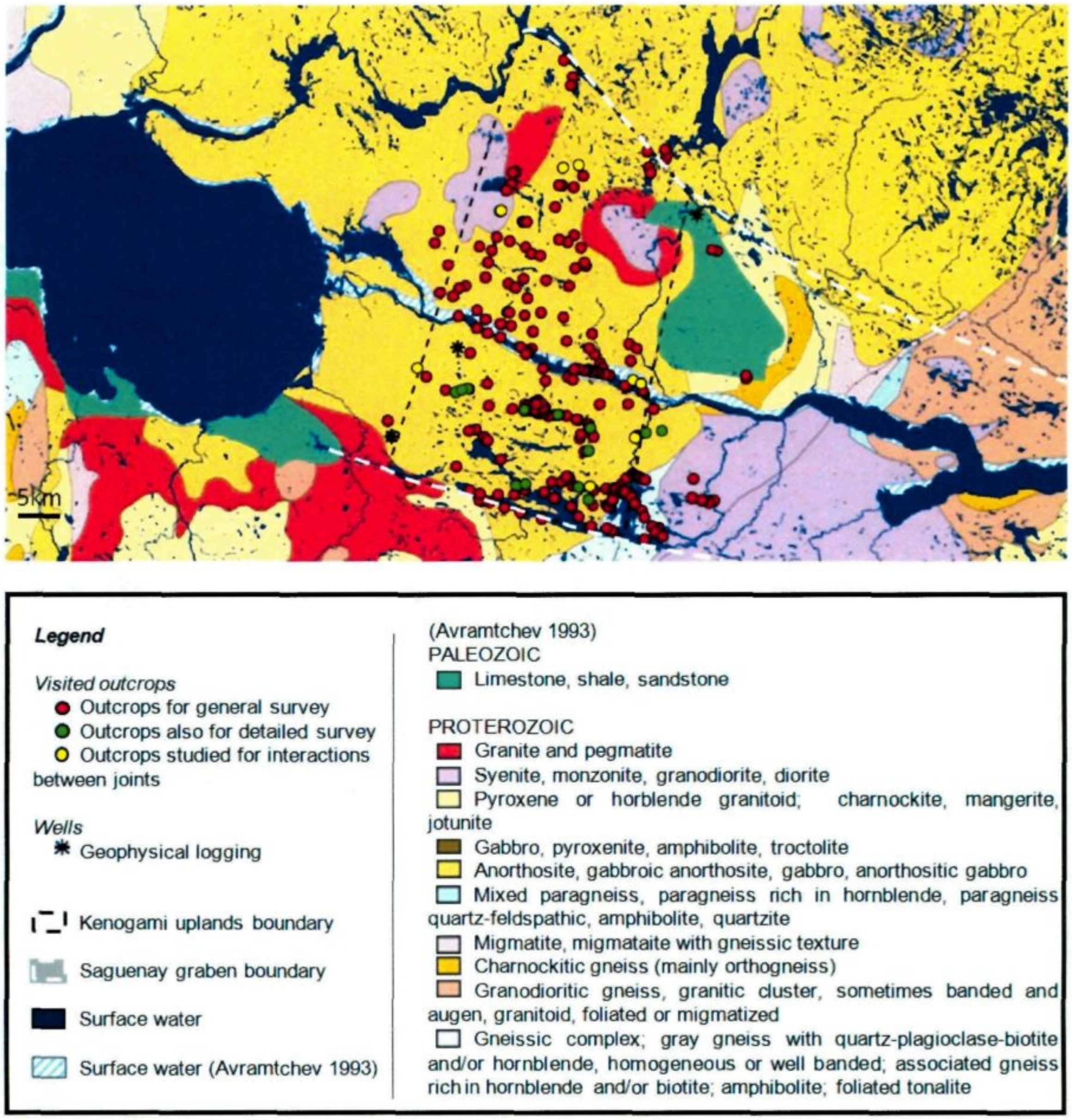

Fig. 3.4 Bedrock geology of the Saguenay region, showing the location of the visited outcrops and the three wells submitted to geophysical logging. Geological map source: Avramtchev (1993).

portions of the Kenogami uplands (Fig. 3.4). The LSJ Anorthosite, covering more than 20.000 km^2, is one of the largest anorthosite massifs of the world (Dimroth *et al.* 1981).

The mineralogy and petrology of the mentioned rocks are discussed in: Woussen *et al.* (1981; 1988), Hocq (1994), Higgins & van Breemen (1992; 1996) and Hébert (2004).

3.3 Tectonic history

The oldest geologic events identified in the Saguenay area occurred between 1900 and 1000Ma (Stockwell 1962; Dimroth *et al.* 1981; Hébert 2004; Roy *et al.* 2006). This period corresponds approximately to the formation of the oldest worldwide orogenic belts and of the amalgamation and dispersion of the supercontinent Columbia[3] (Santosh *et al.* 2009). Paragneisses, granitic gneisses and amphibolites were the first rocks emplaced in the study area, around 1800Ma, being intruded later by other granitic and amphibolite dykes (Dimroth *et al.* 1981). This sequence is locally known as Chicoutimi Gneiss Complex (Woussen *et al.* 1981). It was folded and metamorphosed around 1700±150Ma, during the Hudsonian Orogeny (Stockwell 1962), after which voluminous sheets, dykes, and stocks of granite were put in place. The Chicoutimi Gneiss Complex is nowadays in tectonic contact with the LSJ Anorthosite (Hébert & van Breemen 2004). Some works discuss the origins and ages of this granitic bedrock; e.g. Hervet (1986), Dickin & Higgins (1992), Hervet *et al.* (1994).

The Grenvillian Orogeny occurred between 1190 and 980Ma, and it comprises three clear pulses of NW-directed crustal shortening (Rivers 1997): 1190-1140Ma, 1080-1020Ma and 1000-850Ma (Table 3.1). This thrust orientation is largely acknowledged in literature, as summarized by Tollo *et al.* (2004). The periods of crustal extension that separated these three pulses were coeval with the emplacement of intrusions of

---

[3] The supercontinent Nuna refers to the Paleozoic amalgamation of North American terrains, that is, the portion of Columbia that corresponds to the nowadays North America (Hoffman 1989).

Table 3.1 Summary of the main magmatic and tectonic events in the Grenville Province, focusing in the SLSJ region, in the period 1200-850Ma. D_i, S_i and P_i indicate, respectively, deformation, folitation and folds generated during a tectonic event *i*.

Phases	Magmatic pulses (Hervet *et al.* 1994; Higgins & van Breemen 1992, 1996)	Grenvillian Orogeny (Rivers 1997; Hébert *et al.* 1998; Hébert 2004; Hébert & van Breemen 2004)	
		Grenville Province	*SLSJ*
1	1160-1140Ma 7 ages of AMCG Emplacement and largely synchronous deformation	1190-1140Ma Deformation and metamorphism in terrains in the Ontario area	D_1: thrusting E-W S_1: E-W to ESE-WNW oriented, usually moderately dipping to N.
2	1082-1050Ma 6 ages of AMCG Predominance of strike-slip faulting	1080-1020Ma Thrust of terrains in Ontario area Crustal thickening in the Mauricie region to the southwest of the SLSJ area	D_2: NE-SW shear zone in Saint Fulgence, non-co-axial deformation with NE-SW dextral strike-slip motions; affects the LSJ Anorthosite early D_2: thrusting late D_2 (after collision): strike-slip movement S_2: NE-SW foliation, often dominant and penetrative P_2: open to tight, with plunge parallel to the stretching lineation
3	1020-1010Ma 5 ages of AMCG		D_3: NNW brittle-ductile faults, non-co-axial devormation; sinistral slip *en echelon*
3'		1000-850 Thrusting closer to the Grenville Front Crustal thickening in the Ontario area	

anorthosite, mangerite, charnockite and gabbro (AMCG) across the whole Grenville Province, guided by the shear zones previously and simultaneously formed (Higgins & van Breemen 1996; Rivers 1997; Higgins *et al.* 2002). A fourth period of AMCG magmatism is also recognized (1327±16Ma), although neither deformational nor tectonic events were particularly related to it yet (Higgins & van Breemen 1996; Rivers 1997; Higgins *et al.* 2002).

The NW oriented thrusting in the Grenville Orogen resulted in penetrative deformation (Corrigan & Hanmer 1997), while the final emplacement of solid anorthosite at the present crustal level resulted in local superposed structures. The nature of the process of gravitational ascent of the LSJ Anorthosite through the lower crust remains uncertain, despite proposed hypothesis (Dimroth *et al.* 1981; Woussen *et al.* 1981; Rivers 1997, Duchesne *et al.* 1999). The principal tectonic and magmatic events from the Grenvillian Orogeny are summarized in Table 3.1 and are discussed in the following paragraphs, presenting both the Grenville Province and the SLSJ's aspects.

The first phase of crustal shortening (1190-1140Ma) in the Grenville Province is reflected in the deformation and the metamorphism of the Central Mineral Belt and Parry Sound terrane, in the Ontario region (Rivers 1997). Later, between 1080-1020Ma, these two land masses were emplaced by thrust over the Central Gneiss Belt, also in the Ontario area (Rivers 1997). From this period, an event of crustal thickening was dated at ~1062Ma in the Mauricie region, about 150km south of the LSJ area. Finally, the last phase (1000-850Ma) was characterized by a change in the locus of the thrusting, closer to the Grenville Front (Fig. 3.2; Krogh 1994; Rivers 1997) and by a later extension between 990 and 950Ma in the Central Mineral Belt and the Central Gneiss Belt (Rivers 1997).

More particularly in the SLSJ region, three main events of ductile deformation (Table 3.1) are identified (Hébert 2004; Hébert & van Breemen 2004; Roy *et al.* 2006). The first event is related to a major period of thrust E-W to ESE-WNW, to which can be associated a foliation or a gneissosity (Hébert 2004; Hébert & van Breemen 2004) imprinted over a magmatic bedding (which was described by Woussen *et al.* 1988). The characteristics of this first fabric were strongly deformed by the second event, which is associated to a period of ductile shear oriented ENE-WSW (Hébert 2004; Hébert & van Breemen 2004). The foliation then formed is recognized throughout the SLSJ and it is usually the dominant one (Hébert & van Breemen 2004). Finally, the third event is related to the formation of NNW-SSE brittle-ductile fault zones, really common in the SLSJ (Hébert 2004; Hébert & van Breemen 2004). These fault zones induced sinistral *en echelon* slipping, originating shifts of dozens of meters; e.g. in the contact of the anorthosite with the bedrock in the Kenogami Lake area (Hébert & Lacoste 1998).

A compilation of U-Pb data regarding the SLSJ region (Higgins & van Breemen 1996) proposed three phases of its Mesoproterozoic magmatism: 1160-1140Ma, 1082-1050Ma and 1020-1010Ma (Table 3.1). The first two phases are also correlated to magmatism elsewhere in the Grenville Province (Higgins & van Breemen 1996).

The first phase of magmatism is defined by seven age estimates obtained for the AMCG suites, including the one from the LSJ Anorthosite massif (1156Ma; Higgins & van Breemen 1992). Its early stages were coeval with strike-slip faulting (Higgins & van Breemen 1992, 1996), which is suggested as the upward magma motion mechanism. Both anorthosite and gneiss terrains were plastically deformed in the first phases of ascent; as temperature decreased in the anorthosite, the deformation concentrated in ductile deformation zones (Dimroth *et al.* 1981). The faults generated later guided intrusions of ferrodiorite and leucotroctolite in the anorthosite (Higgins & van Breemen 1992, 1996; Hervet *et al.* 1994). It has been indicated that the Ontario sector of the Grenville Province went under a period of magmatism without anorthosite between 1160-1140Ma (Van Breemen & Davidson 1988; Marcantonio *et al.* 1990), while there was a widespread AMCG magmatism elsewhere in the Province (e.g. McLelland & Chiarenzelli 1990; Doig

1991; Higgins & van Breemen 1992). Nonetheless, it has been affirmed that there is no evidence of collision-type orogeny in the SLSJ region in the period 1160-1010Ma, like thrusting, calc-alkaline magmatism or true regional metamorphism (Higgins & van Breemen 1996).

During the period 1082-1050Ma (Table 3.1), the AMCG magmatism was widespread in the Grenville Province (Higgins & van Breemen 1996). Strike-slip faulting was predominant (Hervet *et al.* 1994), except for the Ontario region, submitted to compression (Higgins & van Breemen 1996).

The last period of AMCG magmatism activity in the SLSJ (1020-1010Ma) seems to be absent in the rest of the Grenville Province, except for later smaller plutons in the Labrador region (Gower *et al.* 1991).

Around 1000Ma, the supercontinent Rodinia was completely assembled, with the completion of the break-up of Columbia (Santosh *et al.* 2009). The formation of Rodinia is related to the consuming plate boundaries that dominated the site of Grenvillian Orogeny, especially at collisional belts. The Grenville Orogeny ended with the emplacement of the last igneous masses and their crystallization at their present level, with the development of ductile shear zones (oriented NNE, ESE and ENE to E-W; Du Berger *et al.* 1991) cutting all Precambrian rocks (phase 3' in Table 3.1; Dimroth *et al.* 1981).

The rifting of Rodinia occurred between 750 and 600Ma. In the portion corresponding to North America, three main tectonic events followed the dispersion of the supercontinent: the Taconic (550-450Ma), the Acadian (410-380Ma) and the Alleghanian (300-250Ma) orogenies[4]. During this whole period (550 to 250Ma), the SLSJ region was marked by extensional faults, which probably formed the Saguenay graben (Hébert 2004).

Around 600Ma, the opening of the Iapetus Ocean created various transcurrent and normal faults in the margin of the new "Quebec Gulf", as well as several lineaments in the Saguenay region (Roy 2009). An extensional regime oriented 022° and transcurrent faults at 120° were then installed (Thomas & Astini 1996). It is possible that the Saguenay graben was formed at this time, and it would constitute an Iapetan aulacogen (Kumarapeli & Saull 1966; Kumarapeli 1985; Allen *et al.* 2009), although there is still no evidence to prove it. Moreover, the limestone found within the graben do not present indications of movement nor talus slopes related to this period (unlike the limestone at Charlevoix region; Rondot 1972).

With the Taconic orogeny, the extensional environment gave way to a collisional one (Osberg 1978). This tectonic event consisted essentially in the formation of new terrains by collision and obduction; e.g. the emplacement of the Appalachian allochthon, essentially to the south of the Saint-Lawrence River, and the displacement along many normal faults from the Iapetus Ocean (Du Berger *et al.* 1991). Some authors (Thivierge *et al.* 1983; Du Berger *et al.* 1991) argued that the Taconic orogeny did not affect the Saguenay area, as it appears to have been part of a "*stable interior plateau*" at that time, as indicated by the absence of slumping and sediment wedges associated to the walls of the Saguenay graben. However, it was recently indicated that this orogenesis promoted extension in some faults at the SLSJ region (Verreault 2000), due to the flexure of the subducted plate caused by the weight of the obducted portion and the loading of the allochtonous over the

[4] The Acadian and the Alleghanian orogenies have a strong dextral strike-slip component, representing brittle non-co-axial deformations.

autochtonous plate. Low angle (10°- 40°) faults are assumed to be formed in the collisional front, while the overweight would have reactivated higher angle faults (~60°).

The Acadian orogeny corresponds to the closing of the Iapetus Ocean, and it was characterized by the collision between Avalonia and Laurentia. The resultant dextral compression, with the main stress field component at 115°, affected the Appalachians (Trudel & Malo 1993). This orientation is parallel to the walls of the Saguenay graben.

The Alleghanian orogeny consisted in the collision between Laurentia-Baltica and Gondwana (Condie 1989; Faure *et al.* 1996). The changes in the orientation of the main stress field component affected major structures in the SLSJ region (Verreault 2000): (1) with σ_1 = NNW-SSE, faults in the Tchitogama and Kenogami Lakes were submitted to compression and dextral movements; (2) with σ_1 = NNE-SSW, the environment was still compressive, though with a sinistral movement; (3) with σ_1 = WNW-ESE, the northern faults were submitted to a sinistral compression, while the southern ones, to a transcurrent environment. All these orientations come from a theoretical study of the stress environment in the Saguenay region that could have been generated by various plate motions through time (Verreault 2000).

It is here suggested that the Saguenay graben was formed between the Acadian and the Alleghanian orogenies, during the Carboniferous, given the compression transformational system that was then installed (Fig. 3.5). Although the normal faults that constitute the northern and southern walls of the graben were already identified, its shear limits were not yet defined. Some possibilities are the shear zone identified by DuBerger *et al.* (1991) and the *en echelon* lineament that defines the contact between the host rock and anorthosite near the Kenogami Lake (Hébert 2004), or even another *en echelon* lineament but in the La Baie area, located to the southeast of the Kenogami uplands, within the SLSJ. This compressional regime is compatible with twisting movements of the graben floor, which could have generated structural basins and saddles.

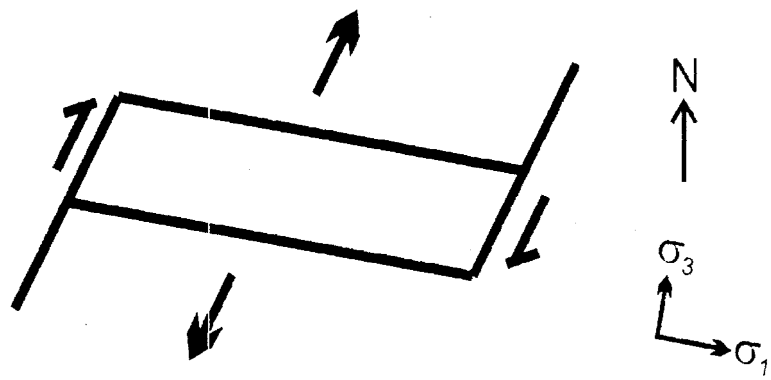

Fig. 3.5 Suggested stress system that would have originated the Saguenay graben during the orogenies in the Carboniferous. The extensional boundaries would correspond to the north and south walls of the graben, while the shear limits were not defined yet.

The fragmentation of Pangea took place between 180 and 60Ma. It started with the opening of the Atlantic Ocean and the formation of great N-S oriented structures, such as the Hudson-Champlain lineament (Roy *et al.* 1998) and the basins of Newark and Connecticut, all in the New York region. The Hudson-Champlain lineament seems to extend to Canada by the Richelieu and Saint-Maurice Rivers, and to the north of the Saint-Jean Lake by a series of segments of large rivers (Fig. 3.3) more or less parallel to the Mistassini River (Roy *et al.* 1998). Thus, it is reasonable to infer that the opening of the Atlantic Ocean probably promoted normal and lateral movements of the Saguenay graben faults (Roy *et al.* 1993, 1998). The influence of the opening of the Atlantic Ocean over the structures of the Saguenay graben has recently been reinforced by apatite fission-track ages obtained in fault zones in the Saguenay region, among other regions in Quebec

(Megan *et al.* 2010; Roden-Tice *et al.* 2011). Initially, the extensional movement was oriented NW-SE, and it probably reactivated the great N-S regional lineaments by sliding (the same orientation as the structures identified in the USA). With the progressive opening of the Atlantic Ocean, the extensional orientation changed to E-W around 140Ma, then reactivating the north and south walls of the Saguenay graben (oriented approximately WNW-ESE) by strike-slip movements. It could have generated a transverse horst within the graben, by one of the structural saddles previously formed, that is, it would have created the uplifted area that is here referred to as Kenogami uplands.

Finally, it has already been indicated that the opening of the Labrador Sea has affected the formation and the pre-existing structures in Canada (Srivastava 1978).

3.4 Local hydrogeology

The main superficial hydrological entities in the study area are the Kenogami Lake and the Saguenay River (Fig. 3.3). The Kenogami Lake is 28km long and 1 to 6km wide. It is locally a hundred meters deep (Walter *et al.* 2010). The Saguenay River is 165km long and around 2km wide. It is up to 275m deep (Walter *et al.* 2010).

Two main types of aquifers are present in the SLSJ region (Fig. 3.6): (1) bedrock aquifers and (2) aquifers constituted of Quaternary granular deposits. The bedrock aquifers are constituted mostly of Precambrian bedrock, overlayed locally and unconformably by remnants of subhorizontal Ordovician limestone units.

The Precambrian bedrock in the region is constituted of crystalline lithologies with very low matrix permeability. The hydrogeological importance of this bedrock is due to the fact that it occurs at the entire region and consequently it accommodates a large proportion of the regional groundwater flow systems (Fig. 3.6). Nonetheless, this bedrock includes a number of higher permeability zones and structures that constitute local aquifers. Bedrock aquifers in the SLSJ region fit in the three types of aquifers present in Precambiran terrains according to Roy *et al.* (2006): (1) along brittle shear zones, (2) in carbonate bands favorable to the formation of karst networks, and (3) in some sedimentary rocks with none or little deformation and not metamorphosed that cover other rocks in discordance. In the latter case, the undeformed sedimentary rocks are Ordovician in age, not Precambrian.

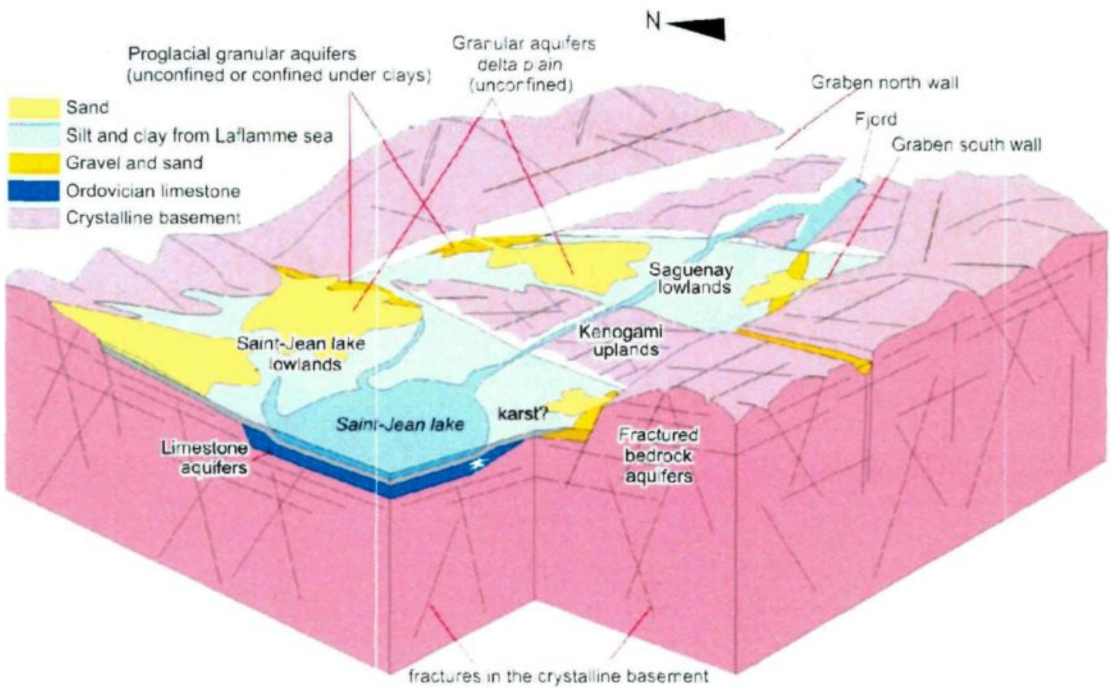

Fig. 3.6 Diagram of the different aquifer types in the Saguenay area. The Kenogami uplands are *constituted of a fractured crystalline rock aquifer.* Adapted from: Rouleau *et al.* (2011).

4

METHODOLOGY

The structural survey involves three main phases, selected after the topics discussed in chapter 2. First, a characterization at the regional scale of the joint system is derived from air photo interpretation, lineament analysis, and a general field survey at selected sites. The latter involves the investigation of the spatial distribution of the main joint sets, completed mostly at sub vertical cuts (247 outcrops), and the study of horizontal outcrops (18 visited, 13 analyzed in detail) in order to identify past stress fields components and joint sets relative ages. The second phase is a detailed structural survey of selected road cuts (18 outcrops) to better define and characterize the main joint sets that constitute the joint system in the study area. In the third phase, geophysical borehole logging is realized in three wells, which provides valuable information at depth, especially regarding subhorizontal joint sets. The first two phases helped answer questions 1 to 3 (identification of joint sets, including at different scales, and their relations with past stress field components) stated as objectives of this study; and the third phase aims at question 4 (possible relationships between joint sets and hydraulic properties). The topics related to these three phases are described below.

4.1 Photo Interpretation and lineament analysis

The interest of analyzing lineaments through aerial photographs and elevation models is that this kind of study provides helpful information to later verify their correlation with the main structural trends, whether related to brittle or ductile structures.

The available digital aerial photos were viewed in stereovision using the software DVP[5]. These photos are from the *Ministère des ressources naturelles et de la Faune* (MRNF), and were taken in 2007[6]. The aim was to select potentially interesting sites for fieldwork and to visualize lineaments at a quasi local scale.

Further lineament analyses were made with the digital elevation model (DEM) of the Kenogami uplands region with the software ArcGIS[7]. The scales selected for the analyses were 1:20.000 (DEM's scale) and 1:1.000, in order to obtain both regional and local observations. The analyses were concentrated within the public intramunicipal territories (TPI – *territoire publique intramunicipal*), as those areas could more easily allow further work such as borehole drilling. However, no holes were made in these areas in the scope of this project, because: (1) fieldwork did not reveal more intense fracturing near identified lineaments, although the latter correspond to geomorphological features; (2) the verification in the field of all the lineaments identified with the DEM would take a longer campaign than the one planned for this project.

---

[5] Groupe Alta. (2007). *DVP version 7 (version 7.2.0.2).*

[6] The photos used are from the following flight lines, performed on the respective days: Q07100, May 19th 2007; Q07101, May 22nd 2007; Q07103, June 7th 2007. All flight lines are from the MRNF.

[7] ESRI. (2008). *ArcGIS 9 (ArcMap version 9.3).*

4.2 Fieldwork

4.2.1 General survey

In the general survey phase, large outcrops are identified (Fig. 4.1a to d) and first submitted to a general description and a limited number of measurements (Appendices 2 and 3). The location and the lithology are described at each visited outcrop; then the most important structures are measured, such as joints (Fig. 4.1d), faults (Fig.4.1i), foliation, dykes, veins and shear zones (Fig. 4.1e). A total of 265 outcrops were visited during the 2010 and 2011 fieldwork campaigns (total of 3 months) in the Kenogami uplands; these are mostly subvertical road cuts (Fig. 4.1a, d to f) and some quarries (Fig. 4.1b, c, g to i), with a limited number of horizontal exposures (Fig. 4.1h). Whenever possible, at least four measurements were taken for each joint set in the same outcrop. A total of 1217 joints were measured during the general survey. Other discontinuities measured in this phase include: 9 dykes, 12 veins, 5 foliation orientations, 14 striae, 4 shear zones and 28 faults.

A few days were dedicated to survey by boat along the shores of the Saguenay River (22 outcrops) and of the Kenogami Lake (25 outcrops) (Fig. 4.1l, m). The landing difficulty and the boat motions at most shore outcrops resulted in a reduced number of measurements for each joint set.

<u>Analysis of the relative ages of joint sets and tectonic events</u>

Thirteen horizontal outcrops were visited in order to observe joint patterns that could provide information on the relative age among the observed discontinuities. This survey was led by Dr. A. J. Fernandes, from the Geological Institute of São Paulo (IG), Brazil. This detailed study consists in the analysis of the interactions between the joints, by

Fig. 4.1 Photos of selected outcrops visited; their identification numbers are indicated, as well as the municipality where they are located. (CONTINUES)

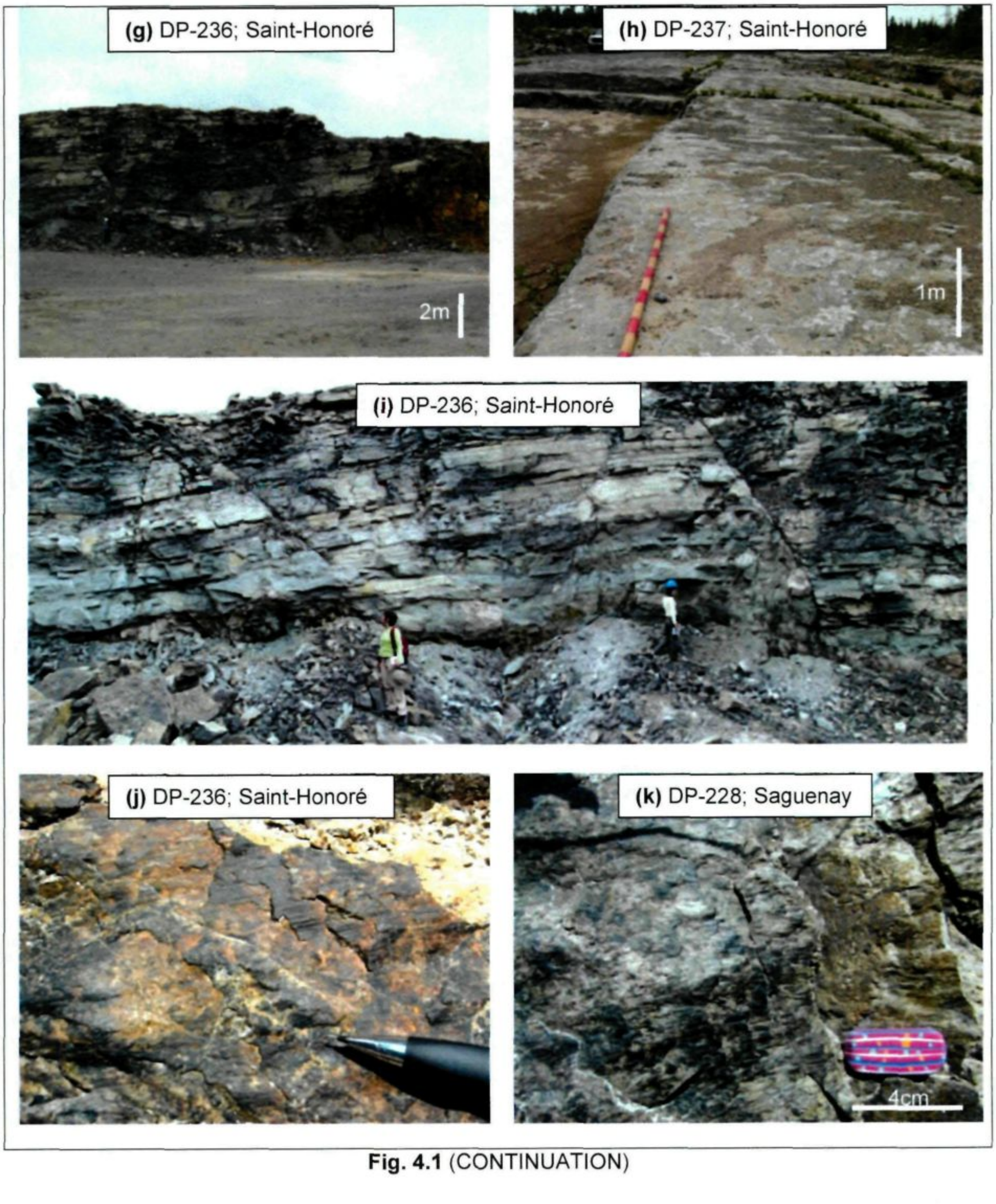

Fig. 4.1 (CONTINUATION)

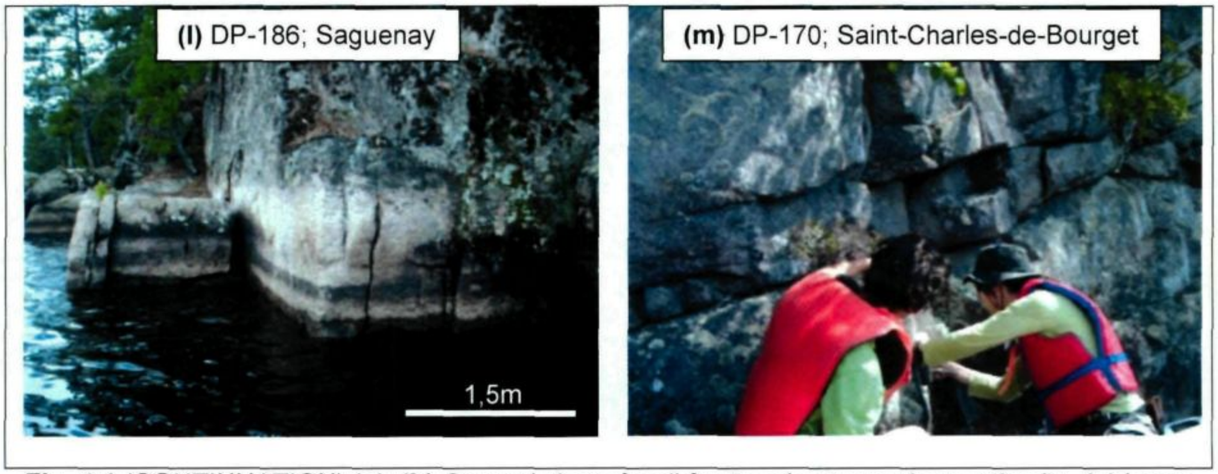

Fig. 4.1 (CONTINUATION) **(a)**, **(b)** General view of well fractured outcrops in anorthosite. **(c)** Large joint oriented E-S, dipping N in anorthosite. **(d)** ENE-WSW to ESE-WNW set of joints is clear along a roadcut, despite the bias introduced by the measurement face orientation (E-W). Outcrop in anorthosite. **(e)** Shear zone in anorthosite. **(f)** Intensely fractured zone of a few tens of meters in anorthosite; less intense fracturing is also observed on the same outcrop. It might indicate a shear zone. **(g)** Contact between an Ordovician unit (limestone) and the Pre-Cambrian basement (granitic rocks). **(h)** Orthogonal fracture pattern in limestone. **(i)** Normal faults in the limestone. **(j)** Steps and striae dipping to SW that indicate the movement of a normal fault in a granitoïd. **(k)** Dark aphanitic rock with a vitreous aspect observed on a supposed fault wall in anorthosite. This material could be formed by fault gouge. The clear steps observed in this aphanitic rock strongly suggest that it is really a fault wall. **(l)** Outcrops of granite on the shores of the Kenogami Lake and **(m)** on the Saguenay River. Photos: (h) D. S. Pino and A. J. Fernandes; (m) M. Chabot; (others) D. S. Pino.

considering the types of termination and the dominancy of a certain joint set, which yield information on the relative ages between the observed sets (Pollard and Aydin 1988, Rives *et al.* 1994, Fernandes 2008).

This information is important because it helps to understand the sequence of tectonic events that generated the joint systems in the fractured aquifer. Identifying the most recent tectonic event is particularly relevant as it is likely the most significant in controlling joint aperture, which plays a major role regarding groundwater flow (Fernandes & Rudolph 2001; Fernandes 2008; Zeeb *et al.* 2010).

Make drawings of sub-horizontal outcrop is a key step of the procedure, which is described hereafter.

1) Take a general look at the outcrop, determining the most representative features and the area to be drawn. In order to properly draw the joint system, it is important to realistically represent their angular relationships. For large or discontinuous outcrops, it is recommended to make more than one drawing.

2) For each of the most important joint sets, start drawing the most remarkable ones. While doing so, pay attention to details that help to understand the interactions between the joints, such as angles between them and terminations. Depending on the size of features, zooms may be needed. Some valuable steps are:

a. Place some markers on the outcrop, (e.g. a hammer, a compass, a knife) that should show up on the drawing. They help to later correlate the photo with the drawing, or to go back to specific points while working in the outcrop.

b. Use a specific type of texture in order to represent materials (e.g. lichen) that obscure the relations between joints, as it is important to report the fact that, at those specific locations, the interactions were not observed.

3) After most of the drawing is done, see if any joint pattern emerges (e.g. *en echelon*, conjugate joints, etc.). Also verify whether the drawing is truly representative of what has been observed in the outcrop.

4) Take photographs of the drafted area with the markers still on it. It is recommended that the photographs are taken perpendicularly to the outcrop face, i. e. looking straight

downward in most cases, and that they are all taken at about the same height, so the observed angles between the joints are more accurate. This also allows further inference of joint spacing of vertical joints. When more than one photograph is needed for the same drawing, showing two markers on every photo also helps to correlate them later and construct back the whole picture.

5) Measure the strike and dip (when the joint is subvertical, measuring only the direction of its trace is reasonable) of all joints and indicate the values in the drawing. Another option is to give a sequential number to each joint and record on a separate data sheet the measurements and observations about each joint.

Examples of results of the procedure described are found in Fernandes *et al.* (2011; 2012).

4.2.2 Geophysical logging

Geophysical loggings provide subsurface data, which are extremely useful complements to the surface information obtained on rock exposures. Geophysical logging was carried out in three wells located in private properties in the study area (Fig. 3.4). This work was conducted by a U. S. Geological Survey (USGS) team, led by R. H. Morin.

Five probes were used in each well (Table 4.1): caliper, multifunctional probe (natural gamma, rock and water resistivity, fluid temperature), acoustic televiewer (ATV), sonic probe and flowmeter. Among these tools, the ATV is the most interesting for structural surveys, as its resulting image is oriented and provides the direction and dip of the identified joints and their location along the borehole (Table 4.1).

Regarding the three wells that were logged, the ATV allowed the identification of a total of 352 joints on 380m of borehole.

Table 4.1 Probes used for geophysical logging in this project.

Probe		Feature measured	Purpose
Caliper		Well diameter	Evaluate the quality of other loggings (tool coupling); Identify zones of weak and fractured rock[a].
Multifunctional	Natural gamma	Natural gamma rays in the rock mass surrounding the borehole	Lithology identification[a]; Stratigraphic correlation among wells[a].
	Rock resistivity	Rock electrical resistivity	
	Water resistivity	Water electrical resistivity	Locate zones of fluid exchange between the borehole and the formation[a].
	Fluid temperature	Fluid (usually water) temperature	
Acoustic televiewer (ATV)		Transit time of an acoustic wave sent by the probe	Locate joints in depth[a, b]; Measurement of orientation and dip at depth of identified joints by means of a proper software[a, c].
Sonic		Transit time of a sonic wave sent by the probe	A proper software[c] provides: the elasticity and shear modulus, Poisson's coefficient and Young's module.
Flowmeter		Water flow	Contribution of each joint to the water flow into the borehole.

[a] Morin *et al.* (1997).
[b] Morin *et al.* (2007).
[c] The software WellCAD 4.2[8] was provided by R. H. Morin (USGS).

4.2.1 Detailed survey

Detailed survey for characterizing joints sets

Two methods were tested to carry out the detailed structural survey: scanline and window sampling (Rouleau & Gale 1985; Priest 1993). In the preliminary fieldwork, three outcrops were tested with scanline, and one with window sampling. The most appropriate outcrops for both methods are clean, approximately planar rock faces that are large regarding the size and spacing of the exposed discontinuities (Priest 1993). Those rock

[8] ALT – Advanced Logic Technology. (2007). *WellCAD version 4.2.*

exposures can be found on beach cliffs, gorges, road cuts, quarries and open pit mines. It is also important that the work place is safe; e.g. with no falling blocks. In the study area, the best available outcrops are located on road cuts and in quarries.

On a scanline survey, all the features that intercept the measuring tape laid on the outcrop are recorded (Fig. 4.2; Appendix 2). The measuring lines tested were about 100m long. In window sampling, on the other hand, area-based measurements are made, that is, all joints with a portion of their trace within a defined area ("window") of the rock face are measured (Fig. 4.3; Appendix 2; Priest 1993). In this study, windows were made of $1x1m^2$ cells, which were disposed in two rows, one above the other, along 30m of the test outcrop, which was a vertical road cut.

Window sampling allows a better assessment of the joint pattern and of their distribution in the outcrop, as all features larger than a specified minimum size are measured. They also contribute to identify the distribution of the visible joint length for each major joint set. This approach could be more interesting in the case of a characterization study of an underground mine gallery. On the other hand, scanline sampling provides direct estimate

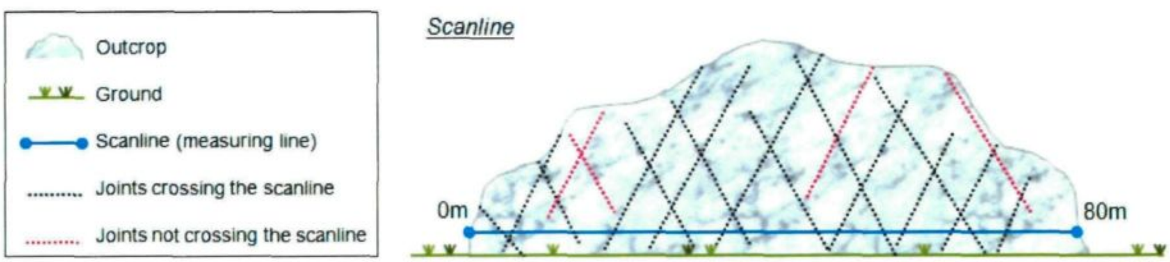

Fig. 4.2 Scheme for scanline method. Only the discontinuities (in black) that cross the scanline (in blue) are measured. The distance at which a discontinuity intercepts the line is always noted (in this example, from 0 to 80m).

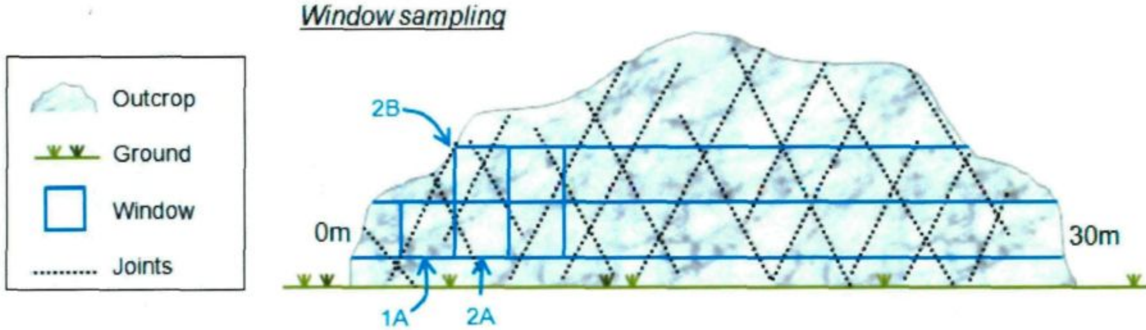

Fig. 4.3 Scheme for window sampling method. All joints are measured within each window cell (e.g. 1A, 2A, 2B, etc), and it should be noted whether the same joint appears in more than one cell. Panoramic photographs (Appendix 4) may be helpful for locating properly the measured joints. This approach works better in smaller outcrops.

of joint spacing and density, these parameters being required in a number of further analysis procedures.

A total of 18 scanlines were made, with lengths varying from 10 to 150m, according to the size of the available outcrops in the study area. They were divided in two orientation groups: E-W (approximately the main orientation of outcrops in the Kenogami uplands) and N-S. The analysis of perpendicular outcrops provides more complete information on the joint system by sampling a wider range of joint orientations. On a total of 888m of scanlines, 1111 joints and 6 veins were measured.

4.3 Processing structural data

4.3.1 Interaction between joints

A second step in the study of the interactions between joints is to analyze the data obtained in the field, comparing the photographs taken, the drawings made and the joint orientations data, in order to define the joint sets and identify the orientation of the horizontal components of the stress field that generated them. It is assumed here that the orientation of σ_1 is the bisectrix of the acute angle between two conjugate joint sets[9]. The drawings may be first analyzed individually, although it is essential to compare drawings from different sites in order to verify if a certain pattern is only local or if it appears at different sites.

Joint patterns also provide valuable information regarding the relative chronology of joints generation (Fig. 4.4; Pollard & Aydin 1988). The most continuous joints tend to be the oldest, while the smaller ones and those that abut on another joint are the youngest (Dunne & Hancock 1994). On the other hand, alternating abutting relationships between joint sets indicates they were formed by the same tectonic event. The sense of shear

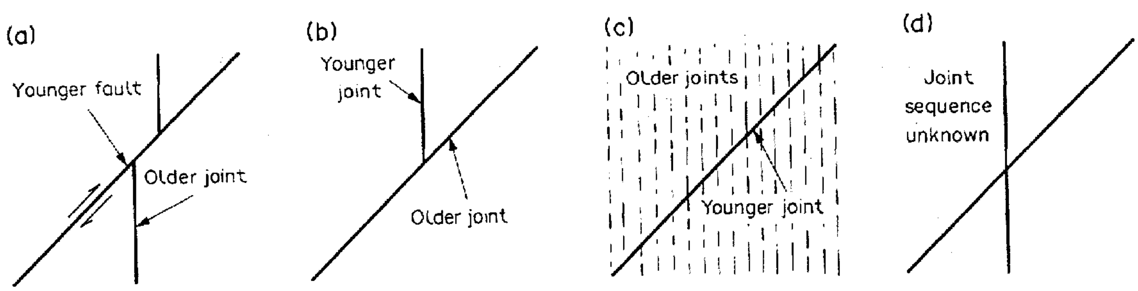

Fig. 4.4 Interactions between joint sets. **(a)** Older joint displaced by a younger one. **(b)** Younger joint abuts in the older one. **(c)** Small older joints are sealed (filled) and cut by a longer and younger joint. **(d)** Two joint sets crossing each other, no formation order can be inferred from this interaction alone. Source: Dunne & Hancock (1994).

---

[9] In a brittle co-axial deformation, the theoritical acute angle between two conjugate joints is 60° for a homogeneous and isotropic material. As a real rock is neither, the acute angle may vary by ± 10° or 15°. Usually, acute angles smaller than 45° suggest non-co-axial deformation, leading to a Riedel fracture pattern where acute angles range between 10° and 20°. Pre-existing planar fractures or weaknesses such as rock banding, foliation and schistosity may also affect the angle between the stress and the fracture.

displacement across the older joint set can also be useful (Fig. 4.4a; Pollard and Aydin 1988; Dunne and Hancock 1994).

4.3.2 Stereoplots

All data collected in the field were initially compiled in Microsoft® Excel 2007 sheets, later being transferred into Microsoft® Access files in the PACES-SLSJ database. Orientation data were processed with Stereo32 (Röller & Trepmann 2008), which allows to construct stereograms, rose diagrams and pole density diagrams. The selected plots use equal area projection in the lower hemisphere. This type of projection is amenable to statistical investigation, particularly pole density analysis (Terzaghi 1965). Other statistical analyses were done with Microsoft® Excel 2007. The density diagrams, along with the identified lineament trends and densities, helped to determine structural domains regarding the homogeneity of the joint system.

4.3.3 Correcting for orientation bias

Various sources of error may affect the characterization of joint systems, at the sampling, the measurement or the estimation phases of a survey. The orientation bias in particular may result in unreliable estimate of the relative abundance of joint sets in the study area (Terzaghi 1965; Rouleau & Gale 1985).

Orientation related errors may be reduced by making observations on a number of appropriately and differently oriented boreholes and/or rock faces. The orientation errors may also be reduced by corrections based on the solid angle α between the joint set and the observation line or the window plane (Terzaghi 1965). Indeed, a sampling bias is introduced in any joint survey by the solid angle α being usually different from 90°, that is, joints making a small angle (e.g. $\alpha < 20°$) with the rock face have fewer chances to be observed than those making a high angle (e. g. $\alpha \sim 90°$).

The basic principles of Terzaghi's correction are here adapted to perform the correction with a computer, accelerating the process. This approach was applied to the data obtained from scanlines and ATV logging (vertical scanline). The computations involved are presented in Appendix 5; the concepts are discussed in the following. The application of Terzaghi's correction over a window is discussed in Appendix 4.

This method of correcting for orientation bias is particularly interesting because it yields an estimate of the true joint density, as opposed to the frequency of their observation. The corrected data can be combined with estimates of other joint system attributes, such as joint aperture and extent, providing significant information to characterize a joint system. Another usual approach is to plot density diagrams of the observed and the corrected data, in order to visualize the effects of the corrections that have been applied.

Other discussions on the application of Terzaghi's method may be found in the work by Mauldon & Mauldon (1997), who analyze one joint of a particular size at a time. In this approach, joints are assumed to be of a finite and known size, and of circular shape. The correction is proposed for two cases (Mauldon & Mauldon 1997): sampling joints over a borehole and over tunnel surfaces. It is indicated that, regarding the joint size, the orientation bias increases as the size of the borehole decreases, that is, the orientation bias is most pronounced for boreholes with radius equal to zero.

Correction over a scanline

The computadorized procedure for Terzaghi's correction over a scanline presented in this work was developed at UQAC, at the *Centre d'études sur les resources minerales* (CERM), under the direction of Dr. D. W. Roy.

First, the angle α between each joint plane and the scanline is calculated using direction cosines. Then, a weight equal to $1/\sin\alpha$ is attributed to each observed joint. This weight indicates how many joints of a certain orientation should be observed along a virtual scanline of the same length as the one used in the survey, but normal to the plane of the joint (see section 4.3.3).

A blind zone of ±20° is drawn around the scanline and indicated in the stereoplot, because the estimate of true joint spacing plotted in that zone becomes increasingly inaccurate (Terzaghi 1965). For the joints in that "blind zone", a new weight equal to zero is attributed, while for the others it is kept at the value $1/\sin\alpha$. By dividing the new estimate of the number of joints, accounting for the weight, by the scanline length, one obtains an estimate of the average true joint density, while the inverse number gives their true spacing.

Because most commercial softwares for plotting a Schmidt stereonet do not consider weighted numbers of joints, each observation is plotted 10 times the value of its weight rounded to the nearest integer. This yields a total number of points in the stereoplot equal to about 10 times the sum of the weights, though the density plot still reflects the corrected density distribution of joints within the rock mass.

With the corrected density plot, it is usually possible to identify one or more pole concentrations that indicate the most important joint sets in the analyzed outcrop. An average pole is then determined for each joint set, and the average poles are used to characterize the type of joint spacing (see section 4.4.3) and to define the unit block (see section 4.4.4).

A complete survey of the joint system at a site requires at least three non parallel scanlines[10] selected in order to cover all possible joint orientations outside of their overlapping blind zones – the angles between these scanlines should be higher than 50°. The observations from each scanline can be combined in the same stereoplot after applying two additional factors to the weights previously computed in order to correct for the bias of each individual scanline. The first factor reduces all the scanlines to the same arbitrary "standard length" (e.g. to 20m); this factor is equal to the standard length divided by the length of the scanline of the considered observation. The second factor is applied for each joint weight; for a given joint, it is equal to the inverse of the number of scanlines for which that joint orientation is outside of the blind zone. The resulting stereoplot gives the distribution of joint densities in a cubic volume with the size of the selected "standard length" and containing a number of joints equal to the sum of the corrected weights. The scanlines grouped this way define a station; several stations are used in the definition of the unit block.

4.3.4 Joint distribution analysis

From Terzaghi's correction, it is possible to analyze the distribution pattern of the joint sets in an outcrop. Only one joint set must be considered at a time; e. g. the set represented by pole P1 (see Appendix 5 for how poles are named) at a given outcrop.

First, a line A is drawn (Fig. 4.5) parallel to the main orientation of the joint pole (e.g. pole P1); its length is that of the scanline on a given outcrop times $\sin\alpha$. A virtual position of the joints along line A can be determined accordingly. A corrected distance diagram is plotted using the virtual position values of the joints on line A. This provides information on

[10] Regarding Terzaghi's correction, the window sampling provides 2D information instead of the 1D from the scanline, that is, a minimum of 2 windows are required for a station, alternatively to the scanlines.

the type of spacing distribution, which may be: (1) random, (2) regular, (3) regularly variable or (4) regularly concentrated (Fig. 4.6).

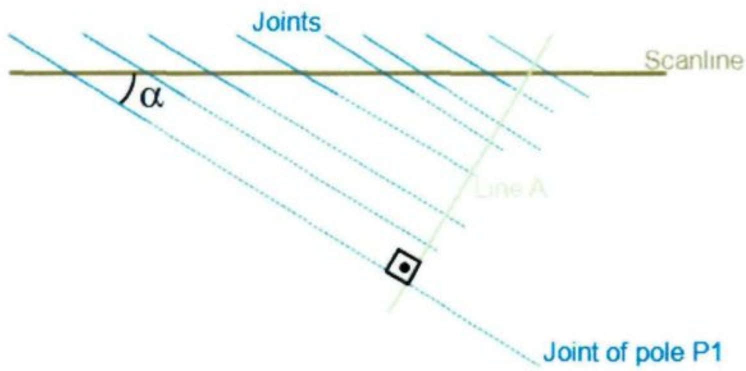

Fig. 4.5 Sketch showing the projection of the position of joints observed on the scanline to a projection line A which is parallel to pole P1 obtained with Terzaghi's correction applied to the measurements done over a scanline. The angle α is calculated by direction cosine. Line A is parallel to the pole P1 and is used to describe the spacing of the considered joint set (virtual position on the corrected distance). This procedure is applied to all poles of joint concentrations.

4.3.5 Unit block

The unit block is defined by the most frequent joint sets (Ruhland 1973), which can be determined by joint density. This requires the definition of at least three main joint sets. The elongation of the block is parallel to the set with the highest density. Common forms include bricks, prisms and plates; the unit block may further be truncated by less frequent joint sets.

The concept of unit block has been proposed in the oil industry (e.g. Ghez & Janot

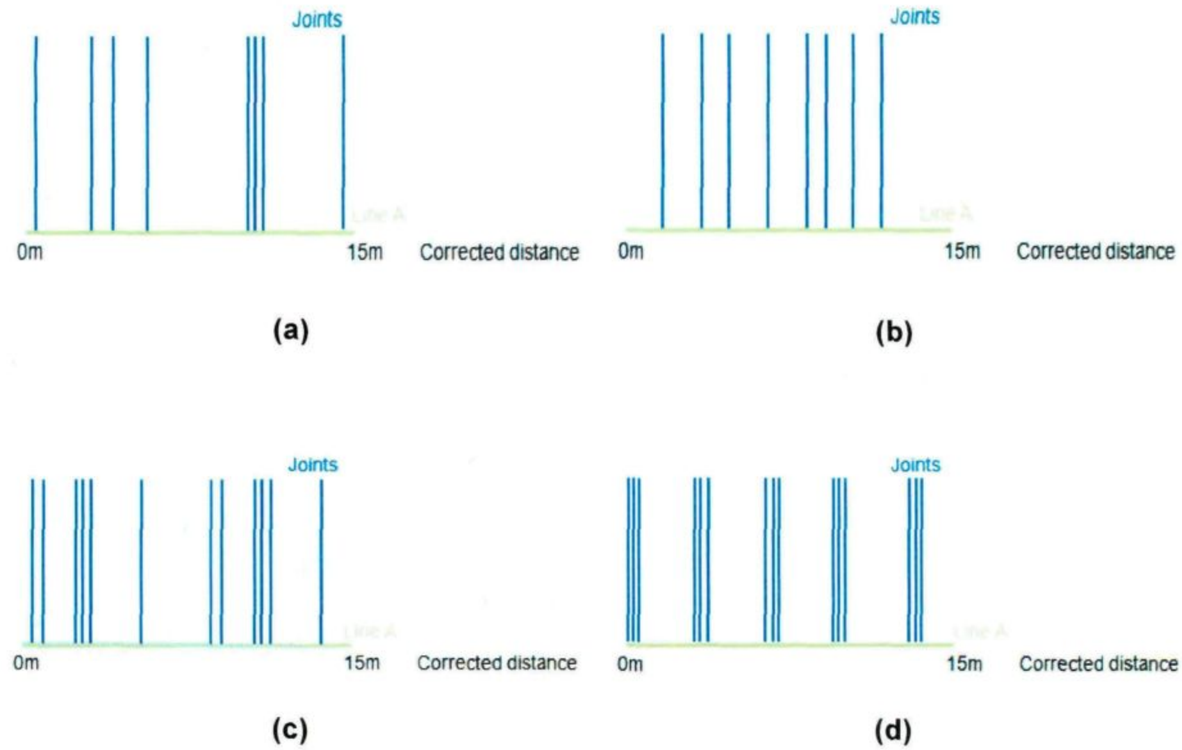

Fig. 4.6 Possible configurations of the corrected distance diagram for pole P1 represented on Fig. 4.4. The joints from this pole may present: **(a)** random, **(b)** regular, **(c)** regularly variable or **(d)** regularly concentrated spacing distribution.

1974), as it represents the basic joint network and may provide information regarding the rock mass behavior and hydraulic properties, e.g. its permeability (Rives *et al.* 1992). In the study of fractured rock aquifers, the joint system and the hydraulic properties of the media are equally important; hence, using the concept of unit block for the structural characterization of this type of aquifers is as well valuable and useful.

Knowledge of the size and shape of the unit block allows the determination of the wet surface per unit volume of rock, which corresponds to the ratio between the total area of fractured surface within the unit block area and its volume. It is also possible to estimate the water volume around the unit block, once a value of joint aperture is assumed or, conversely, of average aperture if the storage capacity of the fractured aquifer is known. Information on recharge or other hydrogeologic factors may still be combined with the previous data in order to evaluate the water flow through the joint system.

4.4 Defining a conceptual model

Finally, the results of these analyses shall provide the basis to define a conceptual model for the bedrock aquifer in the study area. It shall contain information on the following aspects: joint systems, particularly the orientation and density of the main sets; hydrogeological properties related to different lithologies and/or joint systems; the influence of the recent stress fields over the hydrogeological properties.

5

RESULTS

This chapter presents the results obtained by analyzing the data from the general and detailed surveys and from the borehole geophysical logging. First, the results regarding the main joint sets in the study area are presented, combining information from the general survey and the geophysical logging to characterize the joint system of the Kenogami uplands. Second, results from the application of Terzaghi's correction over scanlines and logging data are introduced, as well as the unit block determined for the Kenogami uplands. Finally, data on the interaction between joints are shown.

5.1 Main joint sets

The general survey data for structural characterization of the whole area of the Kenogami uplands is summarized by a histogram of the orientation of the subvertical observation faces (Fig. 5.1), and by a density diagram of the orientation of the poles of the joints observed in these outcrops (Fig. 5.2).

The distribution of outcrop face orientations shows two modes (Fig. 5.1): the main one, at about 120° (ranging between 80° and 130°), is roughly parallel to the axis of the Saguenay graben, while the other one is at about 170° (ranging between 165° and 10°). The low points of the distribution are at 30° and 160°.

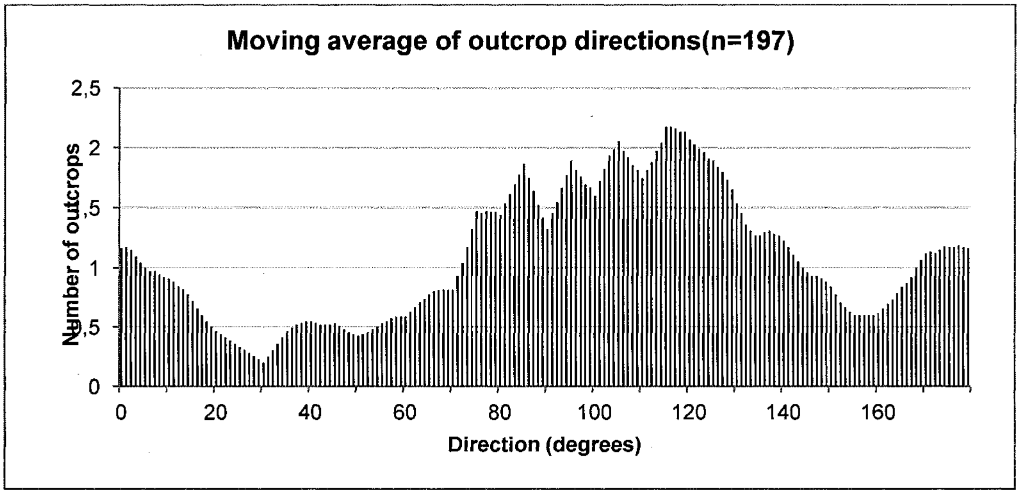

Fig. 5.1 Distribution of outcrop directions. Central moving average (step of 1°) of the number of outcrops with a given direction within a 15° range of directions at each step. Directions of outcrop faces all transformed to 0 to 179°. Ranges of directions below 8° and above 172° are completed by the opposite end of the direction scale.

The density diagram of joint poles (Fig. 5.2) shows five joint sets (A to E; Table 5.1), of which four are subvertical and one is subhorizontal. These five concentrations are all well distributed across the Kenogami uplands; in many of the visited outcrops, up to three of these sets are observed. Although the lithology in the Kenogami uplands is considered fairly homogeneous, this feature may be used to analyze the data from the general survey. Interestingly, the same order of importance among the five joint sets is observed even when the joints are considered according to the different lithologies (Fig. 5.3): the NW-SE set (set A) is always the most abundant. The common spatial distribution of the main concentration and their similar occurrence in the various lithologies indicate that the study area can be considered as a single structural domain.

A few outcrops of Ordovician limestone, also located within the Saguenay graben, but to the east of the Kenogami uplands, are included in this study. They exhibit joint concentrations (Fig. 5.3e) very similar to those of the Precambrian crystalline rocks of the Kenogami uplands; regarding subvertical joint sets, the joint trend NW-SE is dominant, followed by the trend NE-SW. It should also be noted that subhorizontal fractures are more abundant in limestone than in the other lithologies.

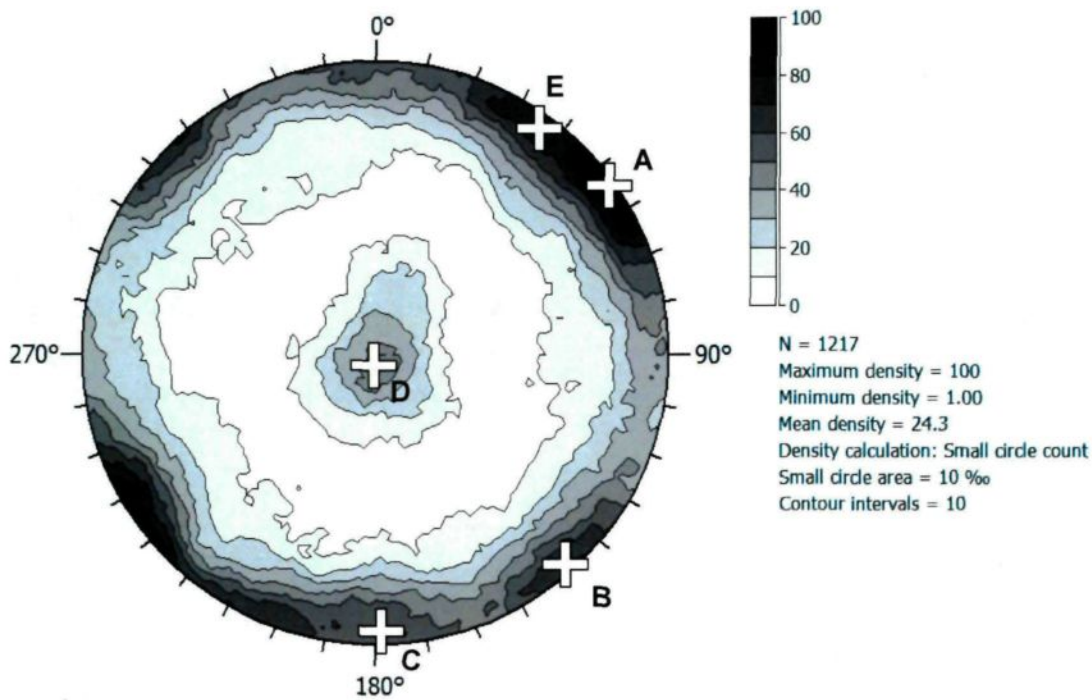

Fig. 5.2 Stereoplot with density contours of the poles of joints measured during the general structural survey; A to E are the main concentrations of joints (see Table 5.1). Equal area projection, lower hemisphere. Software: Stereo 32 (Röller & Trepmann 2008).

Table 5.1 Main concentrations of joints observed during the general structural survey, based on Fig. 5.2.

Joint set	Direction	Dip	General trend
A	144	88	NW-SE
B	229	89	NE-SE
C	288	86	E-W
D	251	03	Hor.
E	126	83	WNW-ESE

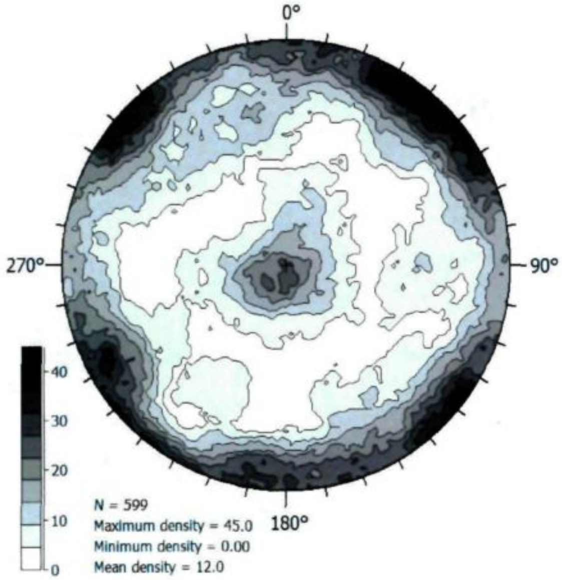

(a) Anorthosite

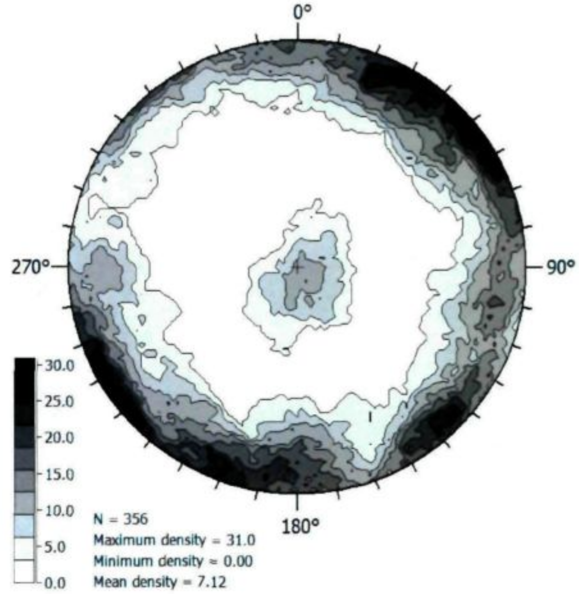

(b) Granites and gneisses

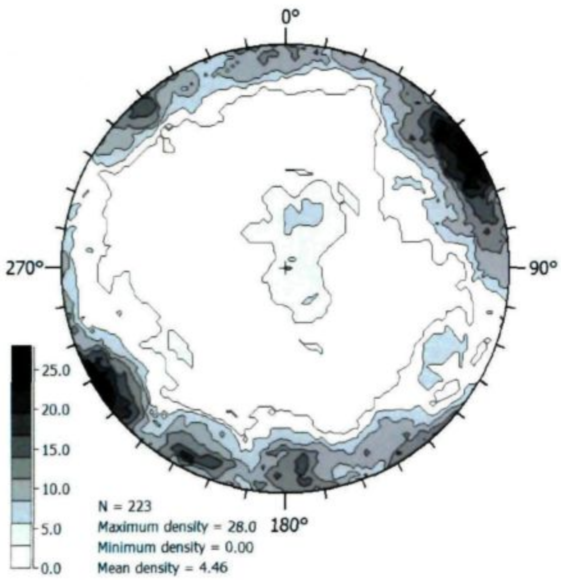

(c) Syenite – monzonite – diorite

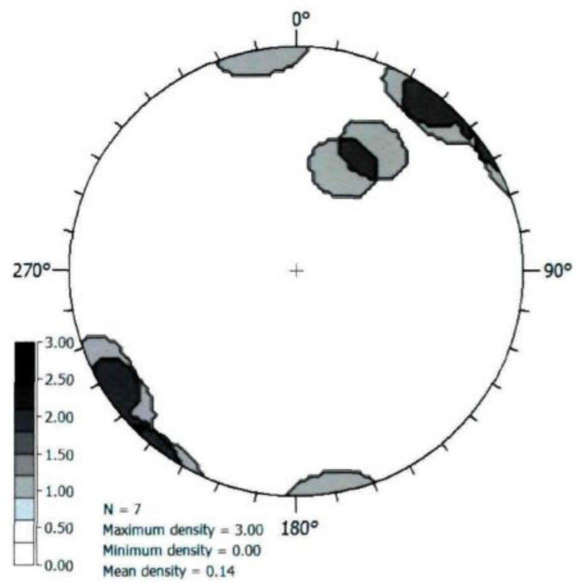

(d) Gabbro

Fig. 5.3 Density diagrams of poles of joints measured during the general structural survey, grouped by lithology. Density calculations by small circle count with area equal to 1%; stereoplots with 10 contour intervals. Equal area projections, lower hemisphere. Software: Stereo 32 (Röller & Trepmann 2008). (CONTINUES)

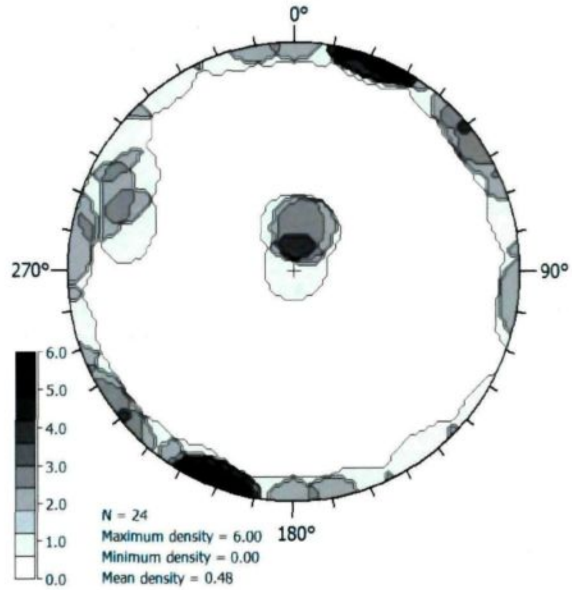

(e) Limestone

Fig. 5.3 (CONTINUATION)

The acoustic televiewer (ATV) logging data from three boreholes provides information on joints at depth (Table 5.2)[11]. The first two boreholes (RM001 and RM004) are located along the western side of the Kenogami uplands, while the third (PZ-S18R) is to the east of it (Fig. 5.4). Rock type interpretations (Table 5.2) were made by J. Roy (IGP, Canada) and R. H. Morin (USGS).

Table 5.2 Vertical boreholes in which the ATV logging was performed.

Well identification	Rock type(s) (from top)	Length (m)	Number of fractures
RM001	Anorthosite**?**	120.40	105
RM004	Granite**?**	111.37	141
PZ-S18R	Limestone	31.59	90
	Sandstone	1.86	2
	Anorthosite	5.57	9

[11] The identifications used for the wells are the same as the one of the Hydrogeological Information System (*Système d'Information Hydrogéologique*, SIH), from the *Ministère du Développement Durable, Environment et Parcs* (MDDEP).

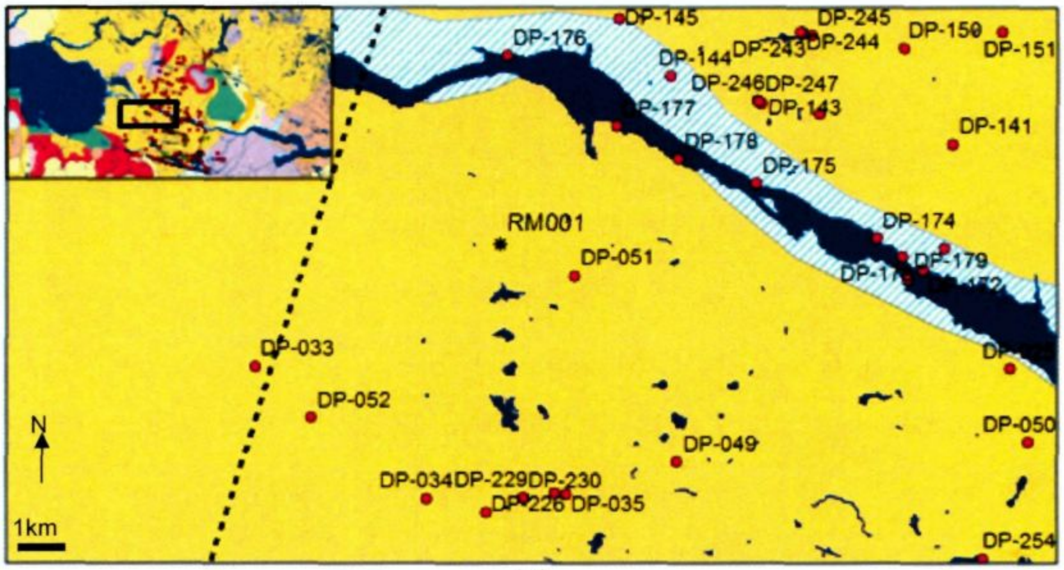

(a)

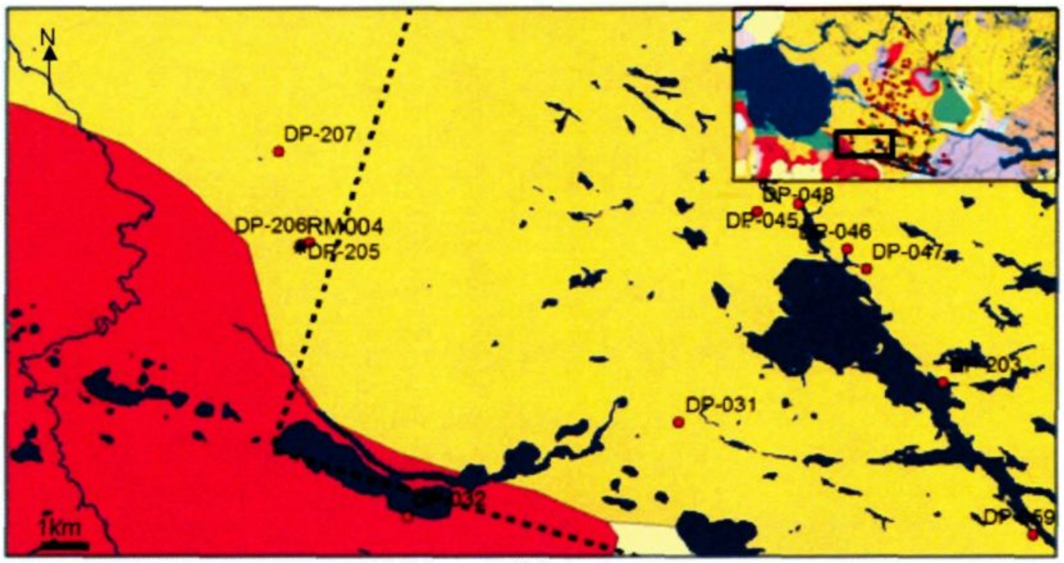

(b)

Fig. 5.4 Location of the logged wells and nearby outcrops: **(a)** RM001, **(b)** RM004 and **(c)** PZ-S18-R. **(a, b, c)** These maps are details from Fig. 3.4, represented as an inset on every map. Black rectangles in the miniature maps show the location of the detailed areas in the study zone. Black stars indicate wells; red dots, visited outcrops; dotted black line is the limit of the Kenogami uplands. Geological map: Avramchev (1993). (CONTINUES)

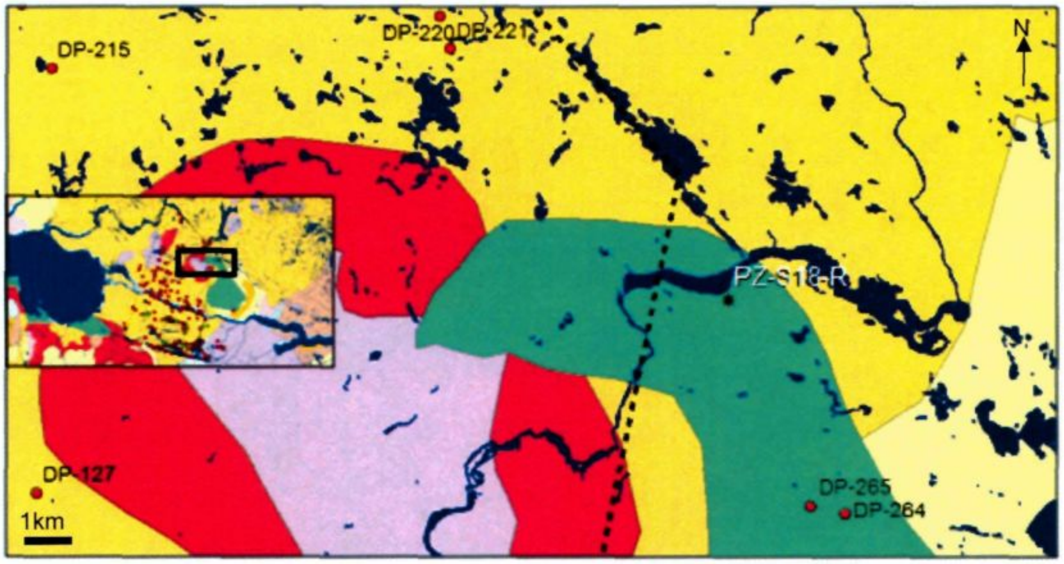

(c)

Fig. 5.4 (CONTINUATION)

The density plots of the joints identified with the ATV (Fig. 5.5) confirm that in vertical boreholes most of the joints observed are subhorizontal; in this case, dipping between 0° and 10°. Some more steeply dipping joints were identified, with dip angles reaching 70° (Fig. 5.5). Particularly in the case of the well PZ-S18-R, high angle dipping joints in the southeast quadrant and oriented around 350° and 095° are concentrated in the anorthosite, while the other joints identified belong to limestone (except for two joints in a thinner layer of sandstone) (Fig. 5.5d). The identification of rock types is based on the lithologic profile made during the construction of this well by members of the PACES-SLSJ team (Appendix 6). Moreover, the orientations of these higher dip angle joints observed at depth are not exactly the same as the ones observed on surface at the nearest outcrops (Fig. 5.6), maybe with the exception of well RM001 and outcrop DP-051 (Figs. 5.5 and

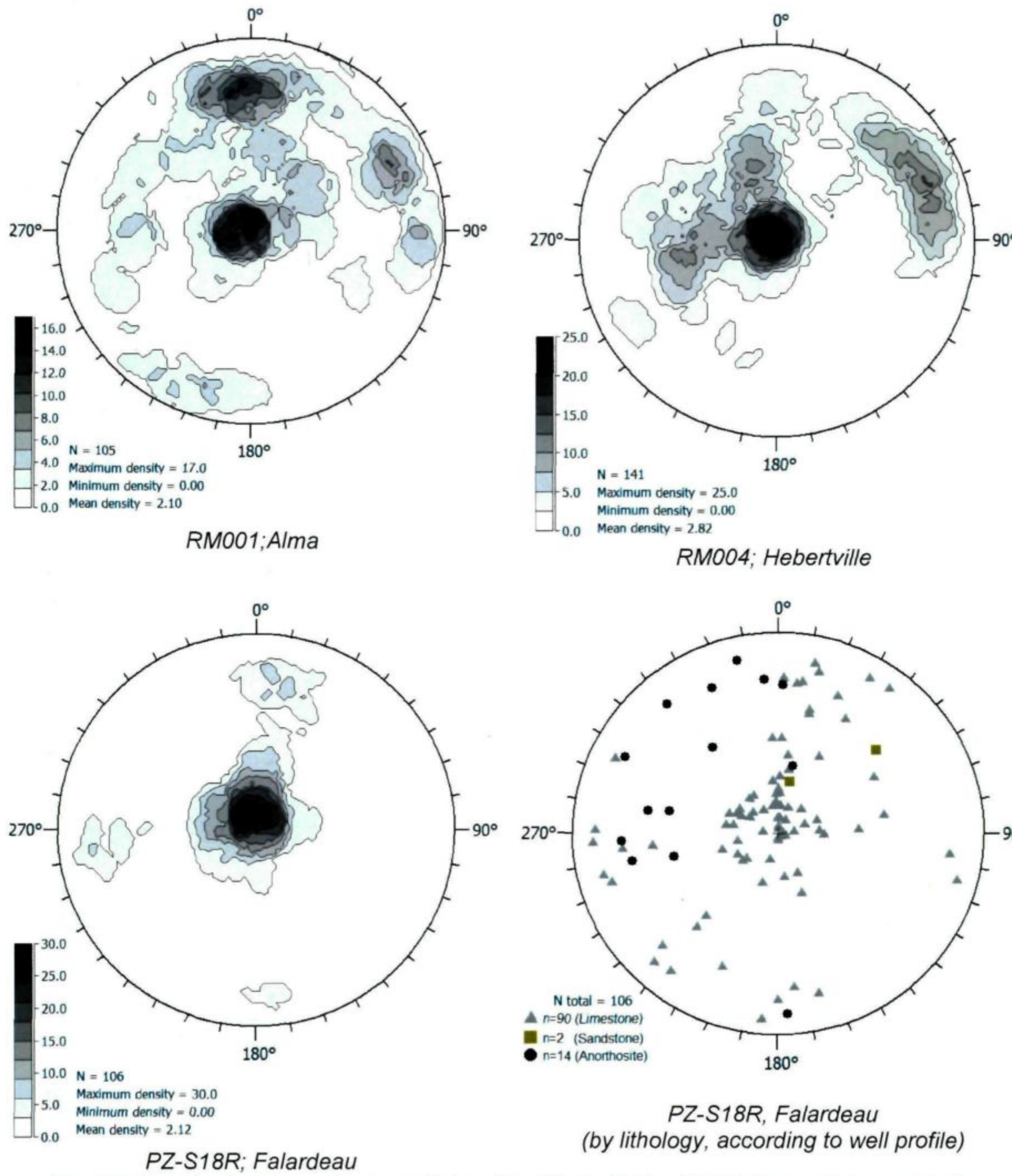

Fig. 5.5 Density diagrams of poles of joints identified with the ATV in the wells logged in the Kenogami uplands. Density calculations by small circle count with areas equal to 1%; stereoplots with 10 contour intervals. Equal area projections, lower hemisphere. Software: Stereo 32 (Röller & Trepmann 2008).

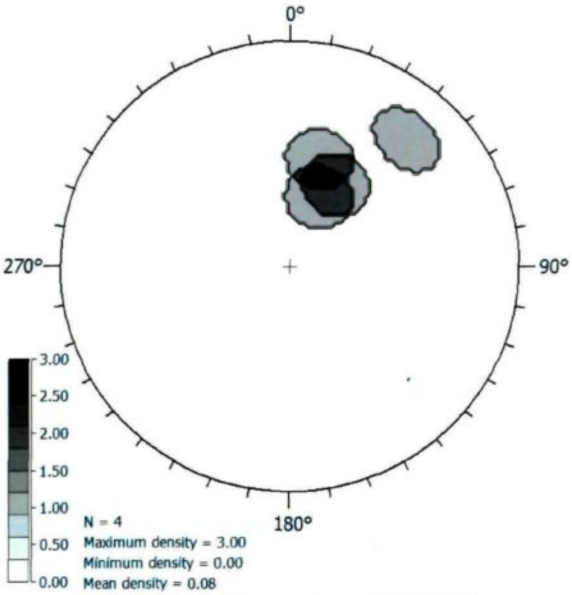

Joint data from outcrop DP-051
Next to well RM001

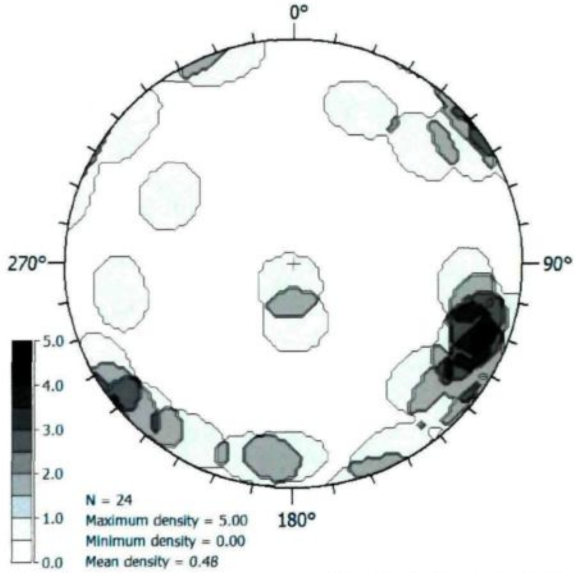

Joint data from outcrops DP-205, DP-206, DP-207
Next to well RM004

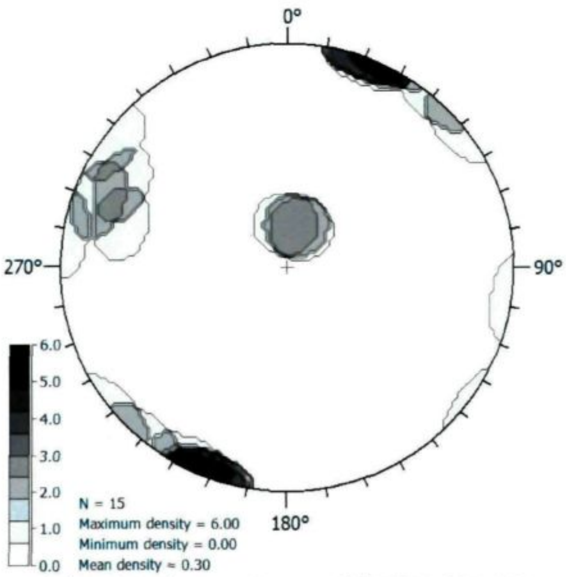

Joint data from outcrops: DP-264, DP-265
Next to well PZ-S18-R

Fig. 5.6 Density diagrams of the joints observed in the nearest outcrops regarding the logged wells (Fig. 5.4). Density calculations by small circle count with areas equal to 1%; stereoplots with 10 contour intervals. Equal area projections, lower hemisphere. Software: Stereo 32 (Röller & Trepmann 2008).

5.6). Distances between wells and outcrops vary approximately from 65m to 4,920m, depending on the outcrop availability in the area of the logged wells (Fig. 5.4).

Finally, regarding the lineaments identified within the public intramunicipal territories, the TPIs (Appendix 7; see also chapter 4), the main orientation is NW-SE, the same orientation as joint set A (Fig. 5.2) in the Kenogami uplands. Another important lineament trend is approximately WNW-ESE, parallel to joint set E (Fig. 5.2) and to the Saguenay graben axis orientation.

5.2 Fault planes and striae

In some fault planes, the presence of steps and striae (Fig. 5.7 and Table 5.3) indicates sense of movement along the faults, which was deduced from the criteria described by Petit (1987).

Faults in anorthosite may be divided in two trends (Table 5.3): NE-SW and NW-SE, both dipping between 60° and 90°. The faults identified in granitoid and in mangerite may also be categorized in these two orientation trends (Table 5.3). Most of the striae were identified in anorthosite (Table 5.3), and they are almost equally distributed between the two fault trends (Fig. 5.7).

The striae on generally steep dipping fault planes have mostly shallow to sub-horizontal plunges, indicating mainly strike-slip motions (Fig. 5.7): striae indicating dextral and sinistral movements are found in both NE-SW and NW-SE fault trends. This suggests the occurrence of two past stress fields or tectonic events. Nonetheless, most striae which did not provide information on sense of fault movement are plunging to SW.

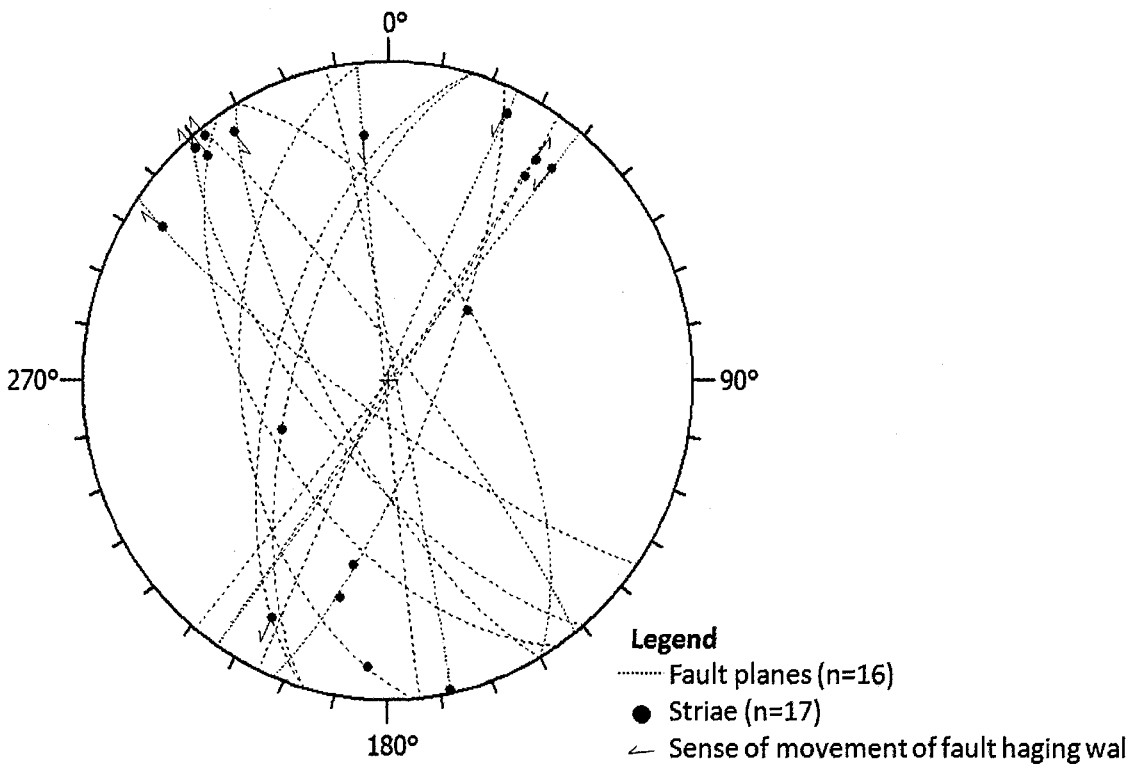

Fig. 5.7 Great circles of faults planes where striae were measured (Table 5.3). Striae and sense of movement regarding the faults' footwalls are also indicated. Equal area projection, lower hemisphere. Software: Stereo 32 (Röller & Trepmann 2008).

5.3 Terzaghi's correction and the unit block

The Terzaghi's correction allows estimating the true density of the various joint sets from their observed abundance along scanlines or within observation "windows". Then, the shape, orientation and dimensions of a representative unit block are derived from these corrected density values and the most frequent orientations over various scanlines. The scanline measurements were performed on 14 selected outcrops along an approximately

Table 5.3 Orientation data of faults and respective identified striae.

Outcrop ID	Lithology	Fault		Stria		
		Direction	*Dip*	*Plunge*	*Plunge quadrant*	*Sense*
DP-228	Anorthosite	140	70	04	NW	Dextral
		146	56	09	NW	Dextral
		125	81	13	NW	Dextral
		174	89	24	NW	Sinistral
		322	84	03	NW	Sinistral
		150	74	08	NW	Sinistral
		348	88	01	SE	N.I.
		205	89	09	NE	Sinistral
		022	77	41	SW	N. I.
				31	SW	N. I.
		034	88	23	NE	N.I.
		034	89	17	NE	Sinistral
		039	89	16	NE	Dextral
DP-233	Mangerite	330	62	62	SE	Sinistral
DP-234	Granitoïde	278	90	N. I.		
		117	77	N. I.		
DP-235	Granitoïde	196	59	18	SW	N. I.
		175	50	11	SW	N. I.
		196	65	59	SW	Sinistral
		180	60	N. I.		
DP-236	Granitoïde (in contact with limestone)	185	58	N. I.		
		029	81	N. I.		
DP-255	Anorthosite	210	85	N. I.		
		189	83	N. I.		
DP-256	Anorthosite	125	46	N. I.		
		219	57	N. I.		
DP-259	Anorthosite	215	82	N. I.		

* N. I.: not identified

E-W profile on the Kenogami uplands (Fig. 3.4), more or less coincident with the road 170, that crosses the study area. Scanline surveys were carried out in four other outcrops[12] near the Kenogami Lake, further to the south. As the latter provided results very similar to the first 14 scanlines (Table 5.4) and a single structural domain was defined in the Kenogami uplands, all of the scanline data were considered together to determine the unit

[12] On outcrops DP-055, DP-059, DP-060 and DP-064.

block. This extrapolation is fairly reasonable, especially considering that the vertical height of the unit block is defined only on ATV measurements on three boreholes located in other parts of the study area than the scanlines (Fig. 3.4).

Table 5.4 Joint pole data obtained by applying Terzaghi's correction to scanline data. These joint orientation values are represented on the density diagram of Fig. 5.9.

Well ID	Trend	Plunge	Average joint spacing (m)
RM001	357	26	25.33
RM001	006	87	5.63
RM004	341	88	361
RM004	057	27	5.01
PZ-S18-R	332	83	3.21
PZ-S18R	007	32	3.92
PZ-S18-R	269	33	6.31
Outcrop ID	**Trend**	**Plunge**	**Average joint spacing (m)**
DP-040	226	37	1.59
DP-040	333	05	3.09
DP-040	012	10	4.52
DP-055	067	03	0.52
DP-055	336	09	1.50
DP-059	183	03	1.00
DP-059	070	01	0.95
DP-060	281	03	1.04
DP-060	133	08	1.19
DP-060	043	06	2.91
DP-064	058	06	0.27
DP-064	153	05	1.06
DP-068	263	10	2.07
DP-068	309	05	2.19
DP-069	316	11	1.61

Outcrop ID	Trend	Plunge	Average joint spacing (m)
DP-156_f1	027	23	16.72
DP-156_f1	055	03	5.46
DP-156_f2	347	04	0.78
DP-156_f2	342	30	1.27
DP-156_f2	059	07	1.48
DP-156_f2	101	10	2.31
DP-157	042	02	2.12
DP-157	142	03	1.17
DP-209	008	04	1.45
DP-222	321	05	0.71
DP-222	029	11	1.70
DP-223	044	14	1.77
DP-223	306	01	4.99
DP-225	294	31	1.85
DP-225	065	44	1.91
DP-226	137	05	0.71
DP-226	025	02	1.80
DP-226	102	58	1.85
DP-226	278	57	2.42
DP-229	161	02	2.25
DP-229	208	15	1.08
DP-230	231	42	0.41
DP-230	178	02	0.78

The comparison of a density diagram of the observed data on a scanline with the diagram of the corrected data (Fig. 5.8) illustrates the importance of such analysis in order to correct the information biased by the angle between each measured joint and the scanline.

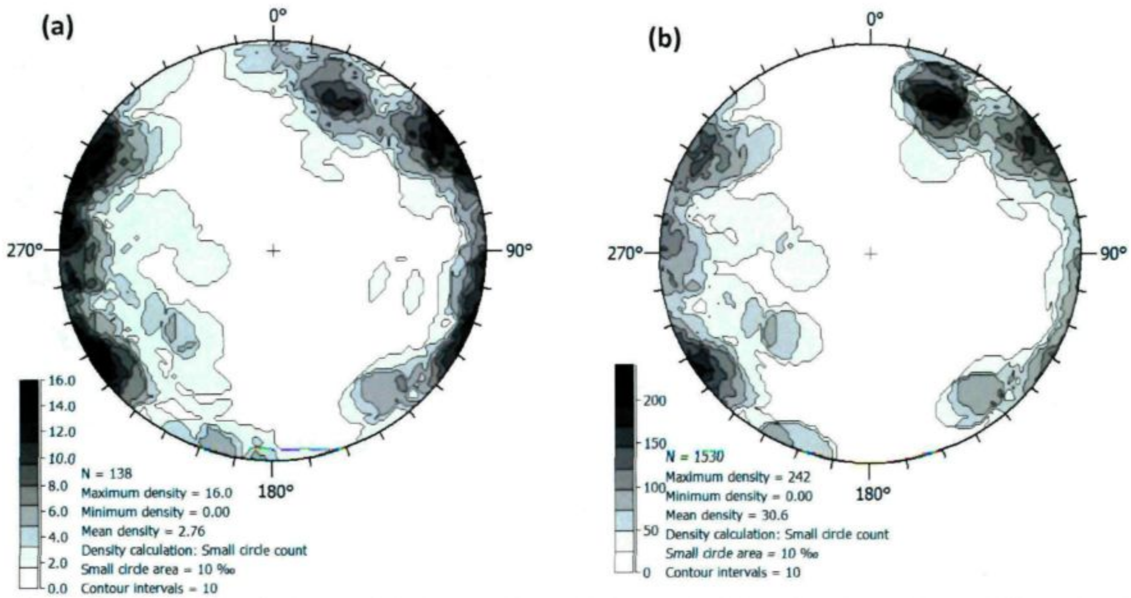

Fig. 5.8 Comparison between **(a)** observed and **(b)** corrected (application of Terzaghi's method) density diagrams of scanline data at outcrop DP-156_face1 (scanline: 086/00). Number of points of corrected values is by ten times that of their weight (see section 4.3.2). Equal area projections, lower hemisphere. Software: Stereo 32 (Röller & Trepmann 2008).

The pole orientation and true spacing data were obtained by applying Terzaghi's correction to all scanline and ATV logging data, and are summarised on Fig. 5.9 and listed on Table 5.4. The four main joint sets observed on Fig. 5.9 and listed on Table 5.5 are used to develop the unit block for the Kenogami uplands (Fig. 5.10). It is defined by the 4 main joint sets (Table 5.5) and it may be often segmented by other sets (smaller pole concentrations on Fig.5.9). Its size is based on the second spacing mode from Table 5.5. The edges from the hexagon that constitutes the base of the unit block Fig. 5.10 are calculated using the law of sines[13]. The values obtained are: 1.55m (edge from set 044/88), 1.36m (edge from set 139/84) and 0.19m (edge from set 095/86).

The spacing of joints that are part of the same set defined by a given corrected pole may be analyzed as discussed at section 4.3.3. As previously mentioned, the joints from a same set may be distributed: (1) randomly, (2) regularly spaced, (3) regularly variable spacing or (4) regularly concentrated (Fig. 4.5).

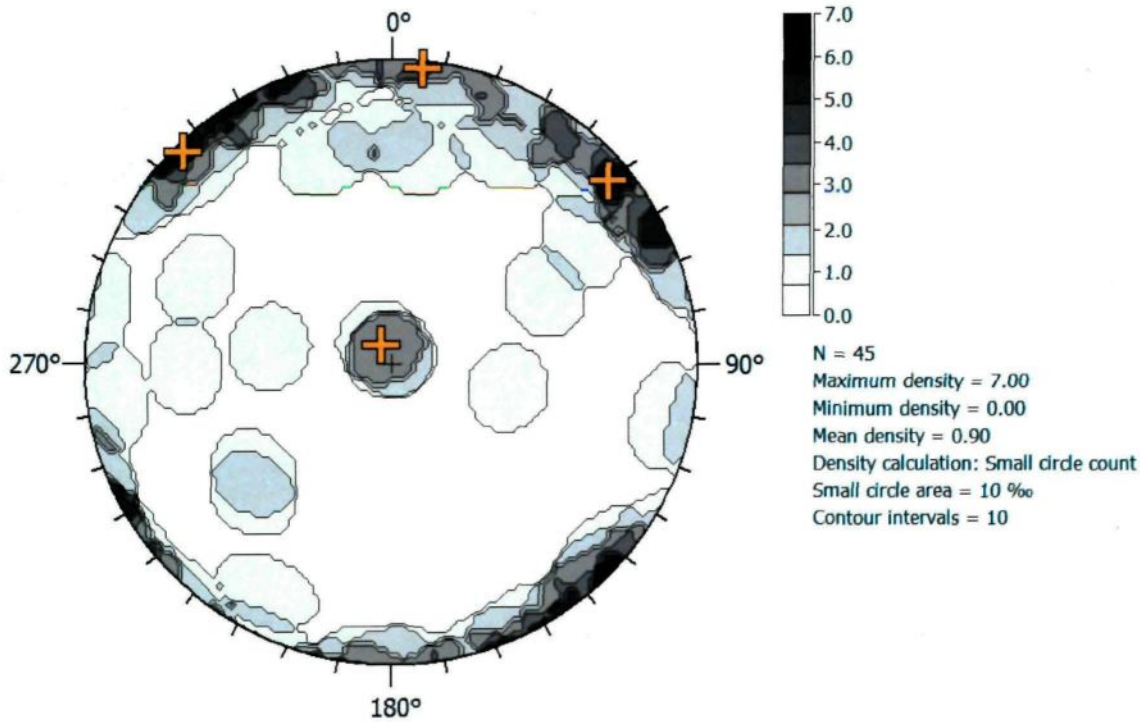

Fig. 5.9 Density plot of all poles of joint sets defined after applying Terzaghi's correction to the 18 scanlines and ATV logging data in 3 boreholes. The main pole concentrations (indicated by orange crosses) define de sides of the unit block. Equal area projection, lower hemisphere. Software: Stereo 32 (Röller & Trepmann 2008).

[13] The law of sines is given by:

$$a/_{sinA} = b/_{sinB} = c/_{sinC}$$

where *a*, *b* and *c* are the lengths of the sides of a triangle and A, B and C are the respective opposite angles.

Table 5.5 Joint sets that define the unit block in the Kenogami uplands. Their poles are indicated by orange crosses on Fig. 5.9.

Direction	Dip	Spacing distribution	Spacing mode 1 (m)	Spacing mode 2 (m)	Type of spacing
044	88	Bimodal	0.0-0.6	1.0-3.0	regularly concentrated
139	83	Bimodal	0.0-0.6	1.5-2.0	regularly variable
070	04	Unimodal	0.0-0.6	-	regularly concentrated
095	86	Bimodal	0.4-0.6	2.0-4.0	regularly concentrated

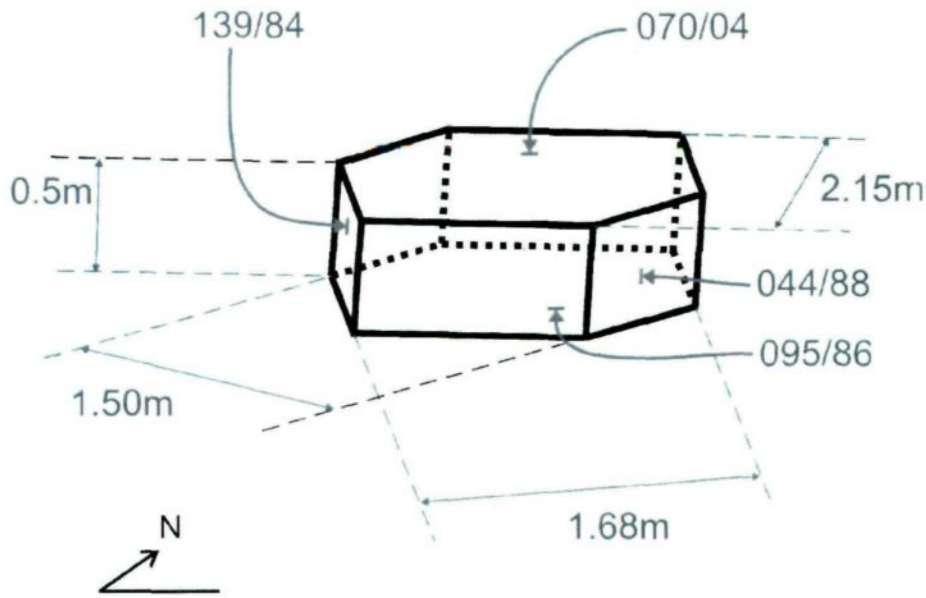

Fig. 5.10 Unit block defined for the Kenogami uplands, using corrected data from horizontal scanlines on outcrops (defining the subvertical sets) and from ATV in vertical boreholes (defining the subhorizontal set). Size is based on the second spacing mode in Table 5.5.

From the 45 poles representing joint sets identified after applying Terzaghi's correction to scanline and ATV logging data, the type of spacing could be defined for 33 sets (Fig. 5.11). In some cases, the classification was not done because there were too few joint measurements of that particular set, preventing the appearance of one of the four patterns previously described. Although the randomness of joint spacing may seem to prevail, the regular types of spacing should not be neglected. They appear particularly as bimodal distributions of joint spacing values (Fig. 5.12; Appendix 8). This pattern was observed many times in the subvertical observation faces, e.g. where more densely fractured zones alternate with zones of a lower degree of fracturing, that is, with lower joint concentration. However, they do not present significant differences regarding indication of water flow. These two types of zones could also be observed in the same outcrop, e.g., DP-059 (Figs. 4.1f and 6.2a). However, the spacing between two densely fractured zones could not be defined within a single outcrop.

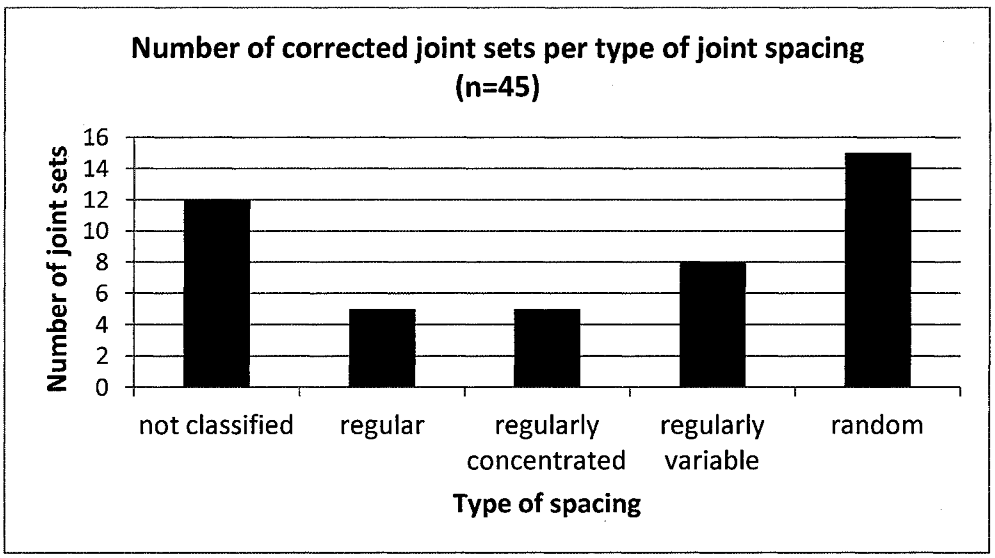

Fig. 5.11 Distribution of type of joint spacing of the joint sets defined after applying Terzaghi's correction to scanline and borehole logging data.

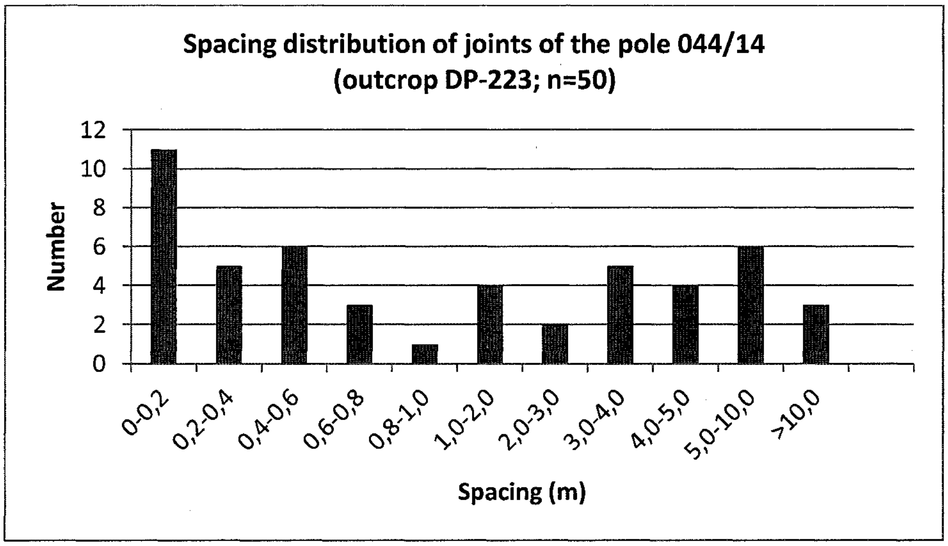

Fig. 5.12 Example of bimodal distribution of joint spacing. Horizontal scale is not uniform.

The suggestion of bimodal distributions by the spacing histograms allowed the determination of a second unit block. The latter was based on the first spacing mode in Table 5.5, with similar geometry but different size (Fig. 5.13) than the first unit block (Fig. 5.10).

Finally, it should be noted that the subhorizontal joints considered for the unit block were more frequently observed during the geophysical borehole logging than in outcrop faces.

5.4 Interaction between joints and relative ages

Thirteen horizontal outcrops were studied in order to determine the interactions between the observed joint sets and their relative ages. The joint sets were classified in 8 groups (Table 5.6 and Fig. 5.14), regarding their orientation and, mostly, their relationship observed in the field.

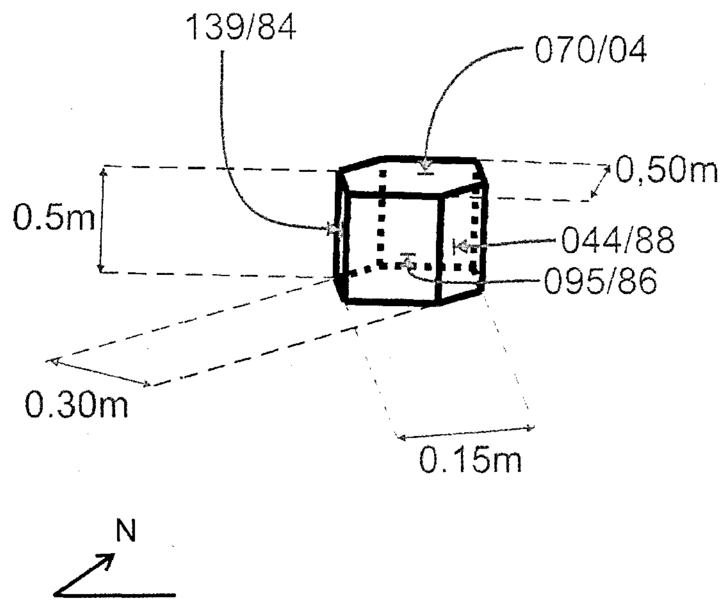

Fig. 5.13 Second unit block defined for the Kenogami uplands, due to bimodal joint spacing distribution. Corrected data from horizontal scanlines on outcrops (defining the subvertical sets) and from ATV on vertical boreholes (defining the subhorizontal set) were used. Notice that this block is smaller than the one presented at Fig. 5.10, although they have a similar geometry.

These groupings have been helpful for defining relative ages among joint sets, in spite of the large number of joint sets considered. Establishing those groupings is important, specially because not all joint sets are observed in each outcrop. Thus, the set in one outcrop can be correlated to the one in another site and then provide a good inference of their formation order. Appendix 9 presents an example of all the steps of this analysis: the drawing and photograph in fieldwork and the later interpretation of the relative ages between the joint sets.

Table 5.6 Grouping of joint sets from horizontal outcrops, based on relative age order.

Order (I = oldest; V = youngest)	Joint sets	Observations
I	060°-075° or 240°-255° 090°-100° or 270°-280° 140°-165° or 320°-345°	Coeval sets
II	020°-030° or 200°-210° 170°-190° or 350°-010°	Coeval sets
III	050°-060° or 230°-240°	
IV	030°-045° or 210°-225°	*En echelon*
V	110°-120° or 290°-300°	Youngest set

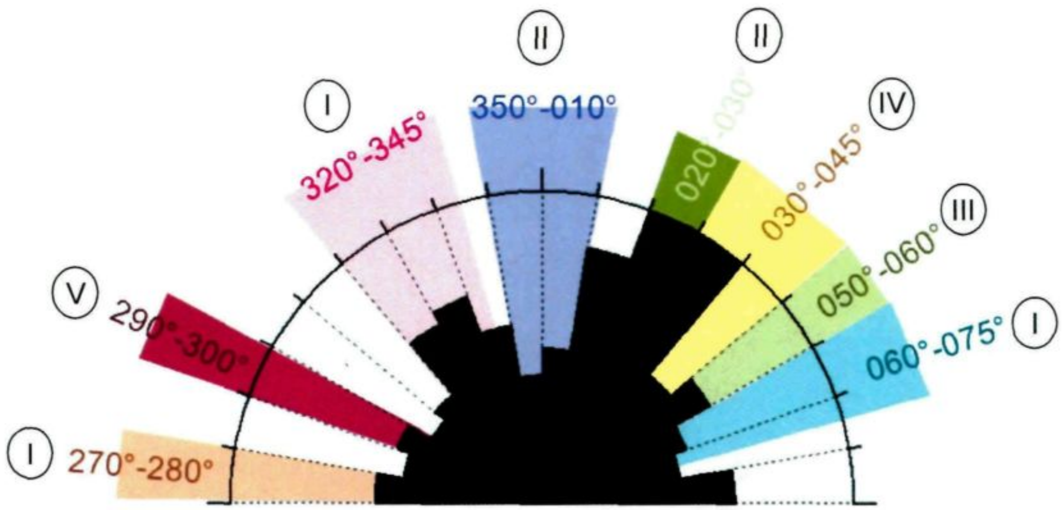

Fig 5.14 Rose diagram of measured orientation of subvertical joints observed at subhorizontal outcrops. All measured values are adjusted to the range 270° to 090°. The indicated groupings are referred to in the text and colors correspond to the ones attributed to joints in Appendix 9. Relative age order (I to V) as indicated on Table 5.6.

6

DISCUSSION

In this chapter, the implications of the previously presented results are discussed: from the occurrence of joint sets to their relationships with each other, as well as their correlation to the Saguenay tectonic history; the definition of the unit block in the Kenogami uplands and its association with hydraulic properties; and, finally, possibilities of integration of these hydrogeological and structural data into numerical and analytical models of groundwater flow.

6.1 Joint sets and structural domains

The subvertical joints oriented NW-SE and WNW-ESE (sets A and E) stand out in the measured population (Figs. 5.2 and 5.3) despite the unfavorable bias due to the measurement face orientation, as most of the visited subvertical outcrops are oriented approximately E-W (Fig. 5.1). Nonetheless, it is also possible to analyze the joint orientation data within the two orientation modes of the outcrops (Fig. 6.1) identified on Fig. 5.1: 080° to 130° (mode 1), 165° to 010° (mode 2), and all the other orientations are intermodal. Regarding mode 1 (Fig. 6.1a), joint sets A, C, D and E are still identified. Next, with mode 2 (Fig. 6.1b), sets B and D are the most easily identified. Finally, in the

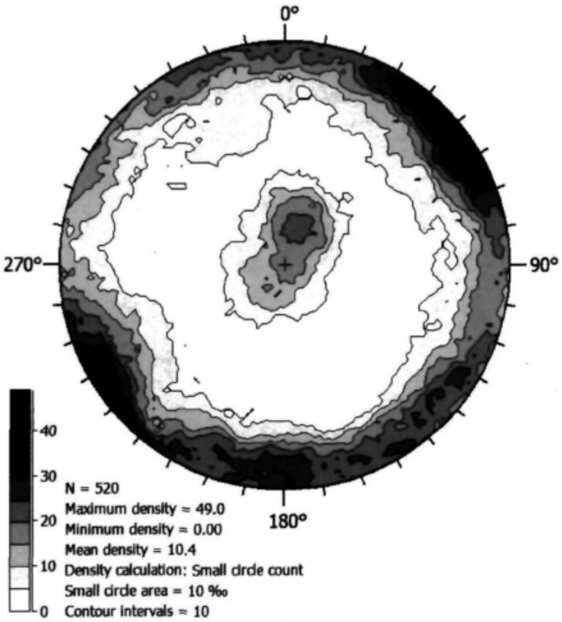

Mode 1: outcrops oriented from 080° to 130°
(a)

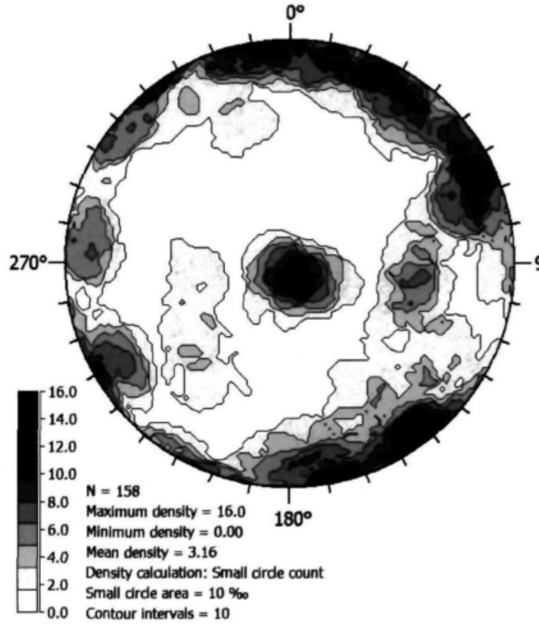

Mode 2: outcrops oriented from 165° to 010°
(b)

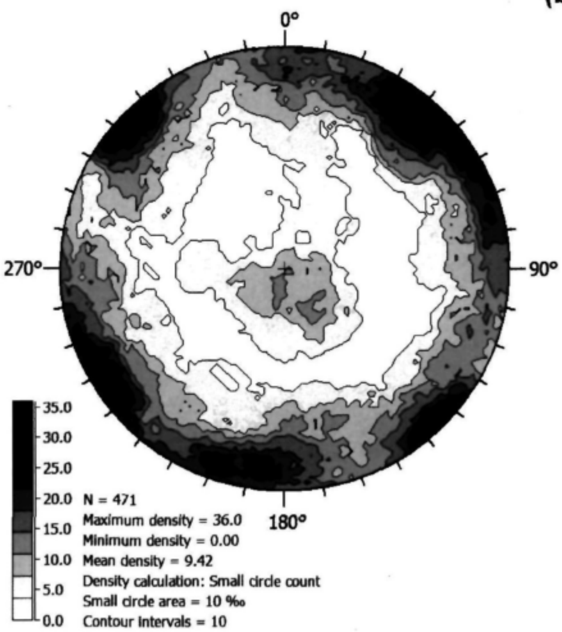

Mode 3: all other outcrop orientations
(c)

Fig. 6.1 Density diagrams of joint poles grouped according to outcrop orientation modes. Joints measured at outcrops oriented **(a)** from 080° to 130°, **(b)** from 165° to 010° and **(c)** all other orientations. Orientation modes are taken from Fig. 5.1. Equal area projections, lower hemisphere. Software: Stereo 32 (Röller & Trepmann 2008).

intermodal outcrop orientations, the joint sets A, B and E are recognized. The ensemble of these analyses indicates that those five joint set orientations are truly significant in the Kenogami uplands. Moreover, the lineament analysis on the TPIs (public intramunicipal territories) indicates that regional and local (outcrop scale) data are in accordance, as most lineaments are oriented WNW-ESE and NW-SE (Appendix 7).

The distribution of the five joint sets observed in the general survey (Fig. 5.2) throughout the entire area suggests that there is a single dominant structural domain in the Kenogami uplands. Another indication is that the same abundance of each joint set is observed regardless of the lithology (Fig. 5.3). The occurrence of a single structural domain allows the combination of the corrected data from all the scanlines to build the unit block. Finally, the joint sets A to E are all related to one of the faces of the unit block.

The subhorizontal joints (set D) are more easily observed in the limestone outcrops located to the east of the Kenogami uplands (Fig. 4.1h, i), although they were also very clear in some anorthosite outcrops within the study area (Figs. 4.1b, f and 6.2a, b). A subhorizontal pattern is also shown by the magmatic bedding observed at an outcrop to the east of Larouche town (Fig. 6.2c, d; outcrop DP-157). This texture was also observed at outcrop DP-217, although not as clear as at the former. The magmatic bedding of the LSJ Anorthosite, described by Woussen *et al.* (1988), includes both banded and massive anorthosite units at outcrop scale (these units form a banded massif at a map scale). However, most magmatic bedding features are believed to have been obscured by deformational events.

In the large limestone outcrops to the east of the Kenogami uplands (e.g. DP-232. DP-235 and DP-237), some of the open subvertical joints observed have been affected by dissolution, as shown by protuberances left within the openings (Fig. 6.3).

Another interesting feature is observed between limestone and granite at outcrops DP-232 to DP-237 (all large wall exposures at a quarry, to the east of the uplands). At this location, the subvertical N-S oriented joints occur mainly in the granite, hardly being observed in the limestone, where the main subvertical joint trend is E-W (secondary in

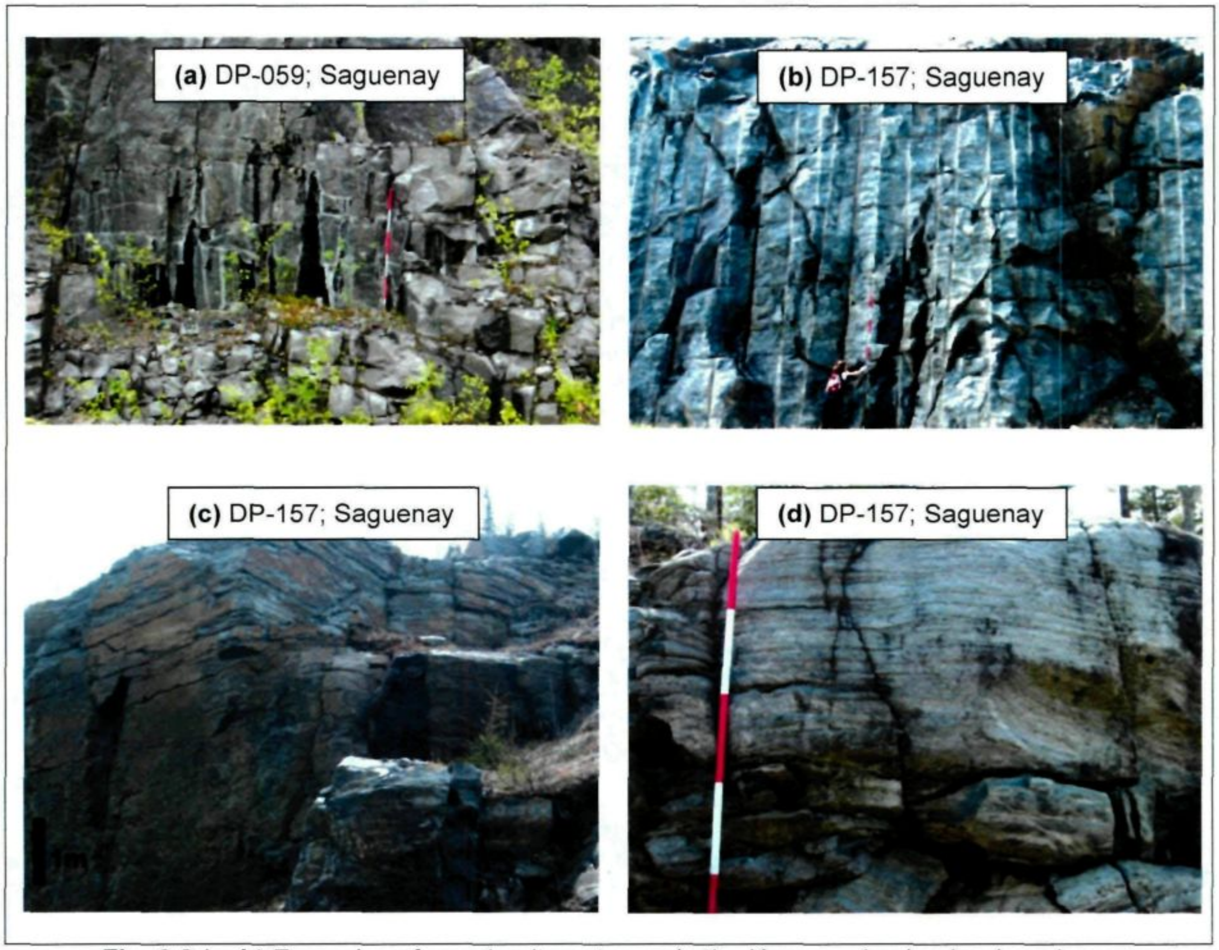

Fig. 6.2 (a, b) Examples of anorthosite outcrops in the Kenogami uplands where large subhorizontal joints are more evident. **(c, d)** Banded anorthosite. The rust color along some subvertical (and horizontal) joints indicates that there was water flow through these discontinuities. Each color division of the sticks measures 30cm (1ft). Photos: D. S. Pino.

Fig. 6.3 Protuberances clearly demonstrating that there was an important dissolution along joints in the limestone. Photo: D. S. Pino.

granite). It should be noted that the occurrence of a joint set in both granite and limestone indicates that it is more recent than the Ordovician (when limestone were formed), or even suggest that previously formed joints in granite were reactivated. These interpretations are supported by similar observations reported for joint systems in Ontario (Clarke 1959; Andjelkovic & Cruden 1998, 2000). Finally, many normal faults are observed in that quarry, as shown on the sketch on Fig. 6.4 (part of which presented on Fig. 4.1i).

On the outcrop represented on Fig. 6.4, a fault oriented 180/60 placed the limestone right beside the gneiss, with an important vertical offset, of about 6m. Nonetheless, striae (oriented 207/18 and 184/11) observed on wall 180/60 suggest an oblique movement.

6.2 Interaction between joints, their relative ages and the stress field

The stress fields and relative chronology of joint sets presented on this section are suggestions, based on the field observations of subhorizontal outcrops and on literature review (chapter 3).

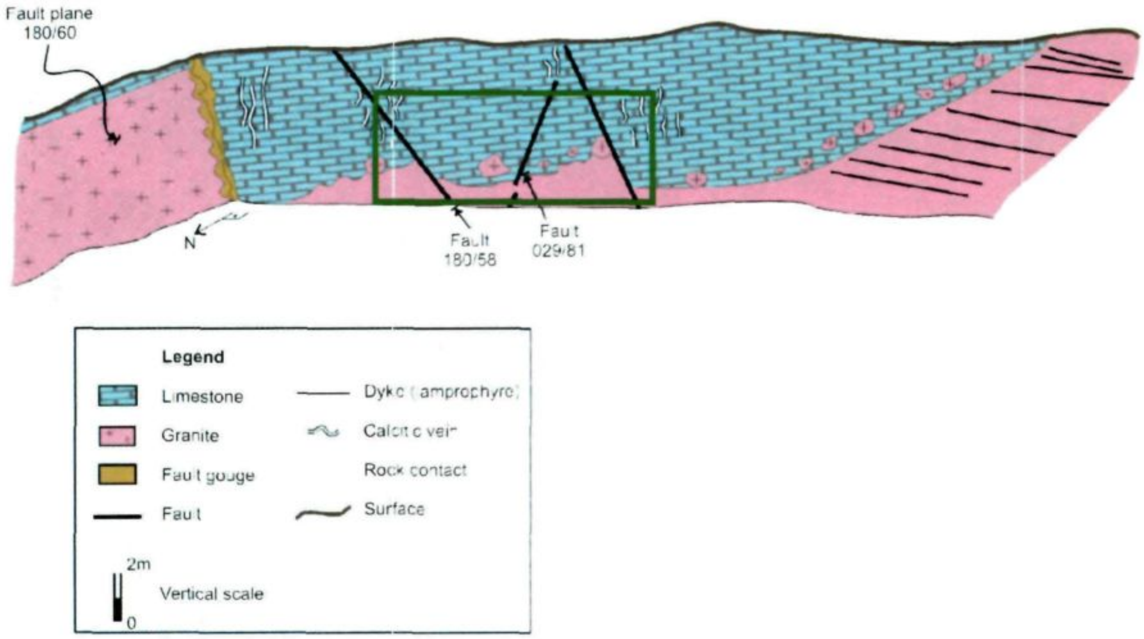

Fig. 6.4 Corner of faces in a quarry, showing a sinistral strike motion of the unconformity, with a small normal dip slip component. The 180/60 fault plane forms the left face of the corner. The normal faults in the center of the sketch cut both granite and limestone. Dykes occur on the right hand side. Sketch from outcrops DP-234 and DP-235 (also the view from DP-232 and DP-237). The frame corresponding to Fig. 4.1i is indicated by the green rectangle.

The three groups (Fig. 5.14) oriented 060°-075°, 090°-100° and 140°-165° are coeval[14], and constitute the dominant joints in most outcrops. The second most important group is 020°-030°. The group 170°-190° is less expressive, even though it seems coeval to the group 020°-030°. Next, the group 050°-060° appears to be younger. Nevertheless, it is interesting to notice that indications of joints of the younger groups being coeval to joints of older groups were observed, as the older ones are also observed abutting in the younger

[14] If Fig. 6.5b is also taken into account, it is possible to infer that the group 060°-075° would represent *P* (synthetic shear joint) in the Riedel system, while 090°-100° and 140°-165° would be *R* (synthetic Riedel shear joint) and *R'* (antithetic Riedel shear joint), respectively.

ones. This may suggest reactivation of older joints, an expected phenomenon in the study area. Finally, the group 030°-045° often appears to form *en echelon* structures; while the group 110°-120° is suggested as the youngest, never being the dominant one.

Conjugate pairs of joints were inferred based on the relations between those groups of joints (Fig. 5.14), as well as the orientation of σ_1 (the major principal component of the stress field) by the time of their formation, yielding four different tectonic events or stress fields (Fig. 6.5). Different sites may be compared as they are all in the same structural domain. Based on the orientation of the inferred major principal stress component and of the conjugate pairs, the four tectonic environments suggested may be related to the tectonic events that affected the SLSJ region (Fig. 6.5).

The correlations shown on Fig. 6.5 were determined by comparing the collected data (angular relationships and relative ages between the joints observed in the field) with information discussed on chapter 3 on the tectonic events that affected the SLSJ region. The comparison between field and theoretical data is presented on the next paragraph; other relationships between the groups are described afterwards, by relative age order of joint set.

The stress field represented on on Fig. 6.5a may be associated with the closing of the Iapetus Ocean (Acadian Orogeny, 410-380Ma), when the main component of the stress field was recognized at 115° (Trudel & Malo 1993). It may also be related to the Alleghanian Orogeny (300-250Ma), as in its phase 2, σ_1 was oriented WNW-ESE (Verreault 2000). Next, the sketch on Fig. 6.5b may be related to phase 1 from the Alleghanian Orogeny, when σ_1 was oriented NNW-SSE (Verreault 2000). The representation of Fig. 6.5c is better (though not perfectly) related to the phase 2 from the

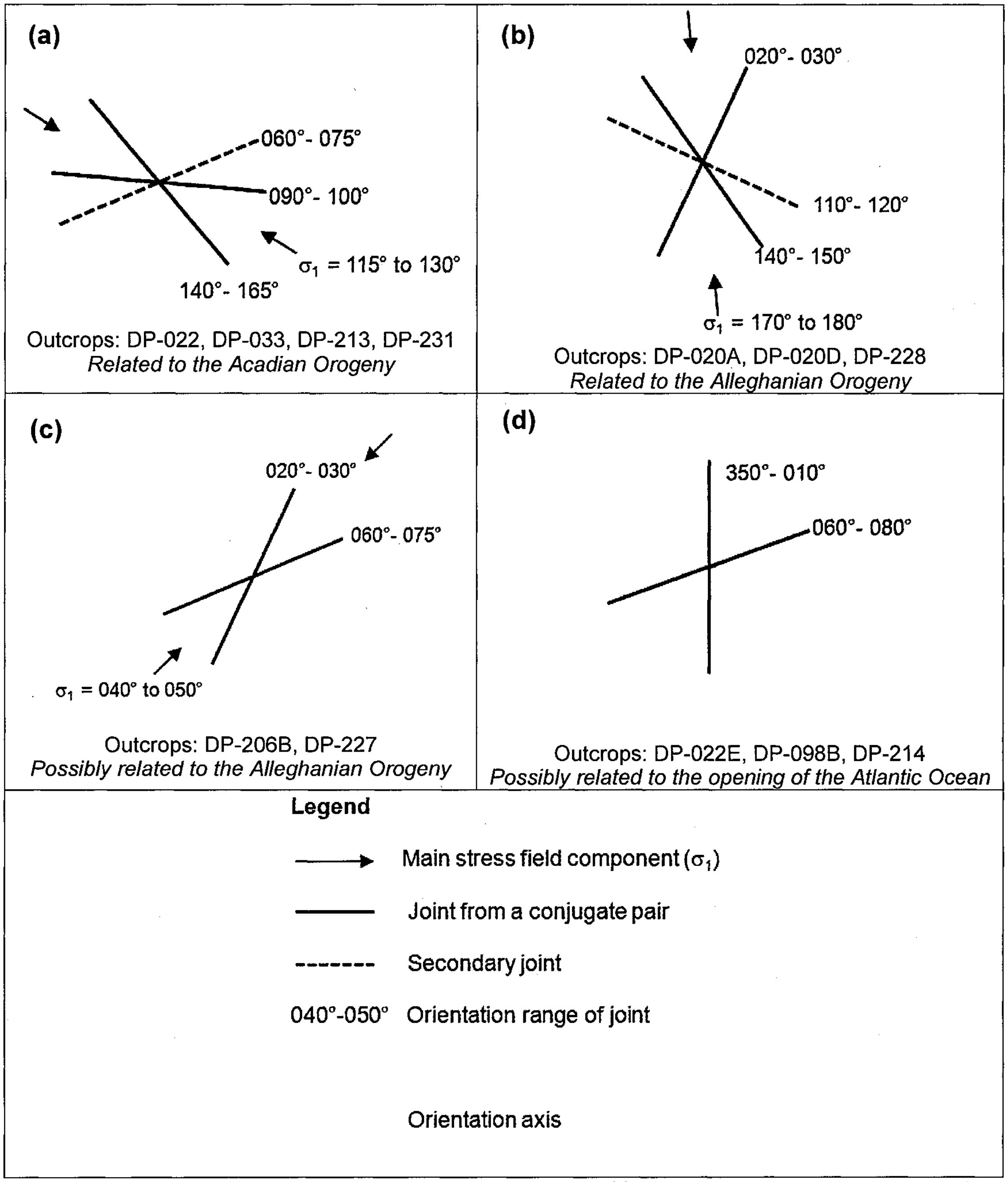

Fig. 6.5 Suggested conjugate pairs of the joint sets identified in 13 horizontal outcrops in the Kenogami uplands. The outcrops where these pairs could be identified are indicated. A correlation is also suggested between the conjugate pairs and the respective main stress field component, with some tectonic events that affected the SLSJ region. The sketches are presented in chronological order, from the oldest tectonic event (a) to the youngest (d).

Alleghanian Orogeny. Finally, the extensional regime on Fig. 6.5d may be related to the opening of the Atlantic Ocean (or the fragmentation of the Pangea; started around 180Ma), given that at that time large N-S structures (e.g. the Hudson-Champlain lineament; Roy *et al.* 1993, 1998; Megan *et al.* 2010; Roden-Tice *et al.* 2011) were originated and/or reactivated.

Finally, regarding the current stress field in the Kenogami uplands, it may be inferred that its main compressional component (σ_1) is oriented NE-SW, as such orientation is consistently found in eastern Canada (Arjang 1991; Hasegawa 1991; Zoback 1992, Assameur & Mareschal 1995) (Appendix 10). This orientation is comparable to the tectonic environments presented on Figs. 6.5a and d, but it differs from the most recent stress field identified in the horizontal outcrops. The trend NE-SW of the current stress field is perpendicular to joint sets A and E (Fig. 5.2) from the Kenogami uplands, and to set 139/84 from the unit block (Fig. 5.10). Joints of these sets would tend to close due to the action of the current stress field, while the joints of sets B (Fig. 5.2) and 044/88 (Fig. 5.10) would tend to remain open.

6.3 The unit block and hydraulic properties

An important issue regarding the correction proposed by Terzaghi (1965) is that it does not account for polymodal distributions of joint spacing; it simply considers the average spacing of all joints over the scanline. In the case of the Kenogami uplands, bimodal distributions were observed along many of the scanlines performed (Appendix 8). Thus, standard statistical parameters which assume an unimodal symmetrical distribution of values, such as the average and the standard deviation, are meaningless. Therefore, intervals corresponding to the bimodal distributions were considered instead (Table 5.5).

Therefore, two unit blocks (Figs. 5.10 and 5.13) were defined for the Kenogami uplands; the average joint spacing values of each unit block were calculated within the range of the respective distribution modes presented on Table 5.5.

The geometry and size of the unit block may be used to relate it to hydraulic properties; the example of the block from Fig. 5.10 is discussed in the next sections.

6.3.1 Hydraulic properties of the unit block

Hydraulic properties of the Kenogami uplands were estimated by Chesnaux (accepted) through an analysis of groundwater flow at a regional scale. Although only the southern part of the Kenogami uplands was considered, the calculated values may be extrapolated to the whole uplands, considering: (1) the relative homogeneity of its lithology; (2) the definition of a single structural domain forming the fractured rock aquifer. The properties estimated by Chesnaux (accepted) are the hydraulic conductivity ($4.3x10^{-7}$m/s), the transmissivity ($2.30x10^{-5}m^2/s$) and the recharge (3.5mm/y; i.e. 0.38% of 930mm over a year. They were calculated based on an analytical interpretation of regional hydraulic head profiles, based on a one-dimensional Dupuit-Forchheimer model in steady state conditions.

It is possible to calculate a mean joint aperture for each joint set of the unit block by applying the calculated value of hydraulic conductivity in Eq. 2.1, assuming that the joints are formed by parallel and smooth walls. Let's consider that each joint set from the unit block contributes equally to the hydraulic conductivity, so that each set presents $K=1.075x10^{-7}$m/s (a quarter of the total value calculated for the Kenogami uplands). Also, for this example, let's take into account a difference of hydraulic head *dh* of 0.1m and a value of water viscosity μ equal to $1.519x10^{-3}$kg/s.m (the latter corresponds to a water temperature of 5°C, a value commonly found in the first 30m of the logged wells in the Kenogami uplands). Water density ρ and gravitational acceleration *g* are assumed to be equal to 999.96km/m³ and 9.81m/s², respectively. Thus, for the joint set 044/88 as an example:

$$K = \frac{(2b)^3}{W}\frac{\rho g}{12\mu}$$

$$1.075x10^{-7} = \frac{(2b)^3}{1.50}x\frac{999.96\,x\,9.81}{12\,x\,1.519\,x\,10^{-3}}$$

$$\therefore 2b \approx 6.69x10^{-5}m$$

A mean joint aperture of approximately 66.9μm is estimated for the joint set 044/88 of the unit block. This aperture value is within ranges proposed for other regions in the Canadian Shield: (1) apertures of 2-200μm, obtained by straddle-packer injection tests and ATV logging (Raven 1986); (2) apertures of 25-375μm for subvertical joints and of 62.5-187.5μm for subhorizontal joints, estimated through groundwater flow simulations (Gleeson 2009; Gleeson *et al.* 2009).

Another value that can be calculated from the characteristics of the unit block is the wet surface per unit volume of rock, that is, the ratio between its surface area and its volume (Pino *et al.* 2011; 2012b). The wet surface indicates the surface area available for water-rock geochemical interaction for the groundwater flow through the joints in that rock mass. As the unit block is a hexagonal prism, its volume may be approximately (due to inclined sides) calculated by multiplying the surface of its base (surface of the hexagon) by its height (the spacing of the subhorizontal set). Thus, its base has approximately a surface area of $8.12m^2$ and the block has a volume of $1.25m^3$. The wet surface is easily calculated as $6.47m^{-1}$.

Next, both the volume of water surrounding the unit block and joint porosity are parameters that provide an estimate of the amount of water storage in the joints of the fractured rock aquifer. Considering the calculated joint aperture for the other sets of the unit block (69.5μm for set 139/84, 75.4μm for set 095/86, and 46.4μm for set 070/04), it is possible to calculate the volume of water surrounding it. Nonetheless, it must be highlighted that the water within each joint that forms the unit block is also considered for the calculi for an adjacent block; thus, it is necessary to divide the values of joint aperture by two. Following these observations, the volume of water around the unit block is estimated at $2.23 \times 10^{-4}m^3$. This value is related to joint porosity (ratio between empty volume – the joint volume in this case – and the total volume of the block). For the unit block of the Kenogami uplands, with the previously mentioned aperture values, a joint porosity of approximately 0.02% is obtained. The joint porosity of 0.02% is comparable to values estimated for a quartzite (down to 0.06%) using both field and laboratory data (Rouleau *et al.* 1996).

6.3.2 Estimating flow velocity

Given a hydraulic gradient value, it is possible to calculate the water flow through each joint set that defines the unit block, combining the elements from Darcy's law (Eq. 6.1) and Eq. 2.1. In Darcy's law (Eq. 6.1), the flow Q [m^3/s] is given by multiplying the hydraulic conductivity K [m/s] by the cross-sectional area to the flow A [m^2] and the hydraulic gradient, which is equal to the ratio between the difference of hydraulic head *dh* [m] and the length *dl* [m] over which the value *dh* is considered (Darcy 1856).

$$Q = -KxAx\frac{dh}{dl} \quad \text{(Eq. 6.1)}$$

To estimate the water flow in a single joint, assuming a parallel-plate mode, Eq. 2.2 and Darcy's law (Eq. 6.1) may be combined as the following:

$$Q = -(2b)^2 x\frac{\rho g}{12\mu} xA_{joint} x\frac{dh}{dl} \quad \text{(Eq. 6.2)}$$

To better assess the unit block, let's consider a system that contains a single joint from the set 044/88 (Fig. 6.6a). It is assumed that the mean joint aperture value (66.9μm) previously calculated may be considered for each single joint. Therefore, for the system represented on Fig. 6.6a:

$$Q = -(2b)^2 x\frac{\rho g}{12\mu} xA_{joint} x\frac{dh}{dl}$$

$$Q = (6.69\,x\,10^{-5})^2\,x\,\frac{999.96\,x\,9.81}{12\,x\,1.519\,x\,10^{-3}}\,x\,(1.55\,x\,1.06\,x\,10^{-4})\,x\,\frac{0.1}{0.5}$$

$$\therefore Q \approx 5.00\text{x}10^{-8}\text{m}^3/\text{s}$$

A flow rate value of approximately $5.00\text{x}10^{-8}\text{m}^3/\text{s}$ is obtained for water flow through a joint of the set 044/88 of the unit block (Fig. 6.6a).

Then, it is also possible to estimate the hydraulic conductivity of an equivalent porous media (Fig. 6.6b), using Darcy's law (Eq. 6.1). It is supposed that it would have the same water flow calculated for the single joint, so:

$$Q = -KxAx\frac{\Delta h}{\Delta l}$$

$$5.00\,x\,10^{-8} = K\,x\,(1.55\,x\,1.5)\,x\,\frac{0.1}{0.5}$$

$$\therefore K \approx 1.08 \times 10^{-7} m/s$$

A hydraulic conductivity value of approximately 1.08×10^{-7}m/s is obtained for the equivalent porous media (Fig.6.7b) of the block diagram that comprehends a joint of the set oriented 044/88 (Fig. 6.6a). This value is in accordance with the hydraulic conductivity calculated by Chesnaux (accepted), as they have the same order of magnitude.

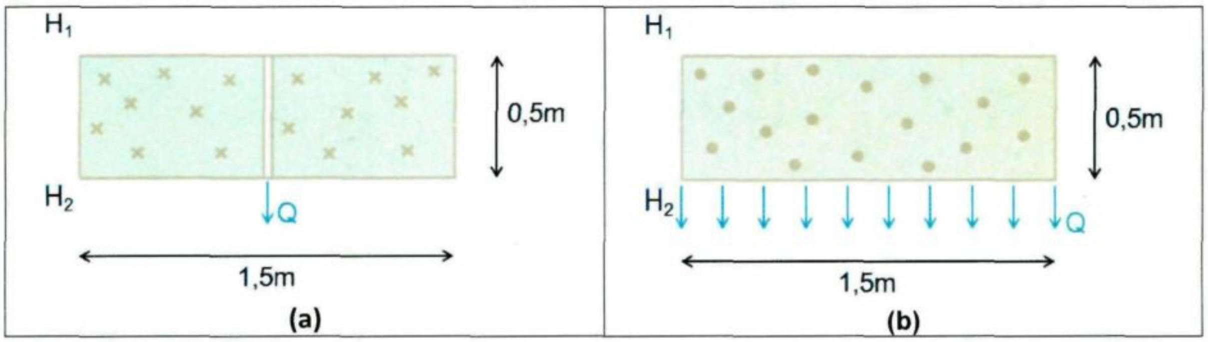

Fig. 6.6 (a) A rock volume that contains one joint of the set 044/88 in its center. Its dimensions are 1.5 x 0.5m, and correspond to the spacing of this joint set and the height of the unit block, respectively. The side not shown in the sketch corresponds to the edge from the hexagonal base of the unit block formed by the set 044/88, with a width of 1.55m (values introduced on chapter 5). **(b)** *Equivalent porous media representation of the previous rock volume.*

The average velocity of water flow is very important for the cases of contaminant flow through fractured aquifers and to the restoration of these aquifers. Given the water flow rate through a joint, the value of the average velocity v_{joint} [m/s] of water through the joint can be estimated. This parameter may be compared to the value of infiltration velocity v_i [m/s] obtained for a porous media with the same water flow rate, and for which a realistic value of effective porosity n_{ef} [dimensionless] is assumed. The velocities for each media are given by the following equations:

$$v_{joint} = \frac{Q}{A}$$

$$v_{joint} = \frac{Q}{2b\ x\ l} \qquad \text{(Eq. 6.3)}$$

$$v_i = \frac{Q}{A\ x\ n_{ef}} \qquad \text{(Eq. 6.4)}$$

Therefore, for the fractured media:

$$v_{joint} = \frac{Q}{2b\ x\ l}$$

$$v_{joint} = \frac{1.08\ x\ 10^{-7}}{6.69\ x\ 10^{-5}\ x\ 0.5}$$

$$\therefore\ v_{joint} = 3.23x10^{-3} m/s$$

For the porous media, assuming an effective porosity of 30%:

$$v_i = \frac{Q}{A\ x\ n_{ef}}$$

$$v_i = \frac{1.08\ x\ 10^{-7}}{(1.55\ x\ 1.50)\ x\ 0.30}$$

$$\therefore\ v_i \approx 1.55x10^{-7} m/s$$

Thus, for a volume of rock mass containing a single joint (Fig. 6.6a) and a similar volume constituted of an equivalent porous media (Fig. 6.6b), the water flow through the joint from the first system has to be about 4 orders of magnitude faster than through the pores from the second one ($3.23x10^{-3}$m/s *versus* $1.55x10^{-7}$m/s), in order to maintain the same flow rate.

6.3.3 Hydraulic conductivity tensor

The hydraulic conductivity tensor of a fractured rock mass allows the quantification of its anisotropy, considering geometrical parameters of the joints, such as their aperture, orientation and spacing (Bianchi & Snow 1968; Snow 1969; Oda 1985; Raven 1986). It is assumed that the joints are parallel and continuous conduits, interference effects at intersections are negligible and there is a single-phase, non-turbulent flow of incompressible Newtonian fluid through the joints (Raven 1986).

The hydraulic conductivity tensor K_{ij} of a continuous media equivalent to a joint system is given by (Snow 1965):

$$K_{ij} = \frac{\rho \; x \; g \; x \; (2b)^3}{12 \; x \; \mu \; x \; W}\left(\delta_{ij} - M_{ij}\right)$$

(Eq. 6.5)

where W is the effective joint spacing, δ_{ij} is the Kronecker delta, and M_{ij} is a 3x3 matrix formed by the direction cosines of the normal to the conduit (that is, of the joint pole). Matrix M_{ij} is given by (Bianchi & Snow 1968; Snow 1969):

$$M_{ij} = \begin{bmatrix} Q_x \cdot Q_x & Q_x \cdot Q_y & Q_x \cdot Q_z \\ Q_y \cdot Q_x & Q_y \cdot Q_y & Q_y \cdot Q_z \\ Q_z \cdot Q_x & Q_z \cdot Q_y & Q_z \cdot Q_z \end{bmatrix}$$ (Eq. 6.6)

where Q_x, Q_y and Q_z are the direction cosines of the joint pole.

Next, regarding the unit block from Fig. 5.10, the input data for Eq. 6.5 is shown on Table 6.1.

Table 6.1 Data available for calculating the hydraulic conductivity tensor for the unit block from Fig. 5.10.

Strike	Dip	Trend	Plunge	2b[1] (m)	Qx	Qy	Qz	μ (kg/s.m)	ρ (kg/m³)	g (m/s²)	W[2] (m)
44	88	314	2	$6.69x10^{-5}$	0,6942	-0,7189	0,0349	0,001519	999,96	9,81	1,5
139	84	49	6	$6.95\ x10^{-5}$	0,6525	0,7506	0,1045	0,001519	999,96	9,81	1,68
95	86	5	4	$7.54\ x10^{-5}$	0,9938	0,0869	0,0698	0,001519	999,96	9,81	2,15
70	4	340	86	$4.64\ x10^{-5}$	0,0656	-0,0239	0,9976	0,001519	999,96	9,81	0,5

[1] Calculated with Eq. 2.1. An example for the joint set 044/88 was previously shown.
[2] Calculated after Terzaghi's correction.

Applying the data from Table 6.1 into Eq. 6.5 for each joint set, the following hydraulic conductivity tensors are obtained:

$$K_{044/88} = \begin{bmatrix} 5.57x10^{-8} & 5.37x10^{-8} & -2.60x10^{-9} \\ 5.37x10^{-8} & 5.19x10^{-8} & 2.70x10^{-9} \\ -2.60x10^{-9} & 2.70x10^{-9} & 1.07x10^{-7} \end{bmatrix}$$

$$K_{139/84} = \begin{bmatrix} 6.17x10^{-8} & -5.26x10^{-8} & -7.33x10^{-9} \\ -5.26x10^{-8} & 4.69x10^{-8} & -8.43x10^{-9} \\ -7.33x10^{-9} & -8.43x10^{-9} & 1.06x10^{-7} \end{bmatrix}$$

$$K_{095/86} = \begin{bmatrix} 1.34x10^{-9} & -9.29x10^{-9} & -7.45x10^{-9} \\ -9.29x10^{-9} & 1.07x10^{-7} & -6.52x10^{-10} \\ -7.45x10^{-9} & -6.52x10^{-10} & 1.07x10^{-7} \end{bmatrix}$$

$$K_{070/04} = \begin{bmatrix} 1.07x10^{-7} & 1.68x10^{-10} & -7.03x10^{-9} \\ 1.68x10^{-10} & 1.07x10^{-7} & 2.56x10^{-9} \\ -7.03x10^{-9} & 2.56x10^{-9} & 5.23x10^{-10} \end{bmatrix}$$

The contribution from the individual joint sets are added resulting in a symmetric tensor K'. It may be later diagonalized in the tensor K, in order to obtain the principal hydraulic conductivities for the Kenogami uplands. The diagonalization of K' was done with the software MATLAB[15].

$$K' = \begin{bmatrix} 2.58x10^{-7} & -8.11x10^{-9} & -2.44x10^{-8} \\ -8.11x10^{-9} & 3.13x10^{-7} & -3.83x10^{-9} \\ -2.44x10^{-8} & -3.83x10^{-9} & 3.21x10^{-7} \end{bmatrix}$$

$$K = \begin{bmatrix} 2.48x10^{-7} & 0 & 0 \\ 0 & 3.14x10^{-7} & 0 \\ 0 & 0 & 3.29x10^{-7} \end{bmatrix}$$

6.4 The conceptual model

A basic unit that characterizes the joint system in the Kenogami uplands was defined through the unit block. This was done at a local scale (block volume of 1.25m³), but the results obtained with Terzaghi's correction (the bimodal spacing distributions; Appendix 8) have allowed the definition of two unit blocks with different sizes (Figs. 5.10 and 5.13). As the two different sizes of block were observed within a same outcrop, it is reasonable to assume that its geometry could be also extrapolated to the regional context. Moreover, defining two unit blocks of different sizes is interesting for numerical modeling: it may be used, for instance, to refine the model mesh; the smaller block may be used to model lineaments related to more densely fractured zones and faults, while the larger block would constitute the rest of the fractured media. The geometry of the unit block may still be used to represent less densely fractured zones, previously discussed (Figs. 4.1f and 6.2a; section 5.3).

As previously discussed, subvertical joints are the main fracturing expression in the Kenogami uplands, and they have an important role regarding groundwater recharge

---

[15] The MathWorks. (2009). *MATLAB version 7.9.0.529.*

paths. Provided the great extent of outcropping crystalline rocks in the Kenogami uplands, and even in the SLSJ region, it is reasonable to assume that the study area is better interpreted as a recharge and transit region rather than simply a water storage zone. Nonetheless, the subhorizontal joint sets should not be neglected: not only they enhance the connections between the subvertical joint sets, but also contribute to the regional groundwater flow, particularly to the lowlands to the east and the west of the Kenogami uplands.

6.5 Recommendations for future studies in the Kenogami uplands

For future works in the Kenogami uplands region, the most immediate recommendation is the development of a regional flow model – possibly based on the discrete fracture network approach, using the unit block and taking into account the present stress field.

It is also advisable to perform more ATV and flowmeter loggings, as well as hydraulic tests (pumping and packer tests) within the Kenogami uplands. The determination of hydraulic properties at several sites in the study area may provide a more definitive assessment regarding their extrapolation to the regional scale, on the basis that the Kenogami uplands can be considered as a homogeneous structural domain whose local structures are repeated at the regional scale. The realization of more ATV logs would improve the data of the subhorizontal joint set from the unit block.

The analysis of thin sections may be interesting as well, in order to verify the existence of infillings, with regard to the various joint sets, and to check the indicators of sense of movement along fault surfaces. The magmatic bedding and the kinematic indicators of shear zones in anorthosite and gabbro could be better described with the help of thin sections.

Finally, regarding lineament analysis, four main advices are given below.

1) Verification of the lineament map by another interpreter, as this is a subjective analysis;

2) A longer fieldwork campaign in order to analyze possible relationships between lineaments and more densely fractured zones, as this could not be documented during this research;

3) Plot of cumulative frequency of wells versus specific capacity for different categories of wells, e.g.: (i) wells at different distances from any type of lineaments, (ii) wells close to lineaments that bear the same trend of measured fractures in nearby outcrops, (iii) wells close to lineaments that do not correlate to any of the fracture trends that were measured in nearby outcrops, (iv) wells close to ductile shear zones, (v) wells close to brittle shear zones, (vi) lineament directions to which the wells are closest. The PACES-SLSJ gathered a large database on wells in the SLSJ region that could be useful for some of these analyses;

4) More detailed analysis of the brittle shear zones found during this research (and other possibly existing ones). Verification of the existence of wells in their surroundings and analysis of the production of wells regarding the core and the damage zone from each shear zone.

7

CONCLUSIONS

This project allowed the characterization of an aquifer in fractured crystalline rocks, regarding the following aspects: joint systems at different scales, past stress fields, hydraulic properties and the possible relationships between these parameters. The methodology adopted proved itself efficient and may be applied to other studies on fractured rock aquifers. The example of the Kenogami uplands has contributed to increase the knowledge on aquifers and groundwater in Quebec, particularly in fractured rock terrains, as most of the PACES (*Programme d'acquisition de connaissances sur les eaux souterraines du Québec*) projects include that type of aquifer.

The results obtained are summarized in the following paragraphs, in relation with the four questions proposed as the objectives (chapter 1) of this study.

In the general survey[16], five joint sets were identified in the Kenogami uplands. The study area is considered to be a single structural domain, as the five joint sets may be found all over the study area and their relative importance is the same in the different lithologies present in the area.

[16] Question 1: Is there a structured joint system in the bedrock, that is, is it possible to identify preferential joint orientations and structural domains?

The lineament analyses[17] at scales 1:20.000 and 1:1.000 allowed the identification of structures mainly oriented NW-SE. This coincides with the main joint set orientation from the general survey. The lineament trending WNW-ESE is also important; it is parallel to the main roads in the study area, which, in turn, are parallel to the Saguenay graben axis, as well as to another joint set identified in the field despite unfavorable bias of orientation of most observation faces. The occurrence of the same structural trends at different scales was also illustrated by the data obtained with the application of Terzaghi's correction on scanlines, as two different sizes of the unit block were defined; this suggests that the geometry of the unit block could be used at other scales as well. Therefore, there is a clear correlation between structures at local and regional scales in the Kenogami uplands.

The observations made on horizontal outcrops[18] allowed the determination of conjugate pairs of joints and of the orientation of the main components of past stress fields. Four different conditions were identified on the 13 outcrops analyzed. Regarding the present stress field (oriented NE-SW), it should be remarked that it tends to close the joints of the main set in the Kenogami uplands, oriented NW-SE, as well as the sets 139/84 and 085/86 from the unit block. On the other hand, the set 044/88 considered in the unit block and the other subvertical sets from the general survey tend to remain open.

The flowmeter test[19] could only be performed at one of the three wells logged in the Kenogami uplands. Nonetheless, when the results are compared to other logs done in the SLSJ during the PACES campaign, it is observed that the conductive joints usually have

[17] Question 2: Can joint systems be defined at different scales (e.g. regional and local ones)? If yes, are there any relationships between the systems observed at different scales?

[18] Question 3: Can any correlation between the joint system(s) and the past and present stress fields be identified?

[19] Question 4: Is there a relationship between the hydrogeological properties obtained from boreholes and the joint system(s)?

directions around 200°, 270° and 330°, and they are all mostly dipping up to 30°. As they all have northerly dip directions and low angle dip, the present day stress field will tend to open them. It may be also suggested that the most conductive joints have a preferential orientations, which could be confirmed with the logging of other wells in the region, particularly in the uplands.

A conceptual model for the fractured rock aquifer in the Kenogami uplands was developed, taking advantage of the unit block. As previously discussed, the unit block may be extrapolated to a regional scale, and the subvertical joints are the most expressive ones in the study area. These are considered as the main path for groundwater recharge, particularly the sets that tend to be open with the present stress field. Nonetheless, the subhorizontal joints should not be neglected: as previously shown, the subhorizontal joints are the most transmissive ones in the wells, particularly in the first 100m. Moreover, the subhorizontal joints enhance the connections between the subvertical joint sets and represent an important path for regional flow, particularly to the adjacent lowlands to the east and the west of the Kenogami uplands.

Finally, the other contributions from this work are: (1) the highlight of the value of constructing a unit block to characterize a fractured media for hydrogeological studies; (2) the exemplification of how to combine the structural data used for the unit block with calculated hydraulic properties; (3) the introduction of a method for applying Terzaghi's correction on computers to obtain information regarding the size and geometry of the unit block, without the need for specialized softwares; (4) the emphasis on the possible polymodal distributions of joint spacing, and the care to be taken when estimating average spacing values over a scanline; (5) the application of the analysis of structures on subhorizontal outcrops for obtaining the orientation of the main components of past stress fields.

8

REFERENCES

Abdssah, D. & Ershaghi, I. (1986).Triple-porosity systems for representing naturally fractured reservoirs. *Society of Petroleum Engineers Formation Evaluation*, **1** (2): 113-127.

Aguilera, R. & Poollen, V. H. K. (1977). Current status on the study of naturally fractured reservoirs. *The Log Analyst*, **XVIII** (3).

Allen, J. S.; Thomas, W. A.; Lavoie, D. (2009). Stratigraphy and structure of the Laurentian rifted margin in the northern Appalachians: a low-angle detachment rift system. *Geology*, **37** (4): 335-338.

Almeida, C. & Oliveira, M. M. (1990). *Caracterização hidráulica de aqüíferos fracturados. In: Livro de homenagem a Carlos Romariz*. Lisboa, Secção de Geologia Económica e Aplicada da FCUL, pp.30-64.

Andjelkovic, D. & Cruden, A. (1998). Inheritance of fractures from Precambrian basement into Paleozoic cover, south central Ontario; implications for neotectonic fault reactivation models. *In:* Geological Society of America, Annual Meeting. *Abstracts with Programs*, **30** (7): 248-249.

Andjelkovic, D. & Cruden, A. (2000). Origin of joints in the Paleozoic rocks of south-central Ontario. *In:* AAPG Eastern Section Meeting. *Abstracts*, **84** (9): 1380.

Angelier, J. (1979). Determination of the mean principal directions of stresses for a given fault population. *Tectonophysics*, **56**: T17-T26.

Apaydin, A. (2010). Relation of tectonic structure to groundwater flow in the Beypazari region, NW Anatolia, Turkey. *Hydrogeology Journal*, **18** (6): 1343-1356.

Arjang, B. (1986). Field stress determinations at the Niobec mine, Chicoutimi, Quebec. Mining Research Laboratories, Division Report MRL 87-15 (TR). 24p.

Arjang, B. (1991). Pre-mining stresses at some hard rock mines in the Canadian Shield. *Canadian institute of Mining, Metallurgy and Petroleum Bulletin*, **84** (945): 80-86.

Assameur, D. M. & Marechal, J. C. (1995). Stress induced by topography and crustal density heterogeneities: implication for the seismicity of southeastern Canada. *Tectonophysics*, **241**: 179-192.

Avramtchev, L. (1993). *Carte minérale de la région du Saguenay – Lac Saint-Jean*, échelle 1:500.000. Ministère des Ressources Naturelles et de la Faune.

Barenblatt, G. I.; Zheltov, I. P.; Kochina, I. N. (1960). Basic concepts in the theory of seepage of homogeneous liquids in fissured rocks (strata). *Journal of Applied Mathematics and Mechanics* (English Translation), **24**: 1286-1303.

Barker, J. A. (1985). Generalized well function evaluation for homogeneous and fissured aquifers. *Journal of Hydrology*, **76**: 143-154.

Barton, C. A.; Zoback, M. D.; Moos, D. (1995). Fluid flow along potentially active faults in crystalline rock. *Geology*, **23** (8): 683-686.

Bianchi, L. & Snow, D. (1968). Permeability of crystalline rock interpreted from measured orientations and apertures of fractures. *Annals of Arid Zone*, **8** (2): 231-245.

Blanchard, R. (1953). Forces hydro-électriques canadiennes. *Revue de géographie de Lyon*, **28** (2): 75-82.

Boulton, N. S. & Streltsova, T. D. (1977). Unsteady flow to a pumped well in a two-layered water bearing formation. *Journal of Hydrology*, **35**: 245-256.

Bull, S.; Cartwright, J.; Huuse, M. (2009). A review of kinematic indicators from mass-transport complexes using 3D seismic data. *Marine and Petroleum Geology*. **26** (7): 1132-1151.

Caine, J. S.; Evans, J. P.; Forster, C. B. (1996). Fault zone architecture and permeability structure. *Geology*, **24** (11): 1025-1028.

Chesnaux, R. (accepted). Regional recharge assessment in the crystalline bedrock aquifer of the Kenogami uplands, Canada. *Hydrogeological Sciences Journal.*

Chesnaux, R. & Allen, D. M. (2008). *Using PETREL and ECLIPSE to model fractured-rock type aquifers.* Final report for Schlumberger Water Services.

Chesnaux, R.; Allen, D. M.; Jenni, S. (2009). Regional fracture network permeability using outcrop scale measurements. *Engineering Geology*, **108**: 259-271.

Clarke, R. J. (1959). *A reconnaissance study of joints in Precambrian and Paleozoic rocks near Kingston, Ontario.* Queen's University. Master's thesis. 118p.

Condie, K. C. (1989). *Plate Tectonics & Crustal Evolution.* 3rd ed. Oxford, Pergamon Press. 476p.

Corrigan, D. & Hanmer, S. (1997). Anorthosites and related granitoids in the Grenville orogen: a product of convective thinning of the lithosphere? *Geology*, **25**: 61-64.

Corthésy, R. (2000). *Mesure de contraintes in situ, mine Niobec.* Centre de développement technologique de l'École Polytechnique.

Cripps, A. C. & McCann, D. M. (2000). The use of natural gamma log in engineering and geological investigations. *Engineering Geology*, **55**: 313-324.

Cruden, D. M. (1988). Subsurface fracture surveys using a borehole television camera and acoustic televiewer: discussion. *Canadian Geotechnical Journal*, **25**: 843.

Darcy, H. 1856. *Les fontaines publiques de la Ville de Dijon.* Victor Dalmont, Paris. 647p.

Degnan, J. R.; Clark, S. F.; Harte, P.T. (2004). Integration of geophysics, geologic mapping and water-level monitoring to characterize the hydrogeology of a fractured bedrock site in Berlin, New Hampshire. Symposium on the application of geophysics to engineering and environmental problems: Environmental and Engineering Geophysical Society Annual Meeting, *ENVO5*: 759-769.

Dickin, A. P. & Higgins, M. D. (1992). Sm/Nd evidence for a major 1.5Ga crust-forming event in the central Grenville Province. *Geology*, **20**: 137-140.

Dimroth, E.; Woussen, G.; Roy, D. W. (1981). Geologic history of the Saguenay region, Quebec (Central Granulite Terrain of the Grenville Province): a working hypothesis. *Canadian Journal of Earth Sciences*, **18**: 1506-1522.

Doig, R. (1991). U-Pb zircon dates of Morin anorthosite suite rocks, Grenville Province, Quebec. *Journal of Geology*, **99**: 729-738.

Domenico, P. & Schwartz, F. (1990). *Physical and Chemical Hydrogeology.* New York, John Wiley & Sons. 824p.

Du Berger, R.; Roy, D. W.; Lamontagne, M.; Woussen, G.; North, R. G.; Wetmiller, R. J. (1991). The Saguenay (Quebec) earthquake of Novermber 25, 1988: seismologic data and geologic setting. *Tectonophysics*, **186**: 59-74.

Duchesne, J. C.; Liégeois, J. P.; Auwera, J. V.; Longhi, J. (1999). The crustal tongue melting model and the origin of massive anorthosites. *Terra Nova*, **11** (2/3): 100-105.

Dunne, W. M. & Hancock, P. L. (1994). *Paleostress analysis of small-scale brittle structures*. *In:* Hancock, P. L. (1994). *Continental deformation*. Oxford, Pergamon Press. Pp. 101-120.

Dutra, T. V. & Aziz, K. (1992). A new double-porosity reservor model for oil/water flow problems. *Society of Petroleum Engineers: Reservoir Engineering*, **7** (4): 419-425.

Environment Canada. (2012). *Water quantity*. Environment Canada. Available at: <http://www.ec.gc.ca/eau-water/default.asp?lang=En&n=2DE7B40F-1>. Accessed on April 9th 2012.

Evans, J. P.; Forster, C. B.; Goddard, J. V. (1997). Permeability of fault-related rocks, and implications for hydraulic structure of fault zones. *Journal of Structural Geology*, **19** (11): 1393-1404.

Faure, S.; Tremblay, A.; Angelier, J. (1996). Alleghanian paleostress reconstruction in the northern Appalachias: intraplate deformation between Laurentia and Gondwana. *Geological Society of America Bulletin*, **108**: 1467-1480.

Fernandes, A. J. (2008). Aqüíferos fraturados: uma revisão dos condicionantes geológicos e dos métodos de investigação. *Revista do Instituto Geológico*, **29** (1/2): 49-72.

Fernandes, A. J. & Rouleau, A. (2008). Simulação de deslocamentos em fraturas em basaltos da Formação Serra Geral (Ribeirão Preto, SP) e implicações para a sua transmissividade. *In:* XV Congresso Brasileiro de Águas Subterrâneas. Natal, Brazil. CD-ROM, 20p.

Fernandes, A. J. & Rudolph, D. L. (2001). The influence of Cenozoic tectonics on the groundwater-production capacity of fractured zones: a case study in Sao Paulo, Brazil. *Hydrogeology Journal*, **9**: 151-167.

Fernandes, A. J.; Perrota, M. M.; Salvador, E. D.; Azevedo, S. G.; Gimenez Filho, A.; Paulon, N. (2007). Potencial dos aqüíferos fraturados do Estado de São Paulo: condicionantes geológicos. *Águas Subterrâneas*, **21** (1): 65-84.

Fernandes, A. J.; Maldaner, C. H.; Rouleau, A. (2011) Análise das Fraturas nos Basaltos de Ribeirão Preto, SP: Aplicação à Elaboração de Modelo Hidrogeológico Conceitual *Revista Geologia USP*. Série Científica.

Fernandes, A. J.; Assis Negri, F.; Azevedo Sobrinho, J. M.; Varnier, C. (2012) Análise de fraturas dos basaltos do Aquífero Serra Geral e o potencial de recarga regional do Sistema Aquífero Guarani. *Boletín Geológico y Minero*, **123** (3): 325-339.

Francese, R.; Mazzarini, F.; Bistacchi, A.; Morelli, G.; Pasquarè, G.; Praticelli, N.; Robain, H.; Wardel, N.; Zaja, A. (2009). A structural and geophysical approach to the study of fractured aquifers in the Scansano-Magliano in Toscana Ridge, southern Tuscany, Italy. *Hydrogeology Journal*, **17**: 1233-1246.

Gaudreault, M.; Rouleau, A.; Archambault, G. (1994). A numerical and field study of the role of stress perturbation on rock mass permeability around mine openings. 47th Canadian Geotechnical Conference, *Proceedings*: 389-398.

Ghez, F. & Janot,P. (1974). Calcul statistique du volume des blocs matriciels d'un gisement fissuré. *Revue de l'Institut Français du Pétrole*, **XXIX** (3) : 375-386.

Gilman, J. R. & Kazemi, H. (1983). Improvements in simulation of naturally fractured reservoirs. *Society of Petroleum Engineers Journal*, **23** (4): 695-707.

Gleeson, T. (2009). *Groundwater recharge, flow and discharge in a large crystalline watershed.* Queen's University, PhD thesis in Doctor of Philosophy. 251p.

Gleeson, T. & Novakowski, K. (2009). Identifying watershed-scale barriers to groundwater flow: Lineaments in the Canadian Shield. *Geological Society of America Bulletin*, **121** (3/4): 333-347.

Gleeson, T.; Novakowski, K.; Kyser, T. K. (2009). Extremely rapid and localized recharge to a fractured rock aquifer. *Journal of Hydrology*, **376**: 496-509.

Gower, C. F.; Heaman, L. M.; Loverage, W. D.; Scharer, U.; Tucker, R. D. (1991). Grenvillian magmatism in the eastern Grenville Province, Canada. *Precambrian Research*, **51**: 315-336.

Grauch, V. J. S.; Sawyer, D. A.; Fridrich, C. J.; Hudson, M. R. (1999). *Geophysical framework of the Southwestern Nevada Volcanic Field and hydrogeologic implications.* U. S. Geological Survey Professional Paper 1608.

Grégoire, M. (1988). *Développement d'un programme de calcul de l'effet des contraintes géomécaniques sur l'ouverture des fractures au pourtour des cavités souterraines cylindriques.* Université du Québec à Chicoutimi. Bachelor's graduation project.

Gustafson, G. & Krásný, J. (1994). Crystalline rock aquifers: their occurrence, use and importance. *Hydrogeology Journal*, **2** (2): 64-75.

Haimson, B. C.; Lee, M. Y.; Feknous, N.; Courval, P. (1996). Stress Measurements at the site of the SM3 hydroelectric scheme near Sept Iles, Quebec. *International Journal of Rock Mechanics and Mineral Sciences & Geomechanics Abstracts*, **33** (5): 487-497.

Hancock, P. L. (1985). Brittle microtectonics: principles and practice. *Journal of Structural Geology*, **7**: 437-457.

Harrap, R. & Lato, M. (2010). *An overview of LiDAR: collection to applications.* Available at: <http://www.geol.queensu.ca/faculty/harrap/pdf/WhatIsLIDAR_release1.pdf>. Accessed on May 29th 2011.

Hasegawa, H. S. (1991). Four seismogenic environments in eastern Canada. *Tectonophysics*, **186**: 3-17.

Hébert, C. (2004). *Histoire tectonomagmatique d'une partie de la région du Saguenay, Québec.* Excursion des amis du Grenville, Ministère des Resources Naturelles de la Faune et des Parcs & Université de Québec à Chicoutimi. 48p.

Hébert, C. & Lacoste, P. (1998). Géologie de la région de Jonquière-Chicoutimi (22D/06). Ministère de Ressources Naturelles du Québec, RG 97-08. 31p.

Hébert, C. & van Breemen, O. (2004). Mesoproterozoic basement of the Lac-St-Jean anorthosite suite and younger intrusions in the Saguenay region, Quebec: structural relationships and U-Pb geochronology. *In*: Tollo, R. P.; Corriveau, L.; McLelland, J.; Bartholomew, M. J. (eds). *Proterozoic tectonic evolution of the Grenville orogen in North America.* Geological Society of America, Memoir 197: 65-79.

Hébert, C.; Chown, E. H.; Daigneault, R. (1998). *Tectono-magmatic history of he Saguenay region (Grenville Province) - Field Trip Guidebook*, vol. A6. Geological Association of Canada, Canada. 68p.

Henriksen, H. & Braathen, A. (2006). Effects of fracture lineaments and in-situ rock stresses on groundwater flow in hard rocks: a case study from Sunnfjord, western Norway. *Hydrogeology Journal*, **14**: 444-461.

Hervet, M. (1986). *Chronostratigraphie et petrographie du complex gneissique de Chicoutimi en bordure du complexe anorthositique du Lac-St-Jean.* Université du Québec à Chicoutimi. Masters thesis in Earth Sciences. 403p.

Hervet, M.; van Breemen, O.; Higgins, M. D. (1994). U-Pb crystallization age near the southeast margin of the Lac-St-Jean anorthosite complex, Grenville Province, Quebec. *In:* Radiogenic age and isotopic studies, Report 8. Geological Survey of Canada Current Research, 1994-F: 115-124.

Higgins, M. D. & van Breemen, O. (1992). The age of the Lac-Saint-Jean Anorthosite Complex and associated mafic rocks, Grenville Province, Canada. *Canadian Journal of Earth Sciences*, **29**: 1412-1423.

Higgins, M. D. & van Breemen, O. (1996). Three generations of anorthosite – mangerite – charnockite – granite (AMCG) magmatism, contact metamorphism and tectonism in the Saguenay - Lac-Saint-Jean region of the Grenville Province, Canada. *Precambrian Research*, **79**: 327-346.

Higgins, M. D.; Ider, M.; Breemen, O. V. (2002). U-Pb ages of plutonism, wollastonite formation, and deformation in the central part of the Lac-Saint-Jean anorthosite suite. *Canadian Journal of Earth Sciences*, **39**: 1093-1105.

Hocq, M. (1994). Géologie du Québec. MM94-01, Ministère des Ressources Naturelles du Québec. 154p.

Hodgson, R. A. (1961). Regional study of joining in Comb Ridge-Navajo Mountain area, Arizona and Utah. *American Association of Petroleum Geologists Bulletin*, **45**: 1-38.

Hoffman, P. F. (1989). Precambrian geology and tectonic history of North America. *In:* Bally, A. W. & Plimer, A. R. (eds). *The geology of North America – an overview.* Geological Society of America, Colorado, pp. 447-512.

Isachsen, Y. W. (1989). Investigation of the Hudson-Champlain lineament, New York, Hudson River portion. *In*: Barosh, P. J. (ed). *New England seismotectonic study activities during the fiscal year 1980.* (1989). U. S. Nuclear Regulatory Commission. Pp. 50-52.

Kazemi, H.; Seth, M. S.; Thomas G. W. (1969). The interpretation of interference tests in naturally fractured reservoirs with uniform fracture distribution. Journal of Petroleum Technology, **246**: 463-472.

Kazemi, H.; Merrill Jr., L. S.; Porterfield, K. L.; Zeman, P. R. (1976). Numerical simulation of water-oil flow in naturally fractured reservoirs. *Society of Petroleum Engineers Journal*, **16** (6): 317-326.

Kemeny, J.; Turner, K.; Norton, B. (2006). LIDAR for rock mass characterization: hardware, software, accuracy and best-practices. *In*: Tonon, F. & Kottenstette, J. (eds). *Laser and photogrammetric methods for rock face characterization.* American Rock Mechanics Association, 42-61.

Kresic, N. (1995). Remote sensing of tectonic fabric controlling groundwater flow in Dinaric Karst. *Remote Sensing of Environment*, **90**: 53-85.

Krogh, T. E. (1994). Precise U-Pb ages for Grenvillian and pre-Grenvillian thrusting of Proterozoic and Archean metamorphic assemblages in the Grenville Front tectonic zone, Canada. *Tectonics*, **13**: 963-982.

Kumarapeli, P. S. (1970). Monteregian alkalic magmatism and the St. Lawrence rift system in space and time. *Canadian Mineralogist*, **10** (3): 421-431.

Kumarapeli, P. S. (1981). Origin and development of the Ottawa graben. Lunar and Planetary Institute, USA. Conference on the processes of planetary rifting, *LPI Contribution*, Issue 457: 114-116.

Kumarapeli, P. S. (1985). Vestiges of Iapetan rifting craton west of the northern Appalachians. *Geoscience Canada*, **12** (2): 54-59.

Kumarapeli, P. S. & Saull, V. A. (1966). The St. Lawrence Valley System: a North American equivalent of the East African Rift Valley System. *Canadian Journal of Earth Sciences*, **3**: 639-658.

Lachassagne, P.; Wyns, R.; Bérard, P.; Bruel, T.; Chéry, L.; Coutand, T.; Desprats, J. F.; Le Strat, P. (2001). Exploitation of high-yields in hard-rock aquifer downscaling methodology combining GIS and multicriteria analysis to delineate field prospecting zones. *Ground Water*, **39** (4): 568-581.

Lajoie, P-L. (2010). *Caractérisation du massif de carbonatite de la mine Niobec sous le niveau 1000 et analyse de la stabilité du pilier de niveau.* Université du Québec à Chicoutimi. Master's thesis in Applied Sciences. 403p.

Lasalle, P. & Tremblay, G. (1978). Dépôts meubles Saguenay – Lac Saint-Jean. Ministère des Resources Naturelles, *Rapport géologique*, **191**. 61p.

Lato, M.; Hutchinson, J.; Diederichs, M.; Kalenchuk, K. (2007). Evaluating block shape and block volume distributions of rock faces using LiDAR and 3DEC. *Geophysical Research Abstracts*, **9** (01171).

Lato, M.; Hutchinson, D. J.; Diederichs, M. S.; Ball, D.; Harrap, R. (2009) Engineering monitoring of rockfall hazards along transportation corridors: using mobile terrestrial LiDAR. *Natural Hazards and Earth System Sciences*, **9**: 935–946.

Lato, M.; Diederichs, M. S.; Hutchinson, D. J. (2010). Bias correction for view-limited LiDAR scanning of rock outcrops for structural characterization. *Rock Mechanics and Rock Engineering*, **43**: 615-628.

Lau, J. S. O.; Auger, L. F.; Bisson, J. G. (1987). Subsurface fracture surveys using a borehole television camera and acoustic televiewer. *Canadian Geotechnical Journal*, **24**: 499-508.

Lau, J. S. O.; Auger, L. F.; Bisson, J. G. (1988). Subsurface fracture surveys using a borehole television camera and acoustic televiewer: reply. *Canadian Geotechnical Journal*, **25**: 844-845.

Long, J. C. S.; Remer, J. S.; Wilson, C. R. Witherspoon, P. A. (1982). Porous media equivalents for networks of discontinuous fractures. *Water Ressources Research*, **18** (3): 645-658.

Lough, M. F.; Lee, S. H.; Kamath, J. (1997). A new method to calculate effective permeability of gridblocks used in the simulation of naturally fractured reservoirs. *Society of Petroleym Engineers: Reservoir Engineering*, **12** (3): 219-224.

Madrucci, V. (2004). Prospecção de água subterrânea em terreno cristalino utilizando-se análise integrada de dados de sensoriamento remoto, geofísicos e técnicas de geoprocessamento, região de Lindóia, SP. Universidade de São Paulo. PhD thesis. 226p.

Marcantonio, F.; McNutt, R. H.; Dickin, A. P.; Heaman, L. M. (1990). Isotopic evidence for the crustal evolution of the Frontenac Arch in the Grenville Province of Ontario, Canada. *Chemical Geology*, **83**: 297-314.

Masoud, A. & Koike, K. (2006). Tectonic architecture through Landsat-7 ETM+/SRTM DEM-derived lineaments and relationship to the hydrogeologic setting in Siwa region, NW Egypt. *Journal of African Earth Sciences*, **45**: 467-477.

Mattila, J. & Tammisto, E. (2012). Stress-controled fluid flow in fractures at the site of a potential nuclear waste repository, Finland. *Geology*, **40** (4): 299-302.

Mauldon, M. & Mauldon, J. G. (1997). Fracture sampling on a cylinder: from scanlines to boreholes and tunnels. *Rock Mechanics and Rock Engineering*, **30** (3): 129-144.

Mazzotti, S. & Townend, J. (2010). State of stress in central and eastern North American seismic zones. *Lithosphere*, **2** (2): 76-83.

McLelland, J. M. & Chiarenzelli, J. (1990). Isotopic constraints on emplacement age of anorthositic rocks, Adirondack Mts, New York. *Journal of Geology*, **98**: 19-43.

MDDEP. (2000). *Portrait régional de l'eau: Saguenay-Lac-Saint-Jean (Région administrative 02).* Ministère du Développement Durable, Environnement et Parcs. Available at: <http://www.mddep.gouv.qc.ca/eau/regions/region02/index.htm>. Accessed on May 10th 2012.

Megan, T. W.; Roden-Tice, M. K.; Tremblay, A. (2010). Late Paleozoic to Early Mesozoic unroofing of the Canadian Shield in southern Quebec based on apatite fission-track analysis. *In:* Geological Society of America, Northeastern Section (45th Annual) and Southeastern Section (59th Annual) Joint Meeting. *Abstracts Programs*, **42** (1): 84.

Miller, S. M. (1983). A statistical method to evaluate homogeneity of structural populations. *Mathematical Geology*, **15** (2): 317-328.

Moore, J. M. & Thompson, P. (1980). The Flinton group: a late Precambrian metasedimentary sequence in the Grenville Province of eastern Ontario. *Canadian Journal of Earh Sciences*, **17**: 1685-1707.

Morin, R. H. & Savage, W. Z. (2003). Effects of crustal stresses on fluid transport in fractured rock: case studies from northeastern and southwestern USA. *Hydrogeology Journal*, **11**: 100-112.

Morin, R. H.; Hess, A. E.; Paillet, F. L. (1988). Determining the distribution of hydraulic conductivity in a fractured limestone aquifer by simultaneous injection and geophysical logging. *Ground Water*, **26** (5) : 587-595

Morin, R.; Carleton, G. B.; Poirier, S. (1997). Fractured-aquifer hydrogeology from geophysical logs; the Passaic Formation, New Jersey. *Groundwater*, **35** (2): 328-338.

Morin, R.; Godin, R.; Nastev, M.; Rouleau, A. (2007). Hydrogeologic controls imposed by mechanical stratigraphy in layered rocks of the Châteauguay River Basin, a U.S.-Canada transborder aquifer. *Journal of Geophysical Research*, **112**.

Mortimer, L.; Aydin, A.; Simmons, C. T.; Love, A. J. (2011a). Is in situ stress important to groundwater flow in shallow fractured rock aquifers? *Journal of Hydrogeology*, **399** (3): 185-200.

Mortimer, L.; Aydin, A.; Simmons, C. T.; Heinson, G.; Love, A. J. (2011b). The role of *in situ* stress in determining hydraulic connectivity in a fractured rock aquifer (Australia). Hydrogeology Journal, **19**: 1293-1312.

Nastev, M.; Savard, M. M.; Lapcevic, P.; Lefebvre, R.; Martel, R. (2004). Hydraulic properties and scale effects investigation in regional rock aquifers, south-western Quebec, Canada. *Hydrogeology Journal*, **12**: 257-269.

Nastev, M.; Rivera, A.; Lefebvre, R.; Martel, R. (2005). Numerical simulation of groundwater flow in regional rock aquifers, southwestern Quebec, Canada. *Hydrogeology Journal*, **13**: 835-848.

Natural Ressources Canada. (1999). *The Atlas of Canada: Political divisions (interactive).* Published online; last modification on 2007. Available at: <http://atlas.nrcan.gc.ca/site/english/maps/reference/national/politicaldivisonsinteractive/1>. Accessed on 2012, February 16th.

Neuman, S. P. (2005). Trends, prospects and challenges in quantifying flow and transport through fractured rocks. *Hydrogeology Journal*, **13**: 124-147.

Noël, J. F. (2009). *Modélisations numérique et analytique d'instabilités en kink dans des masses rocheuses discontinues.* Université du Québec à Chicoutimi. PhD thesis. 245p.

O'Leary, D. W.; Friedman, J. D.; Pohn, H. A. (1976). Lineaments, linear, lineation – some proposed new standards for old terms. *Geological Society of America Bulletin*, **87**: 1463-1469.

Oda, M. (1985). Permeability tensor for discontinuous rocks masses. *Géotechnique*, **35** (4): 483-495.

Odeh, T.; Salameh, E.; Schirmer, M.; Strauch. G. (2009). Structural control of groundwater flow regimes and groundwater chemistry along the lower reaches of the Zerka River, West Jordan, using remote sensing, GIS, and field methods. *Environmental Geology*, **58**: 1797-1810.

Osberg, P. H. (1978). Synthesis of the geology of the Northeastern Appalachians, USA: Caledonian Appalachian Orogen of the North Atlantic region. *Geological Survey of Canada paper*, **24**: 137-147.

Pate, K. & Haneberg, W. C. (2011). Photogrammetric and LiDAR 3-D rock slope discontinuity mapping and interpretation surveys to improve baseline information for supporting design and construction of capital improvement projects at hydroelectric facilities. *In*: 45th US Rock Mechanics / Geomechanics Symposium. San Francisco. American Rock Mechanics Association. ARMA 11-520.

Petit, J. P. (1987). Criteria for the sense of movement on fault surfaces in the brittle rocks. *Journal of Structural Geology*, **9** (5/6): 597-608.

Pino, D. S.; Rouleau, A.; Roy, D.; Daigneault, R. (2010). Hydrogéologie structurale sur le seuil de Kénogami : premiers résultats. *In*: 1er Colloque des Eaux Souterraines du Québec, Chicoutimi, Canada. *Résumés*. Abstract.

Pino, D. S.; Rouleau, A.; Roy, D.; Daigneault, R. (2011a). Analysis of the joint system in the Kenogami uplands bedrock aquifer: methodology and preliminary results. *In:* GeoHydro, Quebec, Canada. *Proceedings Papers*, DOC-2165.

Pino, D. S.; Rouleau, A. ; Roy, D. ; Daigneault, R. (2011b). Analyse du système de fractures dans l'aquifère rocheux du seuil de Kénogami au Saguenay: résultats préliminaires. *In*: Carrefour des sciences de la Terre, Chicoutimi, Canada. *Résumés*, 42. Abstract.

Pino, D. S.; Rouleau, A.; Roy, D.; Daigneault, R.; Fernandes, A. J. (2012a). Joint system and tectonic analysis of a crystalline bedrock aquifer: case study of the Kenogami uplands, Quebec, Canada. *In:* International Conference on Groundwater in Fractured Rocks. Prague, Czech Republic. *Volume of Abstracts*: 30-31.

Pino, D. S.; Rouleau, A.; Roy, D.; Daigneault, R.; Fernandes, A. J. (2012b). Estimation des propriétés hydrauliques d'un aquifère fracturé à partir de données structurales, hydrogéologiques et géomécaniques: cas du seuil de Kénogami, graben du Saguenay. *In:* GRIES, 80e Congrès de l'ACFAS. Available at: <http://www.acfas.ca/evenements/congres/programme/80/200/209/c>.

Pollard, D. D. & Aydin, A. (1988). Progress in understanding jointing over the past century. *Geological Society of America Bulletin*, **100**: 1181-1204.

Price, N. (1966). *Fault and joint development in brittle and semi-brittle rock.* Oxford, Pergamon Press. 176p.

Priest, S. D. (1993). *Discontinuity analysis for rock engineering.* London, Chapman & Hall. 473p.

Ramsay, J. G. & Huber, M. I. (1987). *The techniques of modern structural geology, volume I.* London, Academic Press. 307p.

Raven, K. G. (1986). Hydraulic characterization of a small ground-water flow system in fractured monzonitic gneiss. Inland Waters Directorate; National Hydrogeology Ressearch Institute. *WHRI Paper* n°30, *IDW Scientific series* n°149. 133p.

Rimando, R. E. & Benn, K. (2005). Evolution of faulting and paleo-stress field within the Ottawa graben, Canada. *Journal of Geodynamics*, **39**: 337-360.

Rivers, T. (1997). Lithotectonic elements of the Grenville Province: review and tectonic implications. *Precambrian Research*, **86**: 117-154.

Rivers, T.; Martignole, J.; Gower, C. F.; Davidson, A. (1989). New tectonic divisions of the Grenville Province, southeast Canadian Shield. *Tectonics*, **8** (1): 63-84.

Rives, T.; Razack, M.; Petit, J-P.; Rawsley, K. D. (1992). Joint spacing: analogue and numerical simulations. *Journal of Structural Geology*, **14** (89): 925-937.

Rives, T.; Rawnsley, K. D.; Petit, J.P. (1994). Analogue simulation of natural orthogonal joint set formation in brittle varnish. *Journal of Structural geology*, **16** (3): 419-429.

Robinson, D. A.; Binley, A.; Crook, N.; Day-Lewis, F. D.; Ferré, T. P. A.; Grauch, V. J. S.; Knight, R.; Knoll, M.; Lakshmi, V.; Miller, R.; Nyquist, J.; Pellerin, L.; Singha, K.; Slater, L. (2008). Advancing process-based watershed hydrological research using near-surface geophysics: a vision for, and review of, electrical and magnetic geophysical methods. *Hydrological Processes*, **22**: 3604–3635.

Rocha, M. & Franciss, F. (1977). Determination of permeability in anisotropic rock-masses from integral samples. *Rock Mechanics*, **9**: 67-93.

Roden-Tice, M. K.; Tremblay, A.; Garcia, S. M. (2011) Evidence for Mesozoic fault reactivation and unroofing of the Canadian Shield in southern Quebec based on apatite fission-track analysis. *In:* Geological Society of America, Northeastern (46th Annual) and North-Central (45th Annual) Joint Meeting, *Abstracts with Programs*, **43** (1): 72.

Röller, K. & Trepmann, C. A. (2008). *Stereo 32 – version 1.0.1.* Ruhr-Universität Bochum, Institut für Geologie, Mineralogie & Geophysik.

Rondot, J. (1972). Transgression ordovicienne dans Charlevoix, Québec. *Journal Canadien Sciences de la Terre*, **9**: 1187-1203.

Rouleau, A. (1984). *Statistical characterization and numerical simulation of a fracture system – application to groundwater flow in the Stripa granite.* University of Waterloo. PhD thesis. 416p.

Rouleau, A. & Gale, J. E. (1985). Statistical characterization of the fracture system in the Stripa Granite, Sweden. *International Journal of Rock Mechanics and Mining Science & Geomechanics Abstracts*, **22** (6): 353-367.

Rouleau, A. & Gale, J. E. (1987). Stochastic discrete fracture simulation of groundwater flow into an underground excavation in granite. *International Journal of Rock Mechanics and Mining Sciences*, **24** (2): 99-112.

Rouleau, A.; Cousineau, P.; Denis, C.; Lapcevic, P. (1996). The estimation of hydraulic parameters of a fractures orthoquartzite formation at the laboratory and field scales. *Rock Mechanics*, Aubertin, Hassani & Mitri (eds), 1359-1366.

Rouleau, A.; Walter, J.; Daigneault, R.; Chesnaux, R.; Roy, D.; Germaneau, D.; Lambert, M.; Moisan, A.; Nöel, D. (2011). Un aperçu de la diversité hydrogéologique du territoire du Saguenay-Lac-Saint-Jean (Québec). *In:* GeoHydro, Quebec, Canada. *Proceedings Papers*, DOC-2195.

Roy. D. W. (2009). *Notes sur la géologie des dépôts meubles au Saguenay Lac-Saint-Jean.*16p. UQAC internal document, prepaired for the purpose of the project of Quaternary Mapping from the PACES-SLSJ.

Roy, D. W.; Shmitt, L.; Woussen, G.; DuBerger, R. (1993). Airbone SAR images and the tectonic setting of the 1988 Saguenay earthquake, Québec, Canada. *Journal of Photogrammetric Engeneering and Remote Sensing*, **59**: 1299-1305.

Roy, D. W.; Du Berger, R.; Woussen, G. (1998). Did the opening of the Central Atlantic Ocean reactivate faults in the Charlevoix - Saguenay area?. Eastern section meeting of the Seismological Society of America, *Seismological Research Letters*, **69** (1): 83.

Roy, D. W.; Tremblay, M-L.; Verreault, M. (2006). *Les différents types d'aquifères au Québec. In*: Rasmussen, H.; Rouleau, A.; Chevalier, S. (eds). *Outils de détermination d'aires d'alimentation et de protection de captages d'eau souterraine.* 2nd ed. Centre d'Études sur les Ressources Minérales, Université du Québec à Chicoutimi et Ministère du Développement Durable, Environment et Parcs.

Roy, J.; Morin, R.; Chesnaux, R.; Richard, S.; Pino, D. S.; Rouleau, A.; Roy, D. W.; Noël, D. (2011). Hydrogeological insight from geophysical water-well logging in hard rocks in the Saguenay region, Québec. *In:* GeoHydro, Quebec, Canada. *Proceedings Papers*, DOC-2288.

Ruhland, M. (1973). Méthode d'étude de la fracturation naturelle des roches associée à divers modèles structuraux. *Sciences Géologiques Bulletin*, **26** (2-3): 91-113.

Santosh, M.; Maruyama, S.; Yamamoto, S. (2009). The making and breaking of supercontinents: some speculations based on superplumes, super downwelling and the role of tectosphere. *Gondwana Research*, **15** (3/4): 324-341.

Schwartz, F. W.; Smith, L.; Crowe, A. S. (1983). A stochastic analysis of macroscopic dispersion in fractured media. *Water Resources Research*, **19** (2): 1253-1265.

Selroos, J. O.; Walker, D. D.; Strom, A.; Gylling, B. Follin, S. (2002). Comparison of alternative modeling approaches for groundwater flow in fractured rock. *Journal of Hydrogeology*, **257** (1-4): 174-188.

Singhal, B. B. S. & Gupta, R. P. (2010). *Applied Hydrogeology of Fractured Rocks.* Springer. 408p.

Snow, D. (1965). A parallel plate model of fractured permeable media. University of California. PhD thesis. 331p.

Snow, D. (1968). Rock fracture spacings, openings and porosities. *Journal of Soil Mechanics and Foundations Division*, **94** (1).

Snow, D. (1969). Anisotropic permeability of fractured media. *Water Ressources Research*, **5** (6): 1273-1289.

Snow, D. (1970). The frequency and apertures of fractures in rock. *International Journal of Rock Mechanics and Mineral Sciences*, **7**: 23-40.

Sonier, F.; Souillard, P.; Blaskovich, F. T. (1988). Numerical simulation of naturally fractured reservoirs. *Society of Petroleum Engineers Journal*, **3** (4): 1114-1122.

Srivastava, S. P. (1978). Evolution of the Labrador Sea and its bearing on the early evolution of North Atlantic. *Geophysical Journal Royal Astronomical Society*, **52**: 313-357.

Statistics Canada. (2011). *2011 Census population counts*. Available at: <http://www12.statcan.gc.ca/census-recensement/index-eng.cfm>. Accessed on April 9th 2012.

Stearns, D. W. (1969). Certain aspects of fracture in naturally deformed rocks. *In:* Riecker, R. E. (ed), *Rock mechanics seminar*: 97-118. Massachusetts, Air Force Cambridge Research Laboratory.

Stockwell, C. H. (1962). *A tectonic map of the Canadian Shield. In: The tectonics of the Canadian Shield.* The Royal Society of Canada, Special Publications, **4**: 6-15.

Streltsova, T. D. (1976). Hydrodynamics of groundwater flow in a fractured formation. *Water Resour. Research*, **12** (3): 405-414

Sultan, M.; Wagdy, A.; Manocha N.; Sauck, W.; Gelil, K. A.; Youssef, A. F.; Becker, r.; Milewski, A.; Alfy, Z. E.; Jones, C. (2008). An integrated approach for identifying aquifers in transcurrent fault systems: the Najd shear system of the Arabiam Nubian shied. *Journal of Hydrology*, **349**: 475-488.

Surrete, M. J. (2006). *Quantifying heterogeneity in variably fractured rock using a hydrostructural domain approach, Gulf Islands, British Columbia*. Simon Fraser University. Master's thesis in Earth Sciences. 129p.

Terzaghi, R. D. (1965). Sources of error in joint surveys. *Geotechnique*, **15** (3): 287-304.

Tezuka, K. & Watanabe, K. (2000). Fracture network modeling of Hijiori hot dry rock reservoir by deterministic and stochastic crack network simulator (D/SC). IGA, World Geothermal Congress, *Proceedings*: 3934-3938

Thivierge, S.; Roy. D.R.; Chown, E. H.; Gauthier, A. (1983). Evolution du Complexe Alcalin de St. Honoré (Québec) après sa mise en place. *Mineralium Deposita*, **18** : 267-283.

Thomas, W. A. (1991). The Appalachian-Ouachita rifted margin of southeastern North America. *Geological Society of America Bulletin*, **103** (3): 415-431.

Thomas, W. A. & Astini, R. A. (1996). The Argentine precordillera: a traveler from the Ouachita embayment of North American Laurentia. *Science*, **273**: 752-757.

Tirén, S. (1991). Geological setting and deformation of a low-angle fracture zone at Finnsjon, Sweden. *Journal of Hydrology*, **126**: 17-43.

Tjia, H. D. (1964). Slickensides and fault movements. *Geological Society of America Bulletin*, **75**: 683-686.

Tollo, R. P.; Corriveau, L.; McLelland, J.; Bartholomew, M. J. (2004). Proterozoic tectonic evolution of the Grenville orogen in North America: An introduction. *In*: Tollo, R. P.; Corriveau, L.; McLelland, J.; Bartholomew, M. J. (eds). *Proterozoic tectonic evolution of the Grenville orogen in North America*. Geological Society of America, Memoir 197: 1-18.

Trudel, C. & Malo, M. (1993). Analyses des contraintes par méthodes graphiques dans une zone de coulissage : exemple de la région de Matapédia, Appalaches du Québec. *Canadian Journal of Earth Sciences*, **30** : 591-602.

UNESCO. (1984). Ground water in hard rocks. *Studies and reports in hydrogeology 33.* UNESCO, Paris.

USGS. (2010). *Earthquake Hazards Program: Glossary*. Available at: <http://earthquake.usgs.gov/hazards/qfaults/glossary.php>. Accessed at August 20th 2010.

Van Breemen, O. & Davidson, A. (1988). U-Pb zircon ages of granites and syenites in the Central Metasedimentary Belt, Grenville Province, Ontario. *In:* Radiogenic age and isotope studies, Report 2 Geological Survey of Canada. Paper, **88** (2): 45-50.

Verreault, M. (2000). *Orientation du graben du Saguenay par rapport aux pôles de rotation d Euler successifs de l'Amérique du Nord au cours du Phanerozoïque*. Université du Québec à Chicoutimi, Bachelor's graduation project. 44p.

Wallach, J. L.; Mohajer, A. A.; McFall, G. H.; Bowlby, J. R.; Pearce, M.; McKay, D. A. (1993). Pop-ups as geological indicators of earthquake-prone areas in intraplate Eastern North America. *Quaternary Proceedings*, **3**: 67-83.

Walter, J.; Lambert, M.; Rouleau, A.; Daigneault, R.; Moisan, A.; Germaneau, D.; Chesnaux, R.; DePinel, M. (2010). *Rapport d'étape de la phase I basée sur les données existantes et planification revisée de la phase II*. PACES – Programme d'Acquisition de Connaissances sur les Eaux Souterraines du Québec. 86p and 30 maps.

Warren, J. E. & Root, P. J. (1963). The behavior of naturally fractured reservoirs. *Society of Petroleum Engineers Journal*, **3** (3): 245-255.

Weatherill, D.; Graf, T.; Simmons, C. T.; Cook, P. G.; Therrien, R.; Reynolds, D. A. (2008). Discretizing the fracture-matrix interface to simulate solute transport. *Ground Water*, **46** (4): 606-615.

Woussen, G.; Dimroth, E.; Corriveau, L.; Archer, P. (1981). Crystallization and emplacement of the Lac-St-Jean anorthosite massif (Quebec, Canada). *Contributions to Mineralogy and Petrology*, **76**: 343-350,

Woussen, G.; Martignole, J.; Nantel, S. (1988). The Lac-St-Jean anorthosite in the St-Henri-de-Taillon area (Grenville Province): a relic of a layered complex. *Canadian Mineralogist*, **26**: 1013-1025.

Wynne-Edwards, H. R. (1972). The Grenville Province. *In*: Price, R. A. & Douglas, R. J. W. (eds). *Variations in tectonic styles in Canada.* Geological Association of Canada, Special Paper 11: 263-334.

Zeeb, C.; Göckus, D.; Bons, P.; Ajmi, H. A.; Rausch, R.; Blum, P. (2010). Fracture flow modelling based on satellite images of the Wajid Sandstone, Saudi Arabia. *Hydrogeology Journal*, publié en ligne le 16 juin 2010.

Zhang, K., Wu, Y.S.; Houseworth, J. E.; (2006). Sensitivity analysis of hydrological parameters in modeling flow and transport in the unsaturated zone of Yucca Mountain, Nevada, USA. *Hydrogeology Journal*, **14**: 1599-1619.

Zoback, M. K. (1992). Stress Field constraints on intraplate seismicity in eastern North America. *Journal of Geophysical Research*, **97** (B8): 11,761-11,782.

APPENDIX 1

GLOSSARY

Definitions adopted in the present work, regarding terms of current use.

- Dip: maximum angle from which a planar feature deviates from the horizontal. This angle is measured in a plane perpendicular to the strike.
- Dyke: a sheet-like or tabular igneous intrusion that cuts through a host rock.
- Fault: fracture across which there has been relative displacement (the movement is determined by kinematic indicators). Its two sides are known as *fault walls.*
- Fracture: general term to indicate a physical discontinuity in a rock mass; may refer either to a joint or a fault.
- Groove: a long narrow furrow or channel.
- Joint: "*fractures that show no discernible relative displacements*" (Hodgson 1961; Price 1966; Hancock 1985; Dunne & Hancock 1987; Ramsay & Huber 1987). Joints are considered as the most common result of brittle deformation (Pollard & Aydin 1988).
- Joint set: group of joints whose poles form a concentration on a stereonet of 20° or less in angular width; it is an analytical classification of joints.
- Joint system: the configuration of joints as they are seen in nature.

- Kinematic indicator: geological structures or features that may provide information on the direction, magnitude and mode of transport of a given rock bulk (Bull et al. 2009).
- Lineament: mappable recti-linear feature on the Earth surface, e.g. a straight stream or a ridge, that commonly reflects a subsurface structure (O'Leary *et al.* 1976).
- Pole: line orthogonal in space to a given planar surface.
- Shear: stress that slices rocks into parallel blocks that slide in opposite directions along their adjacent sides.
- Slickenside: striations and grooves on a fault wall parallel to the direction of movement (Tjia 1964).
- Step: breaks on a fault wall. They may indicate the sense of motion of the fault walls: when no infilling is observed, the motion is on contrary to the step; if there is infilling on the fault wall, the motion is on the same sense as the step (Fig. A1.1). Steps are perpendicular or strongly oblique to slickensides. Steps are often observed on joint surfaces in crystalline rocks.
- Strike: direction of the horizontal line on the inclined plane of a geological structure. It is measured from true north.
- Structural domain: defines a region in which the same joint sets were observed everywhere.
- Vein: mineral tabular structure, of hydrothermal origin, that fills fractures of the host rock.

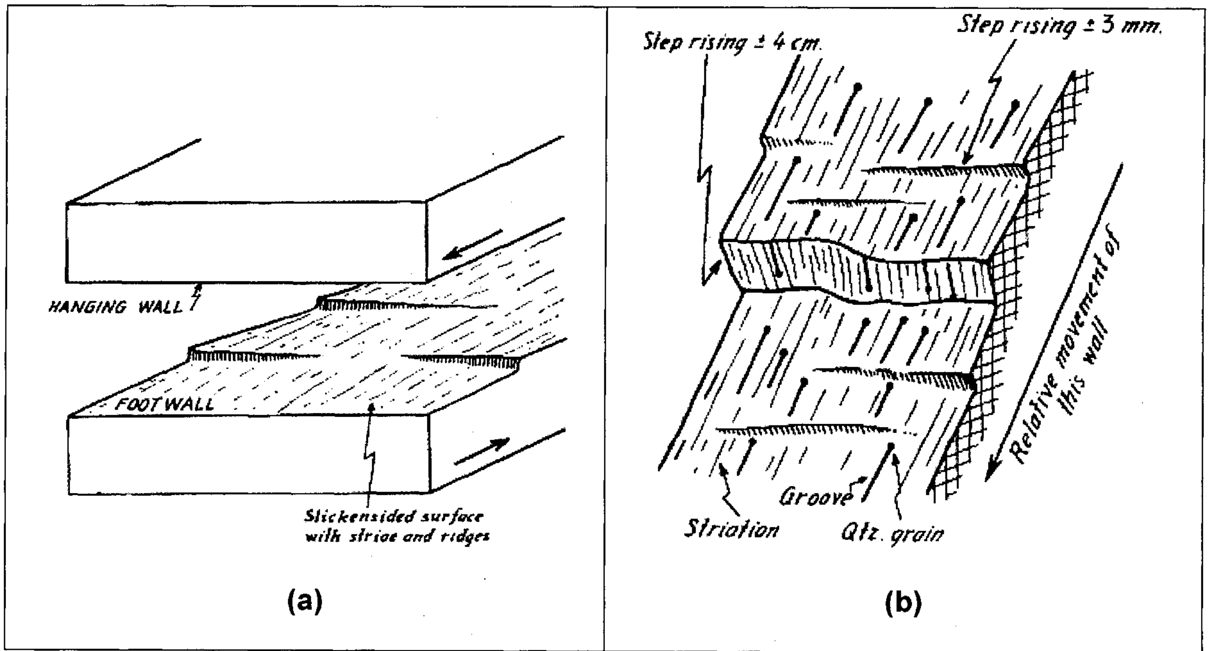

Fig. A1.1 Inferred relative displacement of fault walls based on steps and slickensides. **(a)** The occurrence only of the steps indicates the sense of movement is contrary to this feature. **(b)** The presence also of the slickensides suggests the sense of movement is contrary to the steps. Source: Tjia (1964).

APPENDIX 2

STRUCTURAL SURVEY FORMS

Outcrop description forms developed during structural survey are presented on Figs. A2.1 (detailed survey) and A2.2 (general survey). Table A2.1 presents the acronyms used for filling these forms.

PACES 2010 | Levé en Hydrogéologie Structurale | Fiche de Terrain			
L'équipe			
Affleurement Nº	Zone UTM	X:	Date: ___/___/___
Orient. ligne de levé		Y:	Altitude: m

Nº	Type	Direction	Pendage	Quad. (Pend.)	Distance le long de la ligne de levé (m)	Intersec.	Ouverture unité Type	Longueur (m)	Termin.	Eau	Remplissage (minéraux)
							.	.			
							.	.			
							.	.			

(a)

PACES 2010 | Levé en Hydrogéologie Structurale | Fiche de Terrain			
L'équipe			
Affleurement Nº	Zone UTM	X:	Date: ___/___/___
Orient. ligne de levé		Y:	Altitude: m

Nº	Type	Direction	Pendage	Quad. (Pend.)	Fenêtre (## lettre)	Intersec.	Ouverture unité Type	Longueur (m)	Termin.	Eau	Remplissage (minéraux)
							.	.			
							.	.			
							.	.			

(b)

Fig. A2.1 Outcrop description form for detailed structural survey, for both **(a)** scanline and **(b)** window methods.

PACES 2010 | **Levé en Hydrogéologie Structurale** | Fiche de Terrain		
Général		
L'équipe:		*Date: ___/___/___*
Affleurement	*Localisation*	*Observations*
N°: N° GPS:	Zone UTM: X:	
Direction / Pendage:	Y:	
Dimension:	Altitude:	
Conditions météorologiques	Précision GPS:	
	Environnement	
Température de l'air: °C		

Lithologie		
Nom:		
Minéraux:		
Couleur:	( ) Fraîche ( ) Alterée	
Texture:	Structure:	
Echantillon	N°	Lithologie

PACES 2010 | **Levé en Hydrogéologie Structurale** | Fiche de Terrain		
Général		
L'équipe:		*Date: ___/___/___*
Affleurement	*Localisation*	*Observations*
N°: N° GPS:	Zone UTM: X:	
Direction / Pendage:	Y:	
Dimension:	Altitude:	
Conditions météorologiques	Précision GPS:	
	Environnement	
Température de l'air: °C		

Structures Principales

Nº	Type	Direction	Pendage	Quad. (Pend.)	Intersec.	Ouverture unité Type	Longueur (m)	Termin.	Eau	Remplissage (minéraux)
						.	.			
						.	.			
						.	.			
							.			
							.			
							.			
							.			
							.			
							.			
							.			
							.			
							.			
							.			
							.			
							.			
						.	.			

Zones de Cisaille - général

Nº	Mov	Défor. Type	Défor. Âge	Lithologie Nom	Lithologie Minéraux	Lithologie Texture	Lithologie Structure	Lithologie Direction	Lithologie Pendage	Quad. (Pend.)	Épaisseur (m)	Longueur (m)	Termin.
											.	.	
											.	.	
											.	.	

Fig. A2.2 Outcrop description form for general structural survey.

Table A2.1 Acronyms for outcrop description forms (originally attributed in French).

Structure type	
Rock contact	Cr
Dyke	Dy
Fault	Fa
Fracture	Fr
Foliation	Fo
Gneissosity	Gn
Stria	St
Joint	Jt
Vein	Vn
Mylonite	Ml
Elongated mineral	Am
Axe	Ax
Groove	Cn
Mineral	Mn
Shear zone	ZC
Magmatic bedding	LM

Water	
Flow	Ec
Humidity	Hm
Rust	Ro
Seepage	Su

Joint termination	
Visible	V
Not visible	N

Joint aperture	
Free	L
Filled	R

Shear direction	
Sinistral	S
Dextral	D

Foliation	
Yes	O
No	N

General	
No data	
Does not apply	-
No	N

Texture	
Aphanitic	A
Phaneritic	H
Porphyritic	P
Granoblastic	B
Porphyroblastic	O

Movement indicator type	
negative (observed on the rock)	neg
positive (observed in the filling)	pos
Grades	
Clear "step", visible	A
Ok "step"	B
Uncertain "step"	C

APPENDIX 3

OUTCROP DATA

In the following, summarized data on every outcrop visited during the general survey is presented. Information follows the same format as the fieldwork forms (Appendix 2): outcrop identification, UTM zone and coordinates, outcrop orientation, outcrop dimension, environment, lithology, state of weathering (fresh or weathered), main structures, other observations.

Outcrop ID	UTM Zone	Location		Orientation		Dimension		Environment	Lithology	Fresh or weathered	Structure	Observations
		X	Y	Dir.	Dip	X	Y					
DP-001	19U	325240	5366630	10				roadside	anorthosite	F	fractured	
DP-002	19U	325049	5366701					roadside	anorthosite	F	fractured	
DP-003	19U	323835	5367197					roadside	gabbro		fractured	
DP-004	19U	322643	5367283					roadside	anorthosite		fractured	
DP-005	19U	322505	5367286					roadside	anorthosite	F	fractured	
DP-006	19U	314593	5368528					quarry	anorthosite	F	fractured	
DP-007	19U	315522	5357874					quarry	anorthosite	F	massif	
DP-008	19U	338783	5359324					quarry			fractured	
DP-009	19U	328381	5356417					private property	anorthosite		fractured	
DP-010	19U	326775	5356449					woods	anorthosite	W	massif	
DP-011	19U	330218	5358839					private property	anorthosite	F	fractured	
DP-012	19U	325044	5355094					private property	anorthosite	W	fractured	
DP-013	19U	334431	5353240					roadside	gneiss	W (top)	massif	
DP-014	19U	334452	5353340					roadside	anorthosite	F	fractured	
DP-015	19U	334433	5353458					roadside	anorthosite	F	fractured	
DP-016	19U	334480	5353541					roadside	gneiss	W	fractured; quartz veins	
DP-017	19U	334529	5353601					roadside	anorthosite	F	fractured	
DP-018	19U	334483	5353572					roadside	gneiss	W	massif	
DP-019	19U	332959	5370006	135		30,0	5,0	private property	anorthosite	W	poorly fractured	Covered with lichen; lots of vegetation; hard to reach.
DP-020	19U	332643	5370957	145		40,0	2.5	motocross road	anorthosite	F	fractured	
				169				motocross road	pegmatite	F	fractured	
DP-021	19U	332728	5370888	120		40,0	3,0	motocross road	anorthosite	W	fractured	Between DP-020 and DP-021 there is a granitic intrusion on the anorthosite.
DP-022	19U	331811	5371274	-	0	70,0	60,0	top of outcrop	anorthosite	W	fractured	A lot of vegetation. Granitic vein with 2-5cm width.
DP-023	19U	334187	5367805			90,0	10,0	close to the dam	anorthosite	W	fractured; oriented cristals (E-W)	A lot of lichen.
DP-024	19U	331167	5368416	185				roadside	anorthosite	W	fractured	A lot of lichen.

Outcrop ID	UTM Zone	Location		Orientation		Dimension		Environment	Lithology	Fresh or weathered	Structure	Observations
		X	Y	Dir.	Dip	X	Y					
DP-025	19U	321100	5372894	120		25,0	3,0	roadside	anorthosite	W	fractured; granitic veins	
DP-026	19U	324064	5371790	122		20,0	7,0	private property	anorthosite	W	massif	
DP-027	19U	324629	5371485	35				private property	anorthosite	W	fractured	
DP-028	19U	327758	5368484	135				roadside	anorthosite	W	fractured	
DP-029	19U	326550	5365562	260		100,0	10,0	roadside	anorthosite and gabbro	F	fractured; pegmatite vein	Shear zone.
DP-030	19U	326468	5366069	58	71	85,0	15,0	roadside	anorthosite	F	fractured	
DP-031	19U	310584	5361321	-		15,0	1.5	woods, top of outcrop	anorthosite	W	fractured; granitic vein	
DP-032	19U	305085	5359498	280		15,0	3,0	roadside	anorthosite	W	fractured	Lots of vegetation.
DP-033	19U	306136	5373244	-				grazing	anorthosite	A	fractured	
DP-034	19U	309475	5370536	255		35,0	3.5	roadside	anorthosite	F	fractured	
DP-035	19U	312241	5370573	108		150,0	10,0	roadside	anorthosite	F	fractured	
DP-036	19U	317387	5368085	190		70,0	5,0	roadside	anorthosite	F	fractured	
DP-037	19U	327050	5364580	121		30,0	3,0	private property	anorthosite	W	massif	The top of the outcrop is rounded due to weathering.
DP-038	19U	325391	5364423	6		8,0	2.5	private property	anorthosite	W	fractured	
DP-039	19U	325911	5362815	262		25,0	2,0	roadside	anorthosite	F	fractured	
DP-040	19U	326381	5362925	173		25,0	3,0	roadside	anorthosite	W	fractured	Occurence of exfoliation. Light green weathering. Possible shear zone in opposite side of the road, 10m to north.
DP-041	19U	325534	5364880	296				private property	anorthosite	W	fractured	Not easy to reach, as there is a creek to cross and there are not many places to climb the outcrop.
DP-042	19U	332265	5364620	357		3,0	12,0	private property	anorthosite	W	poorly fractured	Lots of lichen.
DP-043	19U	332027	5364343	-		10,0	4,0	top of outcrop	anorthosite	W	poorly fractured	
DP-044	19U	332003	5364303	-				top of outcrop	anorthosite	W	fractured	Recovered by lichen.
DP-045	19U	313068	5365707	155		15,0	3,0	road near a lake	anorthosite	W	fractured	

Outcrop ID	UTM Zone	Location		Orientation		Dimension		Environment	Lithology	Fresh or weathered	Structure	Observations
		X	Y	Dir.	Dip	X	Y					
DP-046	19U	314018	5364769	79		25,0	3,0	roadside	anorthosite	W	fractured	Partially covered by dirt (60%).
DP-047	19U	314400	5364353	265		15,0	4,0	footpath	anorthosite	W	fractured	
DP-048	19U	312220	5365555	20		40,0	2,0	roadside	anorthosite	W	fractured	Lots of vegetation.
DP-049	19U	314459	5371184	270		20,0	3,0	roadside	anorthosite	W	fractured	Hard to remain stable while on the outcrop.
DP-050	19U	321411	5371426					roadside	anorthosite	W	fractured	
DP-051	19U	312503	5374931	315		20,0	4,0	roadside	anorthosite	W	fractured	Lots of lichen; many fractures on the top, not reachable.
DP-052	19U	307217	5372193	212		10,0	3,0	roadside	anorthosite	W	fractured; grooves (weathering)	
				300		10,0	3,0	roadside	anorthosite	W	fractured; grooves (weathering)	
DP-053	19U	330810	5359519					roadside	anorthosite	F	fractured	
DP-054	19U	328411	5358328	270		40,0	3,0	roadside	anorthosite	F	fractured	
DP-055	19U	326275	5357075	5		50,0	2,0	private property	anorthosite	W	fractured	
DP-056	19U	326905	5358237	104		25,0	5,0	roadside	granite	F	fractured; pegmatitic vein	
DP-057	19U	326440	5358648	264		70,0	10,0	abandoned quarry	granite	W	fractured	Lots of lichen.
DP-058	19U	317438	5357818	305		20,0	4,0	roadside	anorthosite	W	fractured; quartz vein	Lots of vegetation and ants.
DP-059	19U	317672	5358893	188		100,0	10,0	roadside	anorthosite	F	fractured; quartz vein	On both sides of the road.
DP-060	19U	318836	5359081	260		100,0	6,0	roadside	anorthosite	W	fractured	Fractures oriented NW-SE have wavy surfaces.
DP-061	19U	321954	5359267	260		75,0	10,0	roadside	anorthosite	W	fractured	Rust on the top.
DP-062	19U	323071	5359243	242		70,0	8,0	roadside	anorthosite	W	fractured	Green and brown weathering; muscovite near to weathered surfaces.

Outcrop ID	UTM Zone	Location		Orientation		Dimension		Environment	Lithology	Fresh or weathered	Structure	Observations
		X	Y	Dir.	Dip	X	Y					
DP-063	19U	324367	5358847	130		30,0	3,0	roadside	mylonite in gradual contact with anorthosite	W	fractured; granitic and quartz veins (mylonite)	Delta and sigma structures.
DP-064	19U	325103	5358570	115		30,0	3,0	roadside	gneiss in contact with anorthosite	W	fractured; pegmatitic veins (gneiss)	Pegmatite veins in the gneiss
DP-065	19U	329191	5357955	110		20,0	2,0	voltage line	gneiss	W	fractured	
DP-066	19U	329205	5358037	-				voltage line	gneiss	W	fractured	Covered with lichen; lots of vegetation; hard to reach.
DP-067	19U	329297	5358341	-		10,0	5,0	voltage line	anorthosite	W	massif	50% covered by lichen and vegetation.
DP-068	19U	333238	5364951	105		30,0	5,0	Jean Coutu's parking lot	anorthosite	W	fractured	Rust on certain surfaces. Hard to find more than one joint from the same set.
DP-069	19U	335170	5365116	335		80,0	10,0	roadside	anorthosite with pegmatitic vein	W	fractured	Rust on the top.
DP-070	19U	328590	5356168	142		20,0	10,0	woods, voltage line	granite	W	fractured	90% covered by lichen.
DP-071	19U	329611	5358252			50,0	2,5	roadside	gneiss	W	fractured	
DP-072	19U	330147	5357986	175		20,0	10,0	roadside	gneiss	W	fractured	95% covered by lichen.
DP-073	19U	330449	5357775			30,0	10,0	private property; top of outcrop	gneiss with black aphanitic xenoliths	W	massif	
DP-074	19U	331636	5360061	243		4,0	1.8	voltage line	gneiss with xenoliths of anorthosite	W	fractured	
DP-075	19U	331833	5359887	-		20,0	3,0	voltage line; top of outcrop	gneiss with xenoliths of anorthosite	W	fractured; granitic vein	
DP-076	19U	332066	5359777	-		20,0	4,0	voltage line; top of outcrop	gneiss with xenoliths of anorthosite	W	fractured	

Outcrop ID	UTM Zone	Location		Orientation		Dimension		Environment	Lithology	Fresh or weathered	Structure	Observations
		X	Y	Dir.	Dip	X	Y					
DP-077	19U	332145	5359749	-				voltage line	gneiss with xenoliths of anorthosite	W	fractured	
DP-078	19U	332264	5359691	-		40,0	15,0	voltage line	gneiss	W	fractured	Joints filled with granitic material.
DP-079	19U	332397	5359639	-		15,0	10,0	voltage line; top of outcrop	?	W	fractured	
DP-080	19U	332753	5359417	-		50,0	3,0	voltage line	gneiss	W	massif	
DP-081	19U	333070	5359314	-		15,0	5,0	voltage line; top of outcrop	gneiss	W	massif	
DP-082	19U	328799	5356164					private property, voltage line	gneiss	W	fractured	
DP-083	19U	328622	5356298	-		60,0	10,0	top of hill, voltage line	gneiss with K-feldspar and quartz veins	W	fractured	Lots of lichen.
DP-084	19U	328625	5356217	114		70,0	8,0	voltage line	gneiss with feldspar and quartz veins	W	fractured	60% covered by vegetation.
DP-085	19U	328951	5356798	5		80,0	3,0	top of hill	gneiss with xenoliths of anorthosite, pegmatite and granitic veins	W	fractured	
DP-086	19U	329102	5356982	142		20,0	5,0	roadside	gneiss	W	fractured	65% covered by vegetation. It is possible to see the flow in the mafic vein, but not to tell its direction. There are some K-feldspar in the middle of the vein as well.
DP-087	19U	329080	5357032	182		50,0	4,0	woods, voltage line	gneiss	W	fractured	35% recovered by lichen and vegetation.

Outcrop ID	UTM Zone	Location		Orientation		Dimension		Environment	Lithology	Fresh or weathered	Structure	Observations
		X	Y	Dir.	Dip	X	Y					
DP-088	19U	324070	5359558	-		8,0	5,0	swamp; top of outcrop	gneiss	W	fractured	70% covered by lichen and vegetation. Visible fractures are too small and hard to be measured.
DP-089	19U	323829	5359909	-		3,0	2,0	swamp; top of outcrop	gneiss	W	massif	
DP-090	19U	323659	5359903	-		10,0	2,0	top of outcrop	gneiss	W	fractured	30% covered by lichen.
DP-091	19U	341197	5356705			20,0	3,0	voltage line	granite	W	fractured	
DP-092	19U	340560	5356450			5,0	2,5	private property, voltage line	gneiss in contact with lamprophyre		fractured	
DP-093	19U	339774	5356734			10,0	3,0	private property, voltage line	gneiss in contact with lamprophyre	W	massif	Control point.
DP-094	19U	339678	5356759	-				top of outcrop	gneiss	W	fractured	
DP-095	19U	338595	5357124	-		30,0	3,0	voltage line; top of outcrop	gneiss	W	massif	
DP-096	19U	317817	5394964	144		10,0	2,0	roadside	granite	W	fractured	60% covered by vegetation.
DP-097	19U	317179	5394241	225				roadside	diorite / sienite / monzonite with granitic veins	W	fractured	
DP-098	19U	316479	5391794	235		25,0	7,0	private property; top of outcrop	sienite / diorite / monzonite	W	fractured; quartz veins and others	
DP-099	19U	316364	5391783	-		7,0	4,0	woods, private property	sienite / diorite / monzonite	W	fractured	98% covered by lichen.
DP-100	19U	319043	5390497	280		35,0	15,0	woods	gneiss with lamprophyre veins	W	fractured	90% covered by lichen and vegetation.
DP-101	19U	319254	5390474	280		70,0	50,0	roadside	gneiss	W	fractured; K-feldspar veins	
DP-101	19U	319254	5390474	280		70,0	50,0	roadside	migmatite or gneiss with diferential weathering	W	fractured; quartz veins	
DP-102	19U	319555	5390491	136		20,0	4,0	woods	gneiss	W	fractured	Many rusted surfaces.

Outcrop ID	UTM Zone	Location		Orientation		Dimension		Environment	Lithology	Fresh or weathered	Structure	Observations
		X	Y	Dir.	Dip	X	Y					
DP-103	19U	313830	5387610	90		50,0	10,0	roadside	gneiss	W	poorly fractured	
DP-104	19U	315302	5387086	123		40,0	8,0	roadside	gneiss wih granitic veins	W	fractured	80% covered by lichen. No good measurable plans.
DP-105	19U	314803	5385676	70	85	100,0	15,0	quarry	anorthosite with granitic veins	F	fractured	Flanc 1.
				305	87	110,0	20,0	quarry	anorthosite	F	fractured	Flanc 2.
DP-106	19U	308551	5388155	278		10,0		roadside	sienite / diorite / monzonite	W	fractured	
DP-107	19U	309094	5389578	290		50,0	5,0	roadside	anorthosite	F	fractured; dolomite veins	
DP-108	19U	310072	5385463	90		90,0	3,0	roadside	anorthosite	W	fractured	
DP-109	19U	314475	5383946	108		80,0	2,5	roadside	anorthosite	W	fractured	Measurements also taken 20m to E, as the same outcrop.
DP-110	19U	317182	5383091	280		20,0	2,0	roadside	anorthosite with quartz veins	W	fractured	
DP-111	19U	318975	5383700	17		40,0	4,0	roadside	gneiss(?) with quartz and lamprophyre dispersed pockets	W	fractured	
DP-112	19U	321660	5383446	294		30,0	2,0	roadside	gneiss	W	fractured	
DP-113	19U	324370	5382684	290		85,0	2,0	roadside	gneiss	W	fractured	
DP-114	19U	331445	5375597	130		70,0	2,0	roadside	gneiss	W	fractured	
DP-115	19U	332289	5375071	100		30,0	3,5	roadside	anorthosite	W	fractured; pegmatitic vein	Many unreachable joints on the top.
DP-116	19U	326407	5385011	145		15,0	3,0	roadside	diorite	W	massif	
DP-117	19U	325193	5394536	260		20,0	5,0	roadside	diorite / monzonite	W	fractured	Seems to have 3 joint sets, though the outcrop is too small to be sure.
DP-118	19U	323863	5394743	288		30,0	2,5	roadside	sienite / diorite / monzonite	W	fractured	
DP-119	19U	323442	5394802	100		30,0	4,0	roadside	sienite	W	fractured	Lots of big ants.

Outcrop ID	UTM Zone	Location		Orientation		Dimension		Environment	Lithology	Fresh or weathered	Structure	Observations
		X	Y	Dir.	Dip	X	Y					
DP-120	19U	318310	5396463	124		15,0	0,8	roadside	gneiss with granitic veins (K-feldspar)	W	fractured	20m to E, there is a massif outcrop with the same lithology.
DP-121	19U	317967	5396389	19		70,0	2,5	roadside	gneiss with granitic veins	W	fractured	
DP-122	19U	322928	5392175	304		5,0	5,0	roadside	gneiss (with coarser plagioclase cristals)	W	poorly fractured	
DP-123	19U	325094	5388740	15		40,0	2,0	roadside	sienite / monzonite	W	fractured	
DP-124	19U	326258	5385449	134		20,0	8,0	roadside	gneiss	W	poorly fractured	
DP-125	19U	324286	5387969	110		15,0	7,0	roadside	anorthosite	W	poorly fractured	Slippery surface.
DP-126	19U	323333	5388300	125		30,0	2,0	roadside	diorite	W	fractured	
DP-127	19U	325913	5387245	325		100,0	2,0	roadside	gneiss	W	fractured	Lots of vegetation.
DP-128	19U	315937	5388655	96		50,0	2,0	roadside	diorite with granitic veins	W	fractured	
DP-129	19U	317452	5388164	118		25,0	1,5	roadside	diorite	W	fractured	
DP-130	19U	319339	5387449	99		25,0	5,0	roadside	sienite / monzonite	W	fractured	
DP-131	19U	320063	5386664					roadside	sienite / diorite / monzonite	W	poorly fractured	Joints on the top; slippery surface.
DP-132	19U	321029	5386432	99		40,0	4,0	roadside	diorite	W	fractured	
DP-133	19U	325171	5384818	304		25,0	3,0	roadside	monzonite	W	fractured	Outcrop on both sides of the road. W side is more fractured.
DP-134	19U	327080	5376934	350		90,0	10,0	roadside	diorite	W	fractured	Non-continuous outcrop. 30% covered by dirt and vegetation.
DP-135	19U	327320	5374442	150		20,0	2,0	roadside	sienite / monzonite	W	fractured	
DP-136	19U	327904	5373355	130		50,0	3,0	roadside	anorthosite	W	fractured	
DP-137	19U	328158	5372783	165		50,0	7,0	roadside	sienite / monzonite with pegmatitic vein	W	fractured	

Outcrop ID	UTM Zone	Location		Orientation		Dimension		Environment	Lithology	Fresh or weathered	Structure	Observations
		X	Y	Dir.	Dip	X	Y					
DP-138	19U	331577	5373633			25,0	2,0	roadside	anorthosite	W	fractured	
DP-139	19U	326641	5375201	66		60,0	4,0	roadside	sienite / monzonite with pegmatitic vein	W	fractured	
DP-140	19U	323975	5376142	139		30,0	4,0	roadside	sienite / diorite / monzonite	W	fractured	Rust(?).
DP-141	19U	320047	5377399	274		40,0	10,0	roadside	sienite / diorite / monzonite	W	poorly fractured	
DP-142	19U	317420	5378060	5		20,0	2,0	private property, voltage line	sienite / diorite / monzonite	W	massif	Similar outcrops nearby.
DP-143	19U	316263	5378282	74		70,0	25,0	private property	granite	W	fractured	Many unreachable joints on the top.
DP-144	19U	314468	5378870	90		80,0	10,0	roadside	sienite / diorite / monzonite with pegmatitic and lamprophyre(?) veins	W	fractured	
DP-145	19U	313466	5380024	295		30,0	3,0	roadside	sienite / diorite / monzonite	W	fractured	Many unreachable joints on the top.
DP-146	19U	312092	5382917	102		20,0	2,5	roadside	sienite / diorite / monzonite	W	fractured	
DP-147	19U	318046	5382635	320		30,0	2,5	roadside	sienite / diorite / monzonite	W	fractured	
DP-148	19U	319477	5381364	305		30,0	4,0	roadside	sienite / diorite / monzonite	W	fractured	
DP-149	19U	323682	5379015	354		70,0	5,0	roadside	anorthosite	W	fractured; dykes	
DP-150	19U	319104	5379329	295		60,0	4,0	roadside	diorite	F	fractured	
DP-151	19U	321062	5379606	195		15,0	2,0	roadside	sienite / diorite / monzonite	W	fractured	
DP-152	19U	319845	5375330	10		40,0	2,0	roadside	sienite / diorite / monzonite	W	fractured	
DP-153	19U	311301	5382671	356		40,0	3,0	roadside	diorite	W	fractured	
DP-154	19U	310616	5381746	-		70,0	30,0	top of outcrop	gneiss with pegmatitic vein	W	massif	
DP-155	19U	309040	5382227	265		35,0	2,0	roadside	anorthosite	W	fractured	

Outcrop ID	UTM Zone	Location		Orientation		Dimension		Environment	Lithology	Fresh or weathered	Structure	Observations
		X	Y	Dir.	Dip	X	Y					
DP-156	19U	326657	5365600	86	64	100,0	4,0	roadside	anorthosite	F	fractured; shear zone	S-C pair: dextral movement.
DP-157	19U	312019	5370597	260	65	200,0	10,0	roadside	anorthosite and gabbro	F	fractured	Magmatic bedding // schistosity. Tonalitic (?) vein.
DP-158	19U	331129	5370557	120	80	30,0	4,0	Saguenay river	granite	W	fractured	
DP-159	19U	330825	5370629					Saguenay river	granite		fractured	
DP-160	19U	328992	5371902	100	89	15,0	2,0	Saguenay river	granite	W	fractured	
DP-161	19U	328416	5372035					Saguenay river	granite	W	fractured	
DP-162	19U	327733	5372235			10,0	10,0	Saguenay river	granite(?) with pegmatitic veins	W	massif	
DP-163	19U	327430	5372406			30,0	10,0	Saguenay river	granite with pegmatitic veins	W	fractured	
DP-164	19U	327037	5372386			10,0	4,0	Saguenay river	pegmatite	W	fractured	
DP-165	19U	326914	5372348			67,0	8,0	Saguenay river	granite (?)	W	fractured	
DP-166	19U	326537	5372653	136		10,0	4,0	Saguenay river	granite	W	fractured	
DP-167	19U	326301	5372597	110	80	35,0	5,0	Saguenay river	granite	W	fractured	
DP-168	19U	326088	5372577					Saguenay river	granite	W	fractured	
DP-169	19U	325931	5372579					Saguenay river	granite with pegmatitic veins	W	fractured	
DP-170	19U	325396	5372718	150	70			Saguenay river	granite	W	fractured	
DP-171	19U	324829	5372726			70,0	15,0	Saguenay river	granite	W	fractured	
DP-172	19U	319397	5374904	20	85	40,0	10,0	Saguenay river	granite (?)	W	fractured	
DP-173	19U	318998	5375177	70	80	15,0	8,0	Saguenay river	granite	W	fractured	
DP-174	19U	318502	5375548	125	85	20,0	8,0	Saguenay river	granite	W	fractured	
DP-175	19U	316128	5376690	120	80	70,0	5,0	Saguenay river	granite	W	fractured	
DP-176	19U	311230	5379340	100	70	35,0	4,0	Saguenay river	granite	W	fractured	
DP-177	19U	313385	5377889			70,0	10,0	Saguenay river	granite (?)	W	fractured	
DP-178	19U	314597	5377213	50	80	70,0	8,0	Saguenay river	granite	W	fractured	
DP-179	19U	319106	5374735	75	80	30,0	4,0	Saguenay river	granite	W	fractured	Island.
DP-180	19U	330653	5357890	270	60	30,0	2,0	Kenogami lake	granite / gneiss	W	fractured	
DP-181	19U	331407	5357254	356	30	60,0	2,0	Kenogami lake	granite/gneiss with pegmatitic veins	W	fractured	
DP-182	19U	331729	5356495	220	60	150,0	5,0	Kenogami lake	granite with pegmatitic veins	W	fractured	

Outcrop ID	UTM Zone	Location		Orientation		Dimension		Environment	Lithology	Fresh or weathered	Structure	Observations
		X	Y	Dir.	Dip	X	Y					
DP-183	19U	332608	5355722	140	60	60,0	5,0	Kenogami lake	granite	W	fractured	
DP-184	19U	332858	5354937	295	80	70,0	6,0	Kenogami lake	granite	W	fractured	
DP-185	19U	333762	5353804	220	50	30,0	1,5	Kenogami lake	granite with quartz veins	W	fractured	
DP-186	19U	334181	5353154	170	65	40,0	4,0	Kenogami lake	granite	W	fractured	
DP-187	19U	335037	5352593	34	60	50,0	2,0	Kenogami lake	granite	W	fractured	
DP-188	19U	332860	5352326	90	85	70,0	6,0	Kenogami lake	granite	W	fractured	
DP-189	19U	329055	5353322	75	70	40,0	3,0	Kenogami lake	granite	W	fractured	
DP-190	19U	328347	5353657	65	75	80,0	10,0	Kenogami lake	gneiss	W	fractured	
DP-191	19U	326511	5353975	120	85	80,0	10,0	Kenogami lake	granite	W	fractured	
DP-192	19U	320641	5354948	260	85	70,0	4,0	Kenogami lake	granite	W	fractured	
DP-193	19U	318080	5355763	300	75	70,0	6,0	Kenogami lake	granite	W	fractured	
DP-194	19U	316248	5356318	280	80	80,0	10,0	Kenogami lake	granite with mafic dykes (lamprophyre?)	W	fractured	Dykes: 20cm to 1,5m width.
DP-195	19U	314449	5356972	250	80	60,0	8,0	Kenogami lake	granite	W	fractured	
DP-196	19U	313832	5357188	220	80	30,0	8,0	Kenogami lake	granite	W	fractured	
DP-197	19U	313234	5357310	240	75	70,0	20,0	Kenogami lake	granite	W	fractured	
DP-198	19U	312122	5358455	55	75	35,0	7,0	Kenogami lake	granite with feldspar vein (main)	W	fractured	
DP-199	19U	313387	5358031	140	60	20,0	3,0	Kenogami lake	granite (?)	W	fractured	
DP-200	19U	324152	5356360	160	60	20,0	2,5	Kenogami lake	granite/gneiss	W	fractured	
DP-201	19U	322183	5357379	110	65	50,0	2,5	Kenogami lake	granite	W	fractured	
DP-202	19U	321007	5358098	80	65	30,0	3,0	Kenogami lake	granite	W	fractured	
DP-203	19U	315900	5362024	115	60	10,0	5,0	Kenogami lake	mylonite(?) in contact with anorthosite	W	fractured	
DP-204	19U	318730	5358396	90	80	30,0	8,0	Kenogami lake	granite (?)	W	fractured	
DP-205	19U	303053	5365062	155	30	30,0	1,7	private property	granite in contact with anorthosite	W	poorly fractured	Anorthosite dyke.
DP-206	19U	303206	5365093	160	20	40,0	2,0	private property, top of outcrop	granite	W	fractured	
DP-207	19U	302614	5366954	90	70	70,0	3,5	Herbertville Station	anorthosite	F	fractured	

Outcrop ID	UTM Zone	Location		Orientation		Dimension		Environment	Lithology	Fresh or weathered	Structure	Observations
		X	Y	Dir.	Dip	X	Y					
DP-208	19U	319105	5367849	251	75	70,0	4,0	roadside	anorthosite in contact with granite	F	fractured	
DP-209	19U	318886	5367839	70	75	120,0	2,0	roadside	anorthosite	F	fractured	Many subhorizontal joints on the top.
DP-210	19U	324283	5409759	285	50	30,0	2,0	roadside	granite	W	poorly fractured	90% covered by lichen and vegetation. Thin (<1cm) quartz veins.
DP-211	19U	325296	5407705	2	30	20,0	4,0	roadside, top of outcrop	granite / monzonite with mafic minerals concentrations	W	massif	
DP-212	19U	325038	5406682	154	25	100,0	4,0	roadside, top of outcrop	granite / monzonite with mafic minerals concentrations	W	poorly fractured	
DP-213	19U	323921	5396861	285	65	20,0	2,0	roadside	anorthosite	W	fractured	
DP-214	19U	325785	5397107	165	30	15,0	2,5	roadside	anorthosite	W	poorly fractured	30% covered by dirt and vegetation.
DP-215	19U	326361	5395819	170	80	20,0	2,0	roadside	anorthosite	W	fractured	Brittle zone.
DP-216	19U	336150	5397627	80	65	10,0	8,0	woods, voltage line	anorthosite	W	fractured	40% covered by lichen.
DP-217	19U	336356	5398113	135	75	25,0	2,0	roadside	anorthosite(?) with granitic and quartz veins	W	fractured; magmatic bedding	No bedding at the NW part of the outcrop. The bedded rock is very weathered and rusted (suggests water percolation). 70% of outcrop covered by dirt and vegetation.
DP-218	19U	336083	5398825	145	75	15,0	5,0	roadside	anorthosite	W	fractured	
DP-219	19U	333990	5398623	177	45	10,0	2,0	roadside	anorthosite	W	fractured	90% covered by lichen and vegetation.
DP-220	19U	334143	5396722	350	60	80,0	1,5	swamp	anorthosite	W	poorly fractured	60% covered by lichen.
DP-221	19U	334339	5396063	165	60	20,0	6,0	near a lake	anorthosite	W	poorly fractured	

Outcrop ID	UTM Zone	Location		Orientation		Dimension		Environment	Lithology	Fresh or weathered	Structure	Observations
		X	Y	Dir.	Dip	X	Y					
DP-222	19U	322975	5367315	86	70	110,0	3,0	roadside	anorthosite	F	fractured	
DP-223	19U	322827	5367305	80	80	250,0	10,0	roadside	anorthosite with pegmatitic veins and biotite concentrations	F	fractured	
DP-224	19U	321713	5367188	80	75	80,0	5,0	roadside	anorthosite with feldspar veins	W	fractured	Careful: many blocks about to fall.
DP-225	19U	318841	5368006	123	84	25,0	5,0	roadside	anorthosite	W	fractured	Rust on outcrop surface, but not on joints. However, they are filled with mushrooms and lichen, which shows they are at least humid.
DP-226	19U	310645	5370244	260	80	45,0	5,0	roadside	anorthosite	F	fractured	
DP-227	19U	331998	5364351	300	0	30,0	8,0	top of outcrop	anorthosite	F	fractured	
DP-228	19U	332741	5370880	225	0	5,0	3,0	motocross road	anorthosite	F	fractured	
DP-229	19U	311412	5370516	169	80	10,0	2,0	roadside	anorthosite	F	fractured	Perpendicular to the road.
DP-230	19U	311383	5370514	312	75	5,0	10,0	roadside	anorthosite	F	fractured	Perpendicular to the road.
DP-231	19U	331943	5364325	300	0	3,0	5,0	top of outcrop	anorthosite	W	fractured	Magnetite is found in part of the outcrop.
DP-232	19U	345268	5371275		0			top of outcrop	limestone	W	fractured	Calcite partially replaced by silica.
DP-233	19U	345341	5371348	330	62	2,0	4,0	quarry	mangerite	F	fractured	
DP-234	19U	345325	5371309	180				quarry	granitoide with lamprophyre dykes	F	fractured	Mylonitic portions in the granite.
DP-235	19U	345255	5371262	180	60			quarry	granitoide	F	fractured	
DP-236	19U	345238	5371193					quarry	granitoide, limestone	W	fractured	Textbook mini-graben. Contact between limestone and granitoide.
DP-237	19U	345233	5371578		0			quarry	limestone	W	fractured	
DP-238	19U	320648	5367538	110	70	150,0	10,0	roadside	anorthosite	W	fractured	Rust.
DP-239	19U	320525	5367535	275	65	150,0	3,0	roadside	anorthosite	F	fractured	

Outcrop ID	UTM Zone	Location		Orientation		Dimension		Environment	Lithology	Fresh or weathered	Structure	Observations
		X	Y	Dir.	Dip	X	Y					
DP-240	19U	320263	5367632	290	65	120,0	8,0	roadside	anorthosite	F	fractured	
DP-241	19U	320136	5367757	115	60	100,0	5,0	roadside	anorthosite	W	fractured	
DP-242	19U	319897	5367797					roadside	anorthosite	F	fractured	
DP-243	19U	317104	5379698	110	60	2,0	1,0	near a lake	gabbro	F	massif	Bedding approximately parallel to the major lineament that crosscuts the lake.
DP-244	19U	317054	5379687					near a lake	anorthosite	F	poorly fractured	
DP-245	19U	317279	5379627					near a lake	gabbro	W	poorly fractured	Fractures *en échellon*.
DP-246	19U	316180	5378343					cliff	gabbro	F	fractured	Joints approx. parallel to the N30W lineament identified by the digital altitude model.
DP-247	19U	316209	5378327					cliff	gabbro	W	fractured	
DP-248	19U	320178	5367859	185	60	2,0	1,0	transmission tower	anorthosite with magnetite	F	poorly fractured	
DP-249	19U	320191	5367876	130	50	20,0	1,0	transmission tower	anorthosite	W	fractured	Rust.
DP-250	19U	320219	5367931	230	30	2,5	1,5	woods, next to transmission tower	anorthosite	W	fractured	Lots of lichen.
DP-251	19U	318882	5368669	170	70	15,0	2,0	woods	anorthosite	F	fractured	
DP-252	19U	319280	5368491	128	70	30,0	4,0	woods	granitoide with magnetite concentrations (~1cm²)		fractured	
DP-253	19U	320094	5368943	240	70	100,0	10,0	woods	anorthosite with magnetite	F	fractured	Subvertical family forming unit blocks in two scales (10cm and 1m). Zones densely fractured (with fault gouge). There is also a zone that seems preserved from fracturation.

Outcrop ID	UTM Zone	Location		Orientation		Dimension		Environment	Lithology	Fresh or weathered	Structure	Observations
		X	Y	Dir.	Dip	X	Y					
DP-254	19U	320468	5369122	200	30	10,0	0,8	roadside	anorthosite	W	fractured	Superficial white weathering.
DP-255	19U	320259	5368858	0	50	30,0	1,6	roadside	anorthosite	W	fractured	
DP-256	19U	321164	5367548	104	85	50,0	3,0	roadside	anorthosite	W	fractured	Subhorizontal (dip = 07°) fractures spaced 50cm-1m. Chloritization observed in one fracture.
DP-257	19U	321201	5367874	311	70	3,0	2,0	roadside	anorthosite	W	fractured	
DP-258	19U	321277	5368131					roadside	anorthosite	W	fractured	
DP-259	19U	321260	5368217	40	40	30,0	1,5	roadside	anorthosite	W	fractured	
DP-260	19U	321181	5368213	100	75	60,0	3,0	woods	anorthosite	W	fractured	
DP-261	19U	321159	5368214	95	65	2,0	1,5	woods	anorthosite	W	fractured	Rust.
DP-262	19U	320853	5368754					woods	anorthosite	W	fractured	
DP-263	19U	320230	5368644	355	76			woods	anorthosite	W	fractured	
DP-264	19U	257445	5386111	90	80			roadside	limestone	W	fractured	
DP-265	19U	256756	5386259					roadside	limestone	W	fractured	

APPENDIX 4

OTHER SUGGESTED PROCEDURES

The approaches described below were considered during the phases of fieldwork and data analysis; the first two were actually tested. They include: (1) panoramic photographs assemblages; (2) application of Terzaghi's correction over a rock face ("window"); (3) LiDAR. Nonetheless, they were considered relatively time demanding or costly, regarding the results provided, and thus were not used in the scope of this project.

A4.1 Panoramic Photographs

During the general survey, selected outcrops were submitted to series of photographs in order to generate panoramic mosaics. Good outcrops for a panoramic mosaic are wide (at least 50m long), approximately straight and, of course, with as many families of visible joints as possible.

The photographs are taken perpendicularly to the outcrop, to reduce distortion, and far enough from it to make visible the whole outcrop. The distance between photographs along an outcrop should be enough to ensure an overlap of about 50% between photographs. The photograph mosaics (Fig. A4.1) were made using Adobe Photoshop Elements 7[20], and the joints and outcrops contours are drawn with CorelDRAW[21].

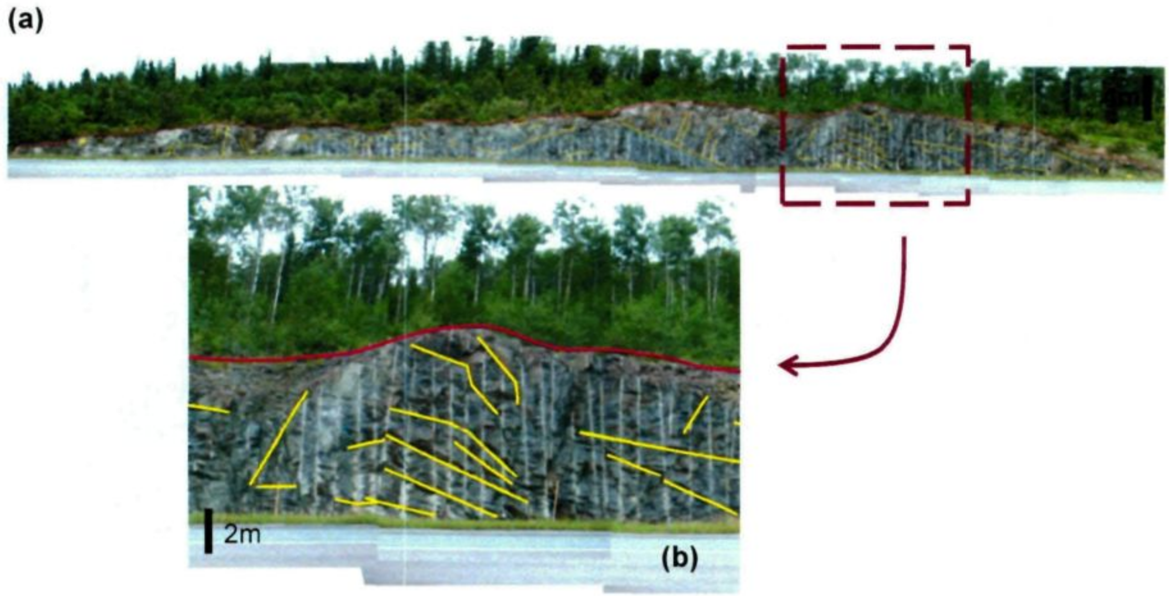

Fig. A4.1 In both figures, red lines delineate the outcrop contour; yellow lines indicate joints. **(a)** Assembling of panoramic photographs. **(b)** Detailed view. Photos: D. S. Pino.

Photograph mosaics may be useful to better visualize the joint sets, particularly the subhorizontal ones; to identify joints that are too high on the outcrop face to be measured; and to help locate sections to be submitted to detailed survey (see section A4.2). As the photographs are taken perpendicularly to the outcrop and with scale markers, they allow the approximation to Terzaghi's correction regarding a window survey.

[20] Adobe Systems Incorporated. (2008). Adobe Photoshop Elements 7 (version 7.0.1).

[21] Corel Corporation. (2005). *CorelDRAW X3 (version 13.0.0.739).*

A4.2 Terzaghi's correction over a window

The correction of the orientation bias over a window is similar to the one applied for a scanline. Let's consider the joint J that intersects the window W at a vector I (Fig. A4.2).

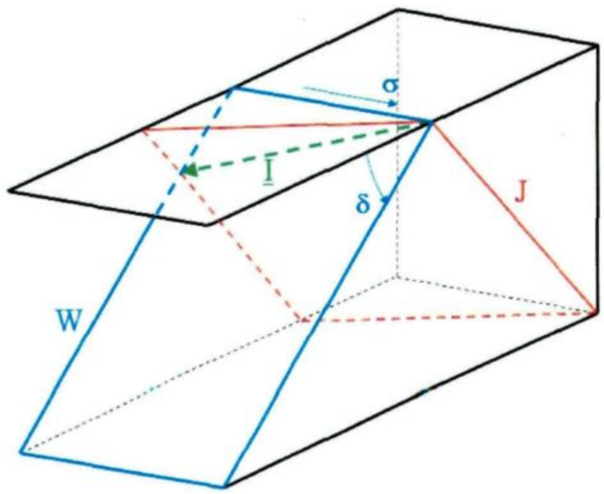

Fig. A4.2 Initial features considered in the bias correction over a window: joint plane (J), outcrop face or window (W), intersection between J and W (I). The window's strike (σ) and dip (δ) are also represented. Original sketch by: D. W. Roy.

The angle α between the joint pole and the window pole is calculated first. It allows the calculation of the direction cosine of the intersection I, by the vectorial product between the joint and the window poles. This direction cosine is used to calculate the angle β between the window strike and the intersection (Fig. A4.3).

The weight attributed to each joint in the window procedure is also given by $1/\sin\alpha$, although it is multiplied by the factor dW/Lt to standardize all weights, where dW is the window diagonal and Lt is the equivalent observation length of the joint (Fig. A4.3). The latter is calculated by trigonometry.

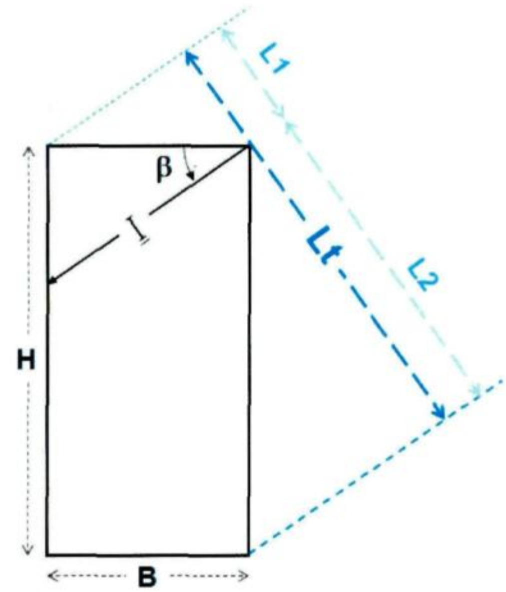

Fig. A4.3 Planar view of the window, defined by its length B and its high H. By trigonometry, the angle β between the intersection I and the window base B provides the value of the equivalent observation length Lt. The maximum value Lt might have is equal to the window diagonal. Original sketch by: D. W. Roy.

The corrected density plot is done in the same way as for the scanline, that is, using the weight multiplied by 10 due to plotting software limitations. Similarly, a blind zone of ±20° with respect to the pole of the window plane is considered for the window[22], and for all joints inside it, a new weight equal zero is attributed.

Finally, the corrected frequency for each joint set is calculated by the inverse of its weight and for the ensemble by the arithmetic average of the individual frequencies. The definition of a station follows the same procedure applied to the scanline; windows and scanlines may be combined in a same station.

[22] The blind zone in the case of a scanline forms a cone, represented by a small circle on the stereoplot. In the case of a window survey, the blind zone is represented by a great circle.

It should be noted that the photograph window approach is not as precise as the scanline one. As mentioned on section 4.3.4, during a scanline study all joints are measured, so it is possible to know the location of each joint on the scanline. In the photograph window approach, though, only the reachable subhorizontal joints are measured (usually up to 1.5m high, or up to 2m when it is possible to climb on the outcrop), and by comparison of joint traces in the outcrop, the orientation values of accessible joints are attributed to the ones located on the top. At this point, it should be mentioned that printing a large photograph of the area where the window survey is planned is truly helpful to asserting the orientation values while taking the measurements. Due to a tight schedule, in the present work the photographs were taken during the same visit as the subhorizontal joints measurements, which later made it harder to make the correlations between the orientations of the measured joints on the bottom of the outcrop and the unreachable ones on the top.

A4.3 LiDAR: Light Distance And Ranging

A ground-based LiDAR, also referred to as a 3D laser scanning, is an instrument that rapidly sends laser pulses and calculates the three dimensional position of reflected objects (Fig. A4.4) (Kemeny *et al.* 2006; Harrap & Lato 2010).

The LiDAR uses the same principles of an ordinary radar; however, it uses a narrow pulsed beam of light instead broad radio waves (Kemeny *et al.* 2006). The speed of light and very precise time devices are used to calculate the distance between the instrument and the object reflecting the beam, as long as the position and pointing direction of the laser are known for each measurement (Harrap & Lato 2010). LiDAR may collect data from airbone or terrestrial vehicles, from fixed positions (e.g. a tripod) and from offshore platforms (Harrap & Lato 2010). Using multiple scanning locations and orientations is always recommended (Lato *et al.* 2010).

Fig. A4.4 Exemple of LiDAR device, a Trimble® VX™ Spatial Station. Source: Trimble. (2010). *Trimble® VX™ Spatial Station Datasheet.*

The interest in the LiDAR device for rock assessments increased with its development (Lato *et al.* 2007, 2009, 2010; Pate & Haneberg 2011). Nowadays, there are equipments capable of collecting data at rates higher than 2000 points per second, with a position accuracy of around 5mm at distances up to 800m (Kemeny *et al.* 2006). It is important to notice that LiDAR's accuracy is limited by the accuracy to which its location is known (Harrap & Lato 2010). Nonetheless, laser scan-based surveys and automated analyses may be faster, less laborious and thus cheaper than traditional surveys and analyses (Kemeny *et al.* 2006).

The data obtained with a laser survey is a "point cloud", consisted of millions of reflection points representing the three dimensional surface scanned and usually coded with the intensity of light return. With data cleaning, a triangulated face is obtained, allowing many other calculations and visualizations, such as extracting information about discontinuities (e.g. orientation, spacing and roughness) and plotting information on stereonets and histograms (Kemeny *et al.* 2006). Moreover, digital images may be overlaid onto the 3D surface.

Finally, two major challenges with LiDAR use may be mentioned (Harrap & Lato 2010): (1) the nonexistence of a software capable of all necessary steps from input to model creation, requiring file transfer between tools and formats; (2) the large amount of data on the point clouds, rendering its processing a very slow procedure.

APPENDIX 5

FORMULAS FOR THE NUMERICAL METHOD OF TERZAGHI'S CORRECTION

Here are explained the procedures for the numerical application of Terzaghi's correction over a scanline and the following analysis of true joint spacing.

A5.1 Terzaghi's correction

The numerical method of Terzaghi's correction applied on this project uses the data from the detailed survey description form. All the calculi were made on Microsoft® Excel tables. The first two lines are reserved to titles and the third to information regarding the scanline (trend and plunge); the structures are listed from the fourth line. As to the columns, they are arranged as in Table A5.1.

A5.2 Joint spacing analysis: virtual position of joints

The application of Terzaghi's correction over a scanline usually provides one or two corrected joint poles. Only the joints whose poles that form 20° or less with a corrected pole are considered to be part of the "corrected joint set" (the joints shown on Fig. 4.5) to calculate the true joint spacing of a corrected set.

The distance d' is calculated by $sin\alpha = d'/d$, where d is the total outcrop or scanline length and d' is the corrected length for the joint set. Then, for each joint previously selected, it is calculated: $sin\alpha_{P1} = d''/(d-x)$, where α_{P1} is the solid angle α from the corrected pole, d'' is the joint corrected distance and x is the distance where the joint is located on the corrected length. This calculus on Microsoft® Excel is shown on Table A5.2.

Once the corrected distance is calculated for all joints, their spacing can be easily evaluated on distance diagrams (as in Fig. 4.6), to analyze its type, or on histograms, if the interest is to identify a polymodal spacing distribution, for example.

Table A5.1 Components of the columns used in the calculus sheet for Terzaghi's correction over a scanline. Values are described regarding the fourth line, i. e., the first line with discontinuity information; the line 100 is here assumed as the last one with such data in order of illustration. Line 101 contains information regarding the main joint pole identified on the corrected density diagram for the scanline.

Col.	Description	Value
A	Number of the discontinuity (ID).	Taken from detailed survey form.
B	Type of discontinuity (see Appendix 2).	Taken from detailed survey form.
C	Discontinuity strike (right hand rule).	Taken from detailed survey form.
D	Discontinuity dip.	Taken from detailed survey form.
E	Dip quadrant.	Taken from detailed survey form.
F	Position of the discontinuity in the scanline.	Taken from detailed survey form.
G	Discontinuity pole trend.	=if(C4<90;C3+270;C4-90)
H	Discontinuity pole plunge.	=90-C4
I	Element Q_x from the direction cosine.	=cos(H3*pi()/180)*cos(G3*pi()/180)
J	Element Q_y from the direction cosine.	=cos(H3*pi()/180)*sen(G3*pi()/180)
K	Element Q_z from the direction cosine.	=sen(H3*pi()/180)
L	Direction cosine $\cos\alpha$ between the discontinuity and the scanline.	=I$3*I4+J$3*J4+K$3*K4
M	Angle α in degrees between the discontinuity and the scanline.	=(acos(abs(L4))*180/pi()
N	Weight attributed to the discontinuity.	=if(M4>=70;0;(1/(cos(M4*pi()/180)))
O	Standard weight.	=N4*10
P	Equivalent number of fractures	=sum(O4:O100)
Q	Direction cosine $\cos\gamma_1$ between the discontinuity and Pole 1.	=I$101*I4+J$101*J4+K$101*K4
R	Angle γ_1 in degrees between the discontinuity and Pole 1.	=(acos(abs(Q4)))*(180/pi())
S	Check if $\gamma_1 \leq 10°$.	=if(R4<=10;O4;0)
T	Check if $\gamma_1 \leq 20°$.	=if(R4<=20;O4;0)

Table A5.2 Components of the two columns to calculate the corrected distance for each joint whose pole makes 20° or less with a corrected pole over a scanline. Like on Table A5.1, values are described regarding the fourth line, i. e., the first line with discontinuity information; the line 100 is here assumed as the last one with such data in order of illustration. Line 101 contains information regarding the main joint pole identified on the corrected density diagram for the scanline.

Col.	**Description**	**Value**
U	First step to calculate the corrected distance.	=sin(M$101*PI()/180)*(F$100-F4)
V	Corrected distance.	=sin(M$101*PI()/180)*F$100-U4

APPENDIX 6

GEOPHYSICAL LOGGING

The geophysical logging profiles for the wells RM001, RM004 and PZ-S18-R are shown in the following (Figs. A6.1 to A6.3). ATV interpretations done by R. H. Morin, log displays by J. Roy.

As the only geophysical logging discussed so far is the ATV, due to its input in defining the unit block subhorizontal side, this appendix also presents commentaries on other loggings that were performed in the same boreholes in the study area. The interpretation of these logging data benefited greatly from the contributions of J. Roy (IGP, Canada) and R. H. Morin (USGS).

A8.1 Other remarks on geophysical logging

In the three wells logged within the Kenogami uplands, the caliper logging confirmed the occurrence of fractures at depth (peaks in an otherwise linear log). Particularly high peaks were observed in the log of the well RM004, for depths higher than 91m (300ft). Regarding the well PZ-S18-R, the caliper also indicated a change of drill diameter below 123m (405ft), from 6" to 5"¼.

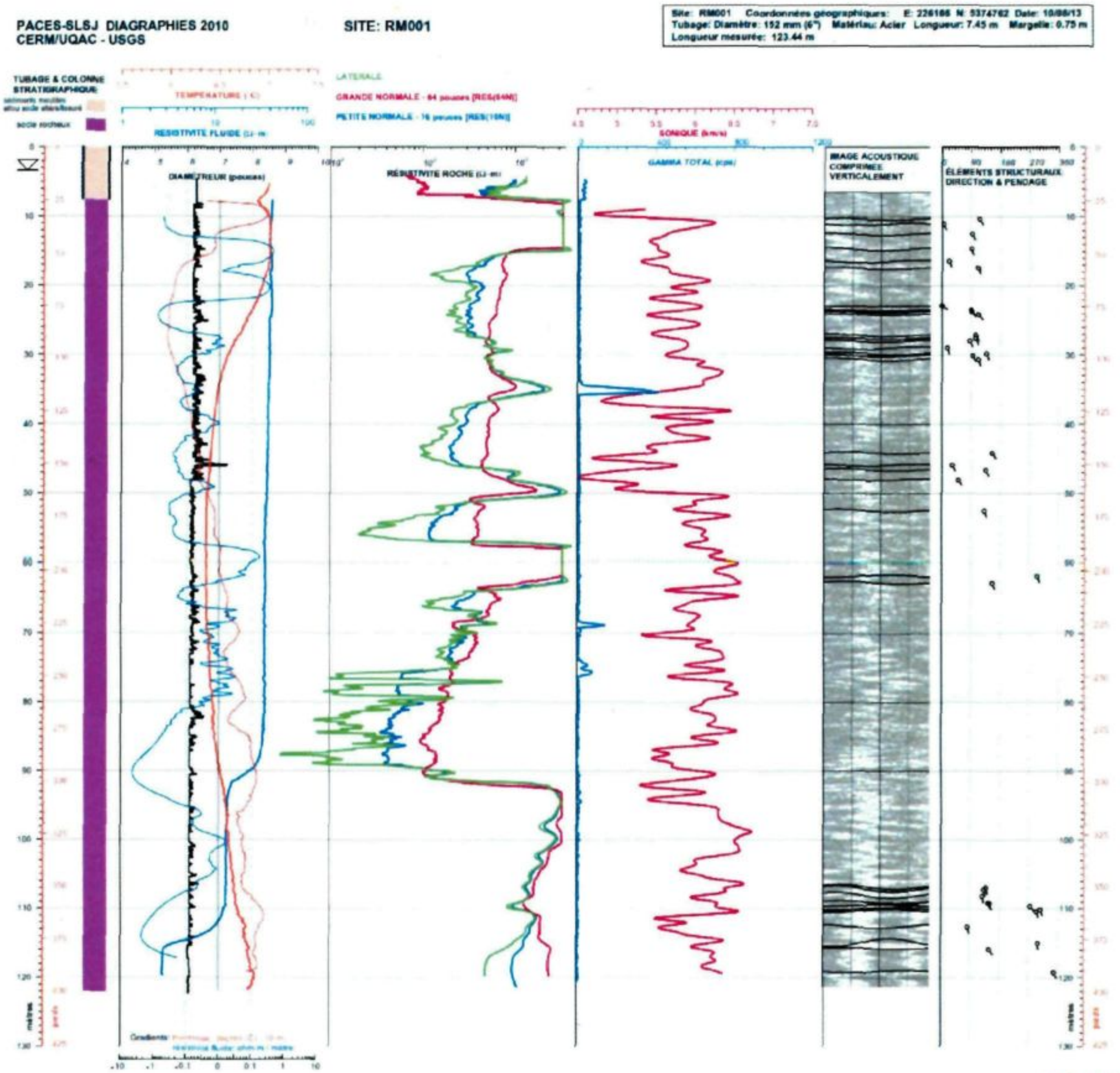

Fig. A6.1 Logs for the well RM001. From left to right: (1) stratigraphic profile, (2) water temperature and resistivity and borehole caliper, (3) rock resistivity, (4) sonic waves and natural gamma, (5) ATV image with identified joints (black sinusoids) and (6) orientation data of joints on the ATV image.

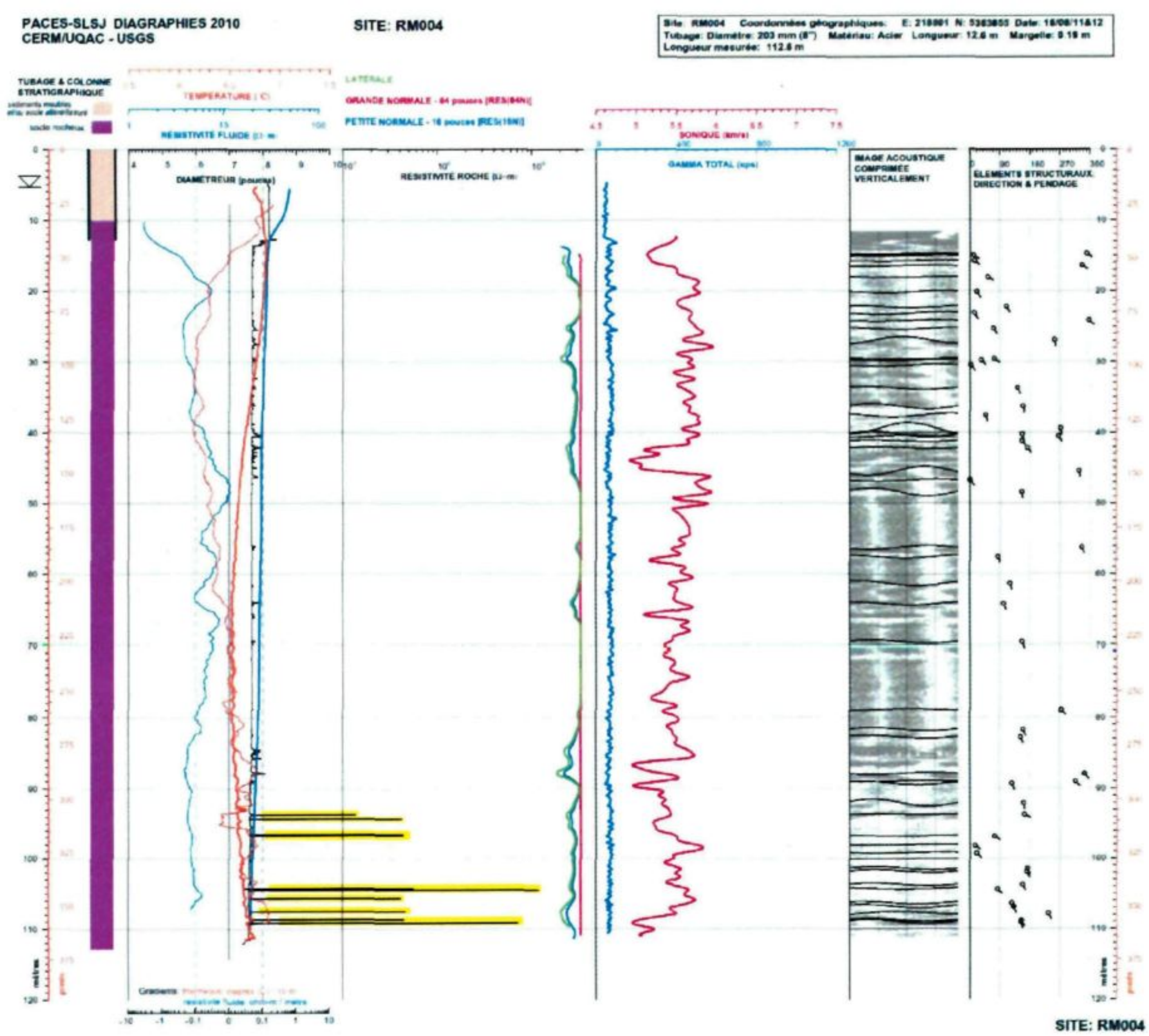

Fig. A6.2 Logs for the well RM004. From left to right: (1) stratigraphic profile, (2) water temperature and resistivity and borehole caliper (the peaks in yellow indicate instabilities of the signal received by the probe, not joints), (3) rock resistivity, (4) sonic waves and natural gamma, (5) ATV image with identified joints (black sinusoids) and (6) orientation data of joints on the ATV image.

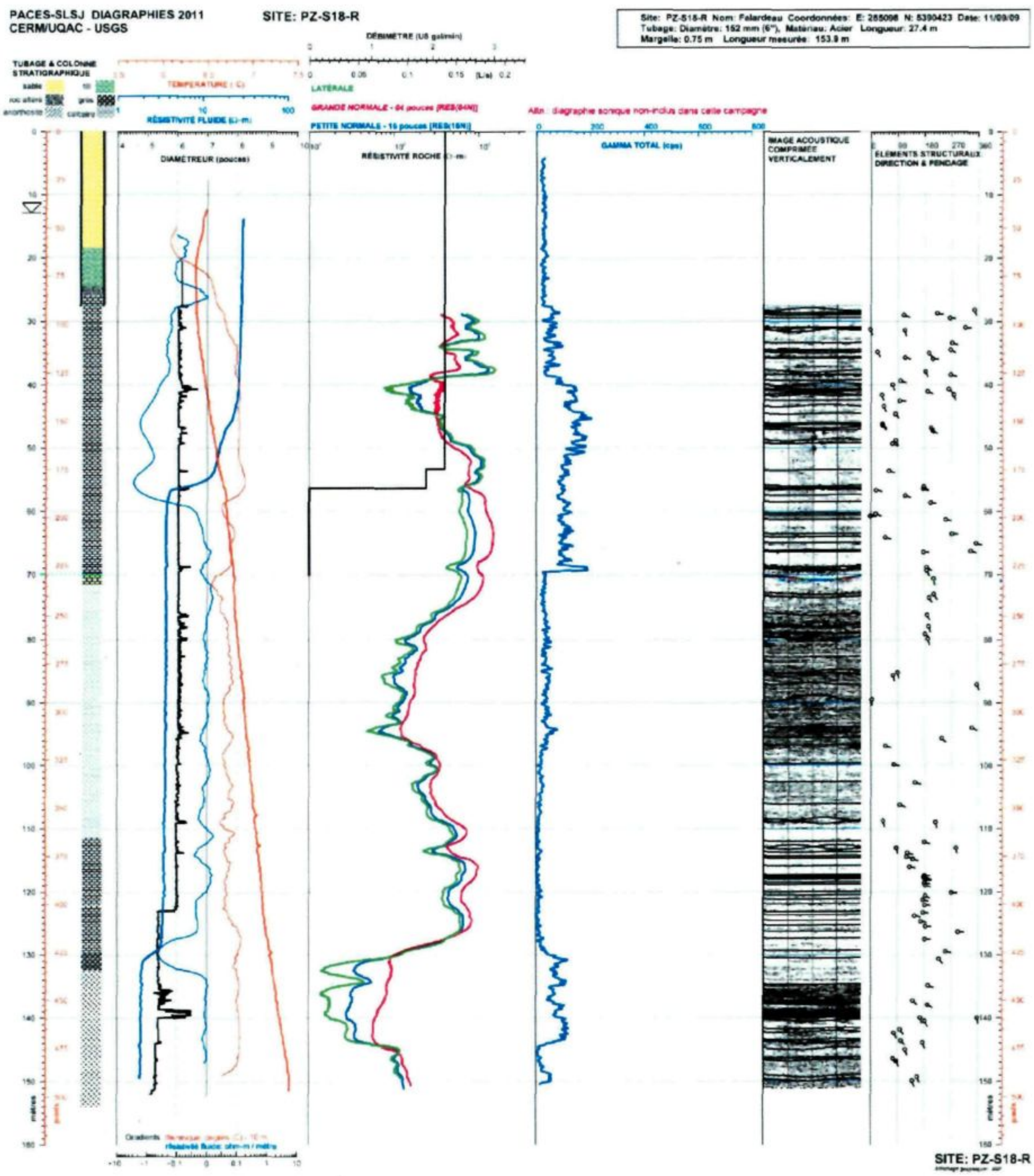

Fig. A6.3 Logs for the well PZ-S18-R. From left to right: (1) stratigraphic profile, (2) water temperature and resistivity and borehole caliper, (3) rock resistivity and flowmeter, (4) natural gamma, (5) ATV image with identified joints (black sinusoids) and (6) orientation data of joints on the ATV image.

The natural gamma log, combined with a rock resistivity log, allowed the identification of a few lithologies in the wells logged. Well RM001 has a still undefined stratigraphy, but it has two main lithologies (one with high values of resistivity and sonic wave velocity, and another one with lower velocity and moderate resistivity values) and four possible dykes or thinner layers. These punctual higher responses of natural gamma could also represent joints filled by clay, which normally give higher values of this parameter due to the acquisition of radioisotopes by adsorption or ion exchange. Well RM004 has a single lithology, given that the values of natural gamma and rock resistivity are relatively constant. It is probably granite, as it presents natural gamma values higher than RM001, which was supposedly in anorthosite[23], and it is located near the contact between anorthosite and granite (Figs. 3.4 and 5.4). Finally, on well PZ-S18-R the following lithologies were identified: limestone at the interval 64.01-128.02m (210-420ft), possibly gneiss at 128.02-143.26m (420-470ft) and anorthosite at 144.78-148.74m (475-488ft), while no lithology could be assigned to other depth intervals.

Regarding water resistivity, on well RM001 two levels are identified: one down to 91m (300ft), and the other from 100m to the end of the well. Water in the first level presents a higher resistivity, around 40Ω.m, indicating good quality water (low value of total dissolved solids, TDS); the reduction of water resistivity after 100m to approximately 2Ω.m indicates lower quality water (high TDS). It is interesting to notice that most joints are located in the first 100m. Well PZ-S18-R also shows a decrease of water quality with depth: 30Ω.m down to 53m (175ft), 4Ω.m at 53-128m (175-420ft), and 2Ω.m at 128-149m (420-490m). Finally, on well RM004, an almost constant resistivity is observed (approximately 25Ω.m; medium water quality), which reinforces the hypothesis of a single lithology.

---

[23] The natural gamma log from well RM001 is comparable to another well that is known to be in the anorthosite, although it is located outside the Kenogami uplands. For details, see Roy *et al.* (2011).

The water temperature logs indicate, in general, that water temperature tends to increase below 91m (300ft).

The sonic logging on well RM004 indicates an average velocity of the primary compressional waves (Vp) equal to 5,5km/s. More pronounced negative peaks are observed at 42m (140ft) and 82-85m (270-280ft), which could be related to the decreases in natural gamma at such depths. A positive peak is observed at 97m (320ft), with no other remarkable changes. Regarding well RM001, the average Vp is 5,5km/s down to 46m (150ft), after which it increases to 6,3km/s. More variations (peaks) are present in the log for the well RM001 than for RM004. At 38m (123ft) on well RM001, a decrease in Vp coincides with a large peak in natural gamma and rock resistivity values. This suggests that a joint located at 38m is filled with a material more active (higher response to natural gamma rays) than the surrounding rock, probably rich in potassium[24]. At 47m (155ft), another decrease in Vp is also possibly related to the presence of a joint at that depth. Lastly, the increase in average Vp observed after 91m is due to a lithology change, as also suggested by the great increase in rock resistivity and the decrease in water resistivity. The sonic logging could not be performed on well PZ-S18-R due to probe malfunction.

The flowmeter on well PZ-S18-R allowed the identification of two productive joints: one at 53.5m (175ft), oriented 331/18, and the other at 56.5m (180ft), oriented 287/11. The deeper joint is responsible for ~86% of the water inflow in the well (1.9USG/min or 0.13L/s), while the shallower joint contributes with only ~14% of the inflow (0.3USG/min or 0.02L/s). The flowmeter logging could not be performed on wells RM001 and RM004

[24] Potassium-40 and the products of radioactive decay of uranium and thorium are the main radioisotopes of interest in natural gamma loggings (Cripps & McCann 2000). Potassium is suggested as the most probable radioisotope present in the material filling the interpreted joint at well RM001.

because the water level could not be stabilized during the pumping test; it decreased very quickly even after the pump level and the pumping rate were lowered.

APPENDIX 7

LINEAMENT MAP WITHIN THE TPIS (INTRAMUNICPAL PUBLIC TERRITORIES)

Lineaments were traced using a shaded digital elevation model (DEM) in the Kenogami uplands (Fig. A7.1). Attention was focused within areas called TPI, *territoire publique intramunicipal* (intramunicipal public territories), as explained on chapter 4.

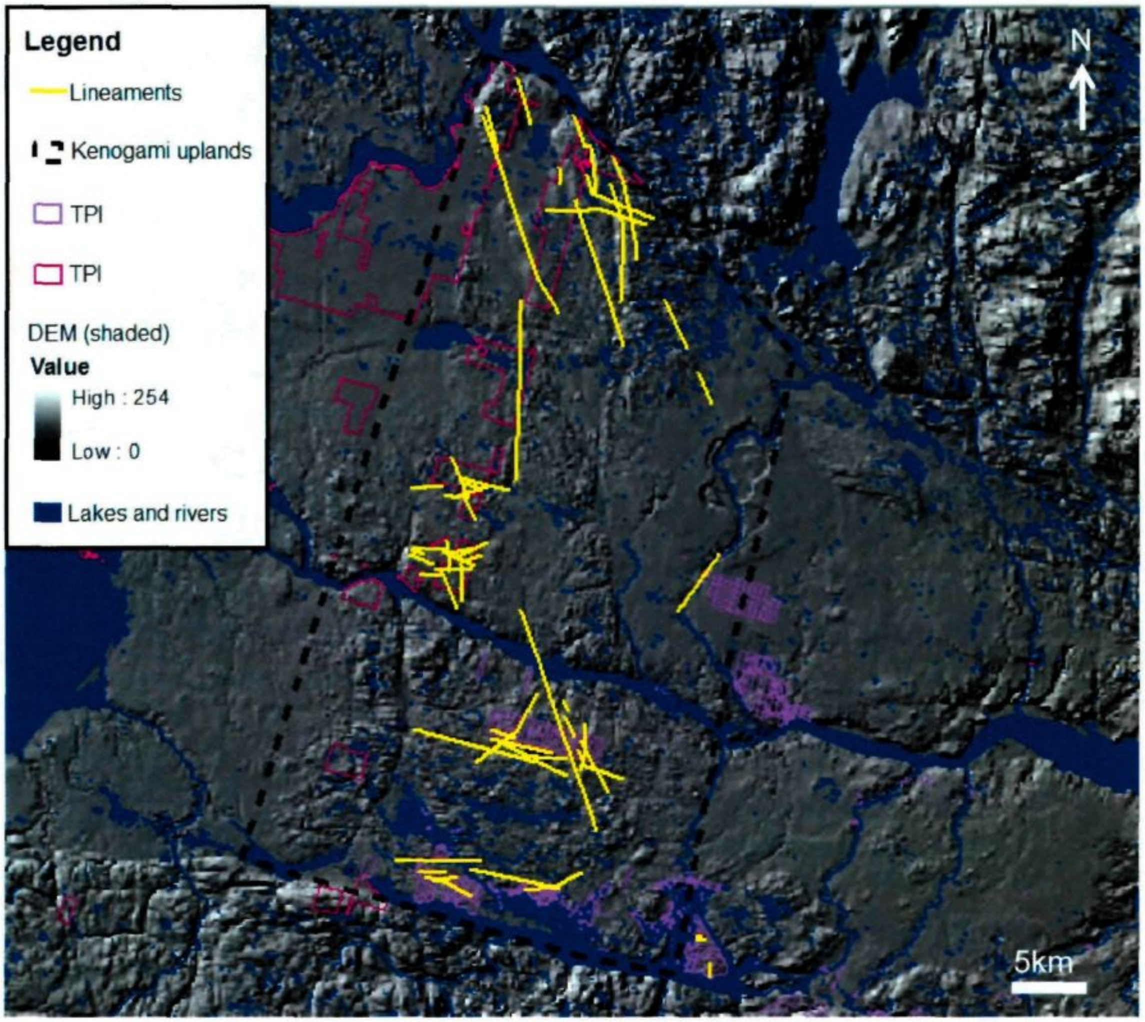

Fig. A7.1 Lineaments (yellow) identified within TPIs in the Kenogami uplands region. Observation scales were 1:20.000 (DEM's scale) and 1:1.000.

APPENDIX 8

JOINT SPACING DISTRIBUTION

Joint spacing distributions are represented in histrograms (Figs. A8.1 to A8.5). This analysis reinforces the argument that average joint spacing values over a scanline may be misleading, as exemplified here by the recurrent occurrence of bimodal distributions in the Kenogami uplands. This topic is not treated in literature, although it is possible to find a discussion on the evolution of joint spacing (Rives *et al.* 1992).

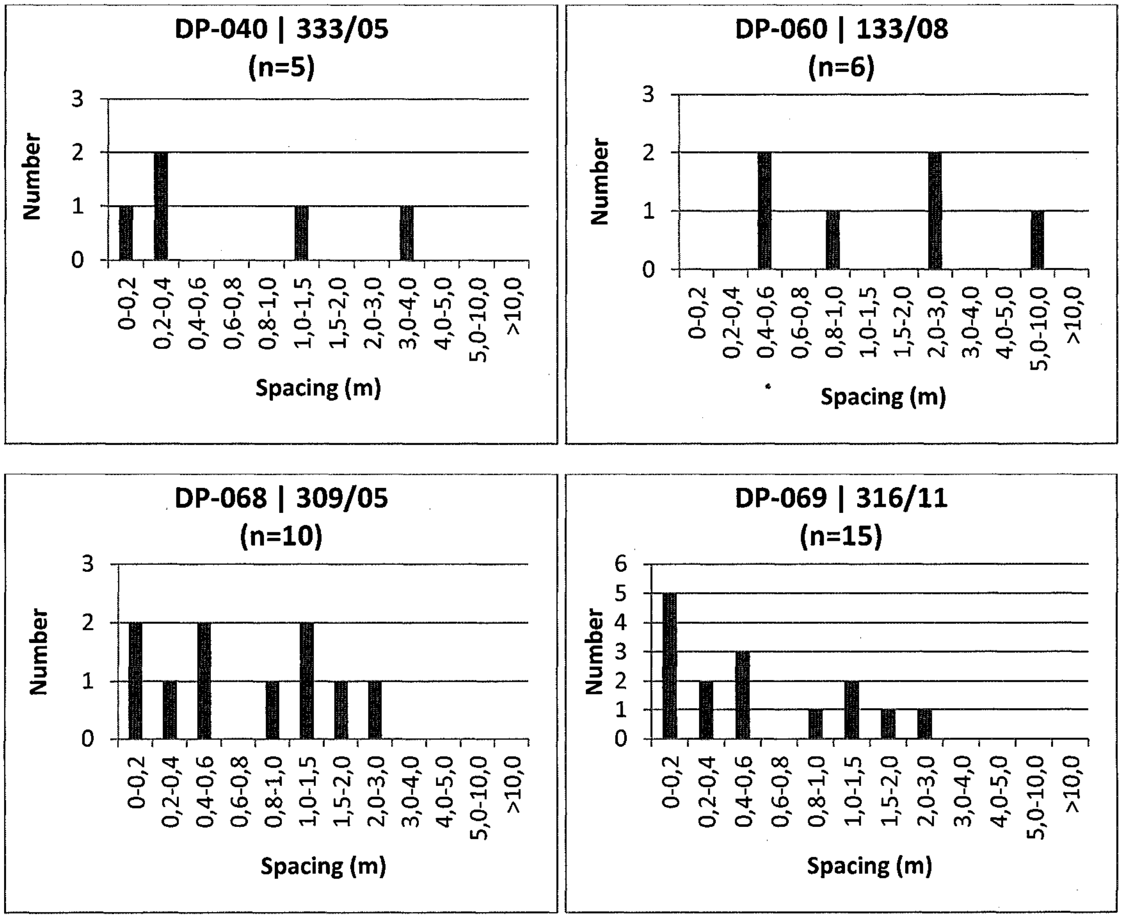

Fig. A8.1 Joint spacing distribution regarding joint sets that represent the set 044/88 from the unit block. Outcrop identification and respective pole of the joint set are indicated above every histogram. Spacing measured on lines orthogonal to joint plane. Spacing classes vary in width: 0.2m for spacing sizes between 0.0 and 1.0m; 0.5m, between 1.0 and 2.0m; 1m between 2.0 and 5.0m; 5.0m between 5.0 and 10.0 m; and all sizes above 10m. Observe the bimodal distribution trend. (CONTINUES)

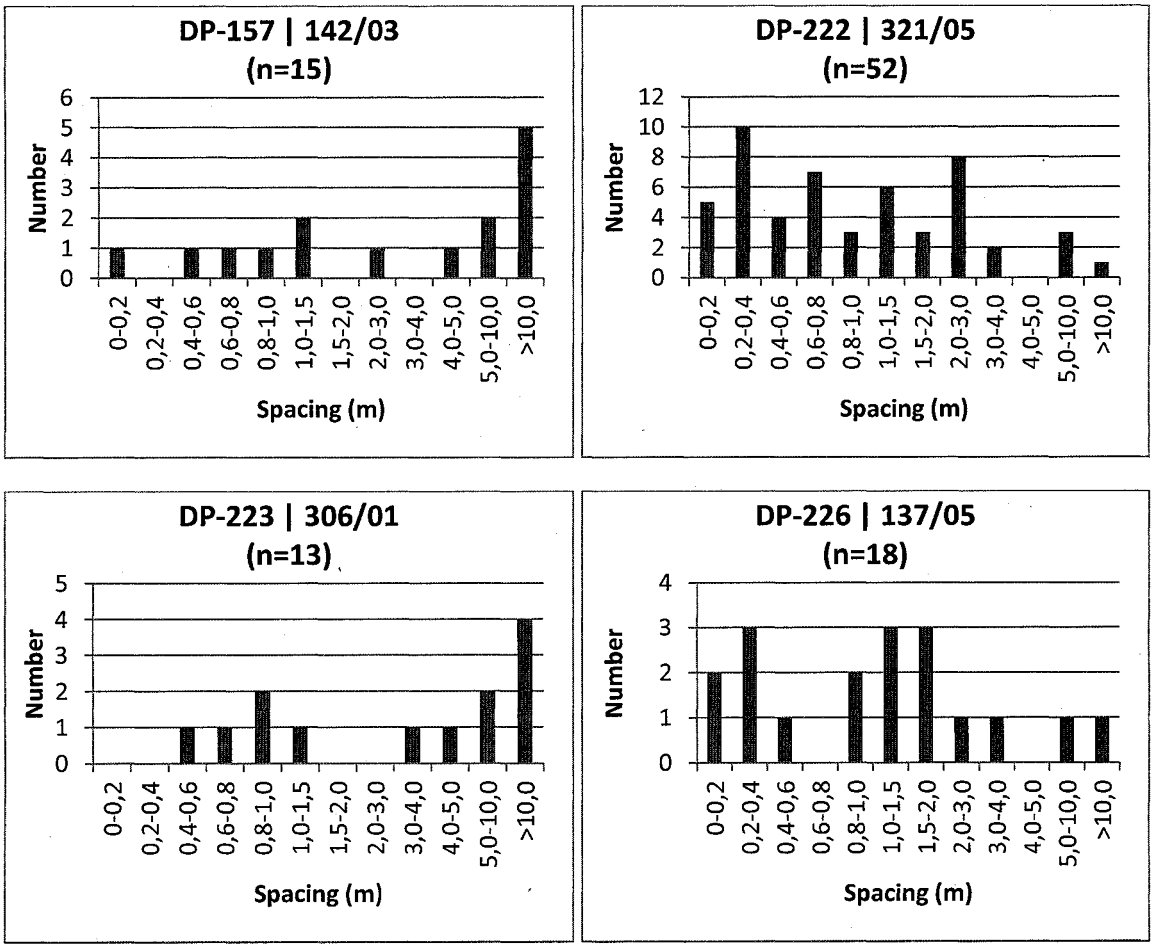

Fig. A8.1 (CONTINUATION)

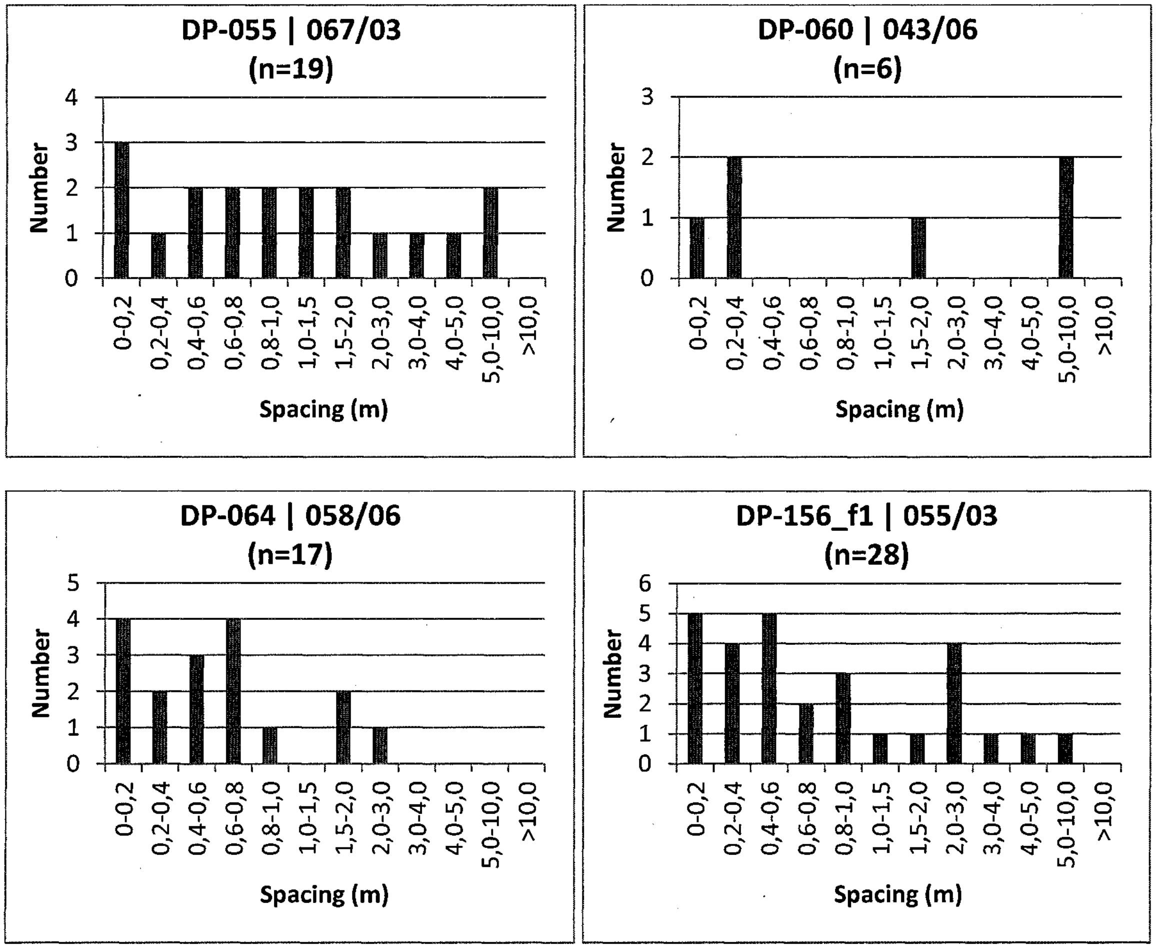

Fig. A8.2 Joint spacing distribution regarding joint sets that represent the set 139/84 from the unit block. Outcrop identification and respective pole of the joint set are indicated above every histogram. Spacing measured on lines orthogonal to joint plane. Spacing classes vary in width: 0.2m for spacing sizes between 0.0 and 1.0m; 0.5m, between 1.0 and 2.0m; 1m between 2.0 and 5.0m; 5.0m between 5.0 and 10.0 m; and all sizes above 10m. Polymodal distributions seem to prevail. (CONTINUES)

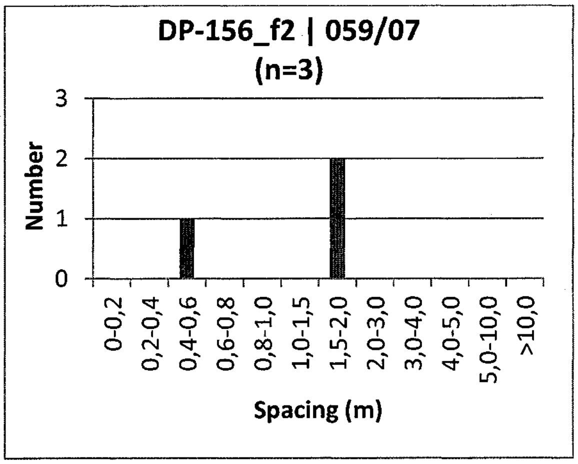

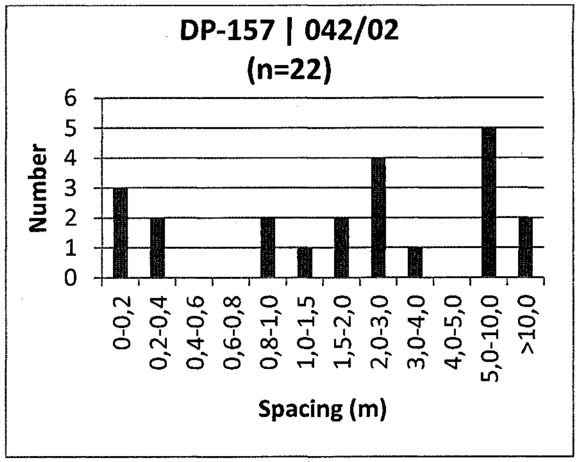

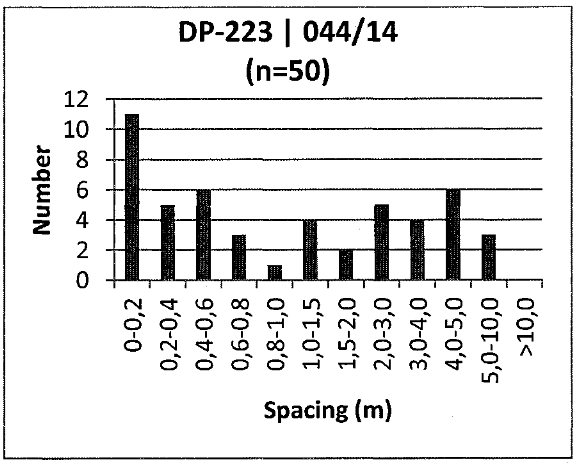

Fig. A8.2 (CONTINUATION)

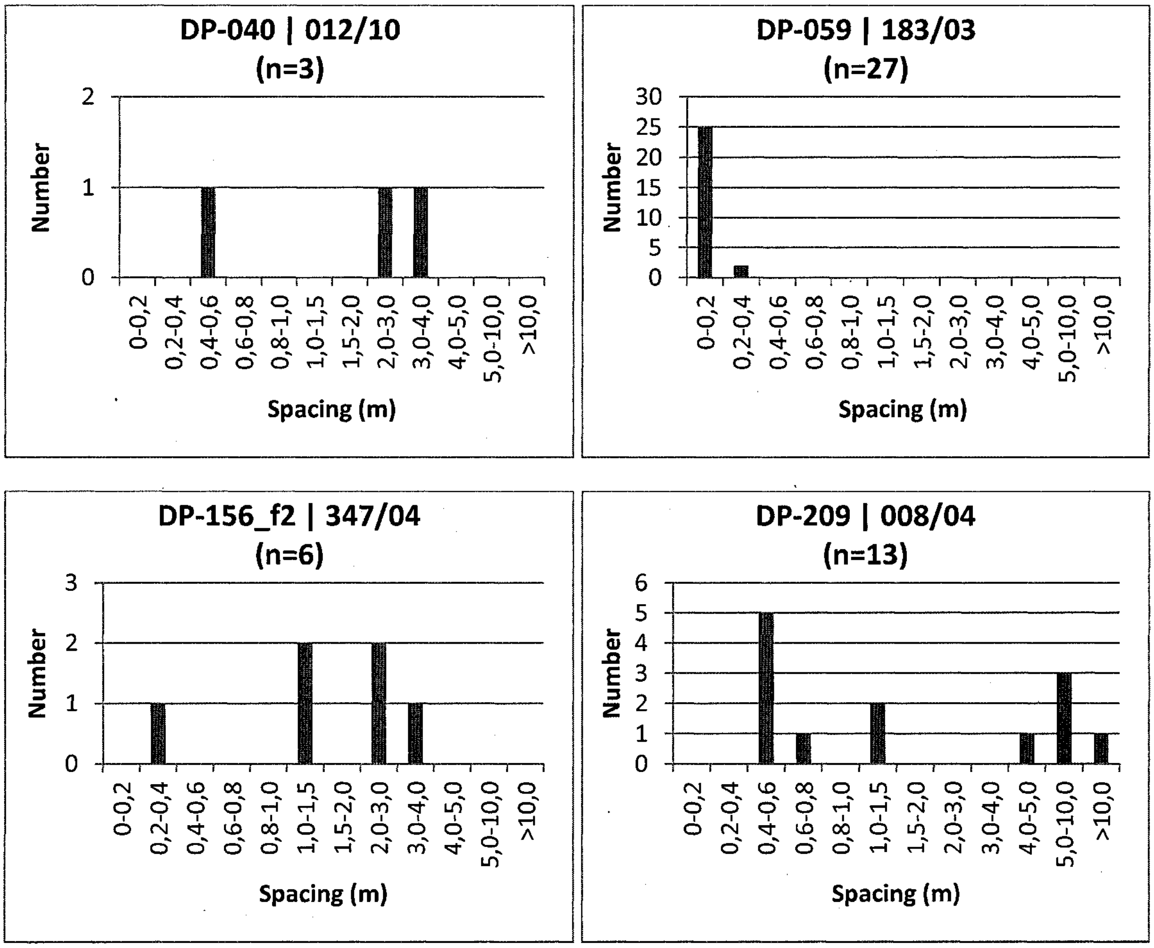

Fig. A8.3 Joint spacing distribution regarding joint sets that represent the set 095/86 from the unit block. Outcrop identification and respective pole of the joint set are indicated above every histogram. Spacing measured on lines orthogonal to joint plane. Spacing classes vary in width: 0.2m for spacing sizes between 0.0 and 1.0m; 0.5m, between 1.0 and 2.0m; 1m between 2.0 and 5.0m; 5.0m between 5.0 and 10.0 m; and all sizes above 10m. Although not as clear as for the two other subvertical joint sets, bimodal distributions also seem to emerge from this data.

(CONTINUES)

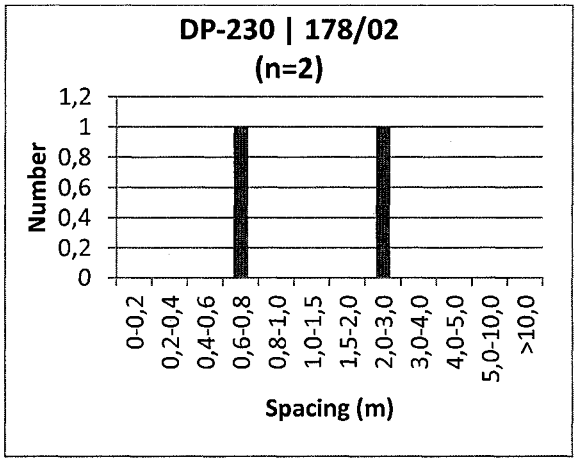

Fig. A8.3 (CONTINUATION)

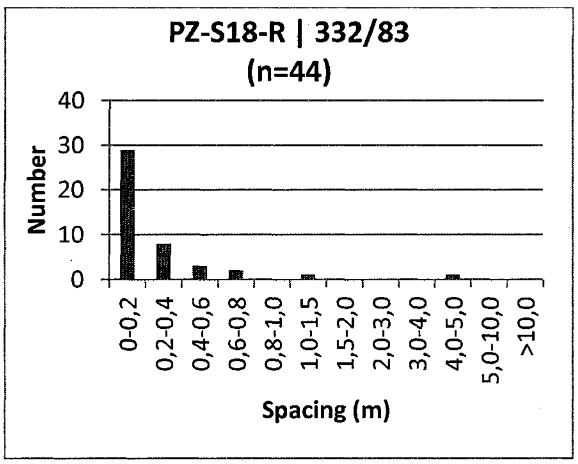

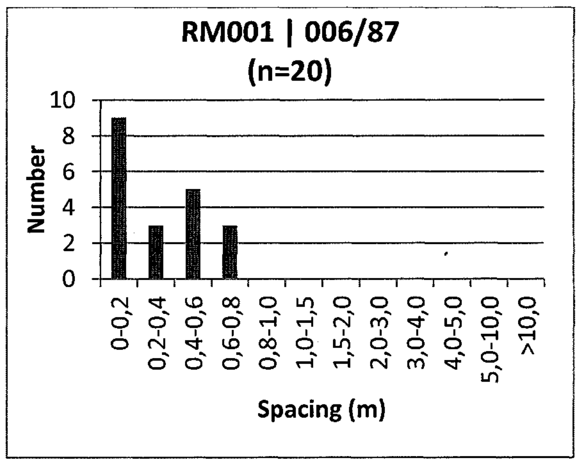

Fig. A8.4 Joint spacing distribution regarding joint sets that represent the set 070/04 from the unit block. Outcrop identification and respective pole of the joint set are indicated above every histogram. Spacing measured on lines orthogonal to joint plane. Spacing classes vary in width: 0.2m for spacing sizes between 0.0 and 1.0m; 0.5m, between 1.0 and 2.0m; 1m between 2.0 and 5.0m; 5.0m between 5.0 and 10.0 m; and all sizes above 10m. In this case, most joints present a small spacing (unimodal distribution). (CONTINUES)

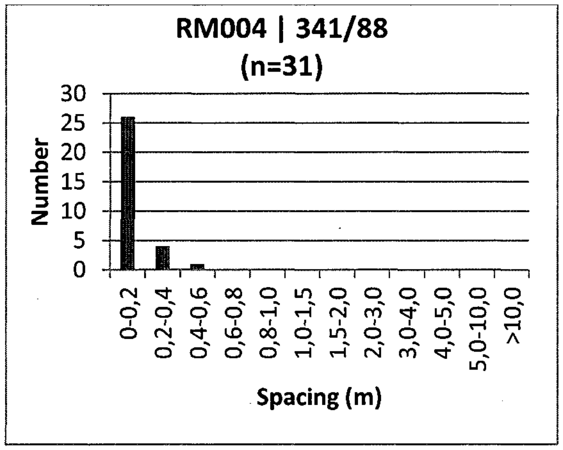

Fig. A8.4 (CONTINUATION)

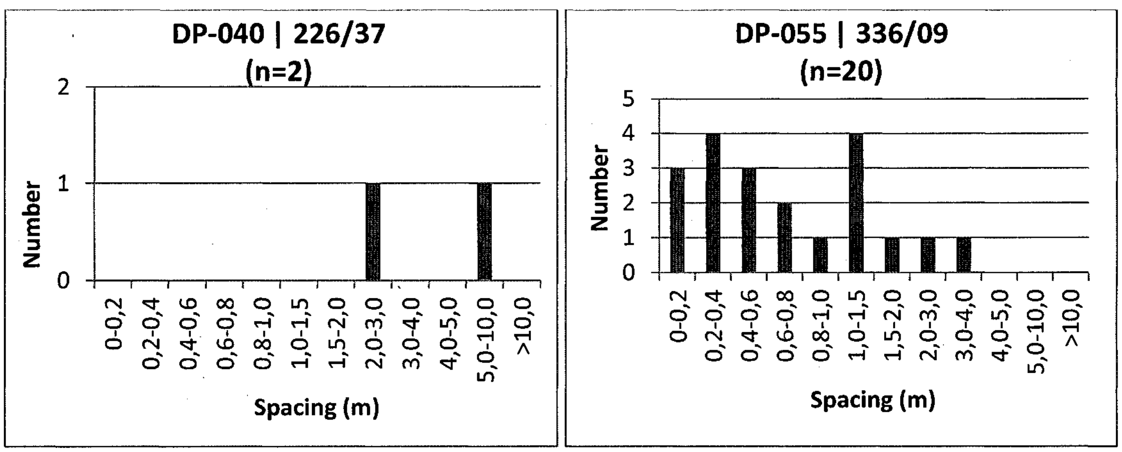

Fig. A8.5 Joint spacing distribution regarding all other joint sets that do not correlate to the unit block. Outcrop identification and respective pole of the joint set are indicated above every histogram. Spacing measured on lines orthogonal to joint plane. Spacing classes vary in width: 0.2m for spacing sizes between 0.0 and 1.0m; 0.5m, between 1.0 and 2.0m; 1m between 2.0 and 5.0m; 5.0m between 5.0 and 10.0 m; and all sizes above 10m. Observe the polymodal (mostly bimodal) distribution trend. (CONTINUES)

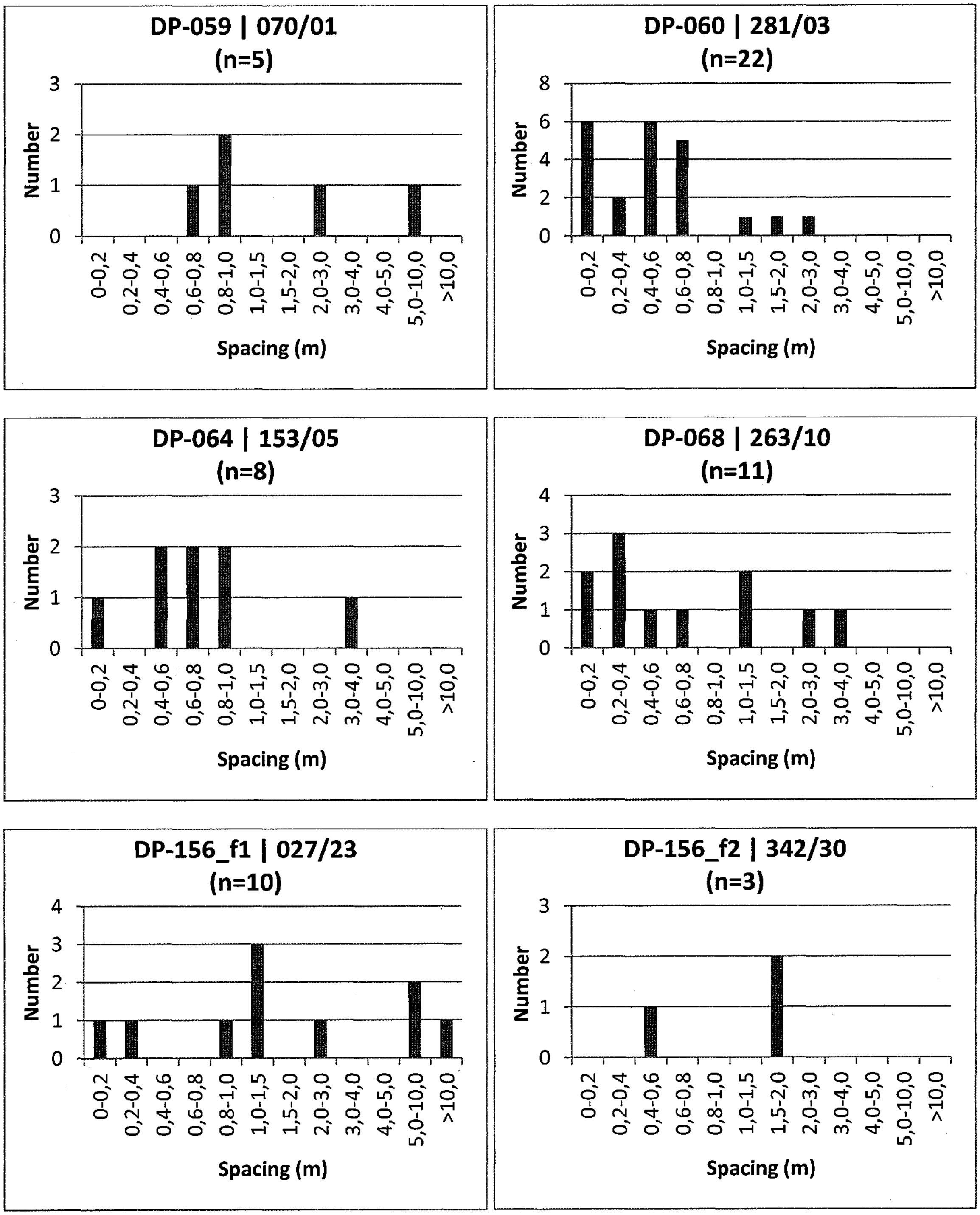

Fig. A8.5 (CONTINUATION)

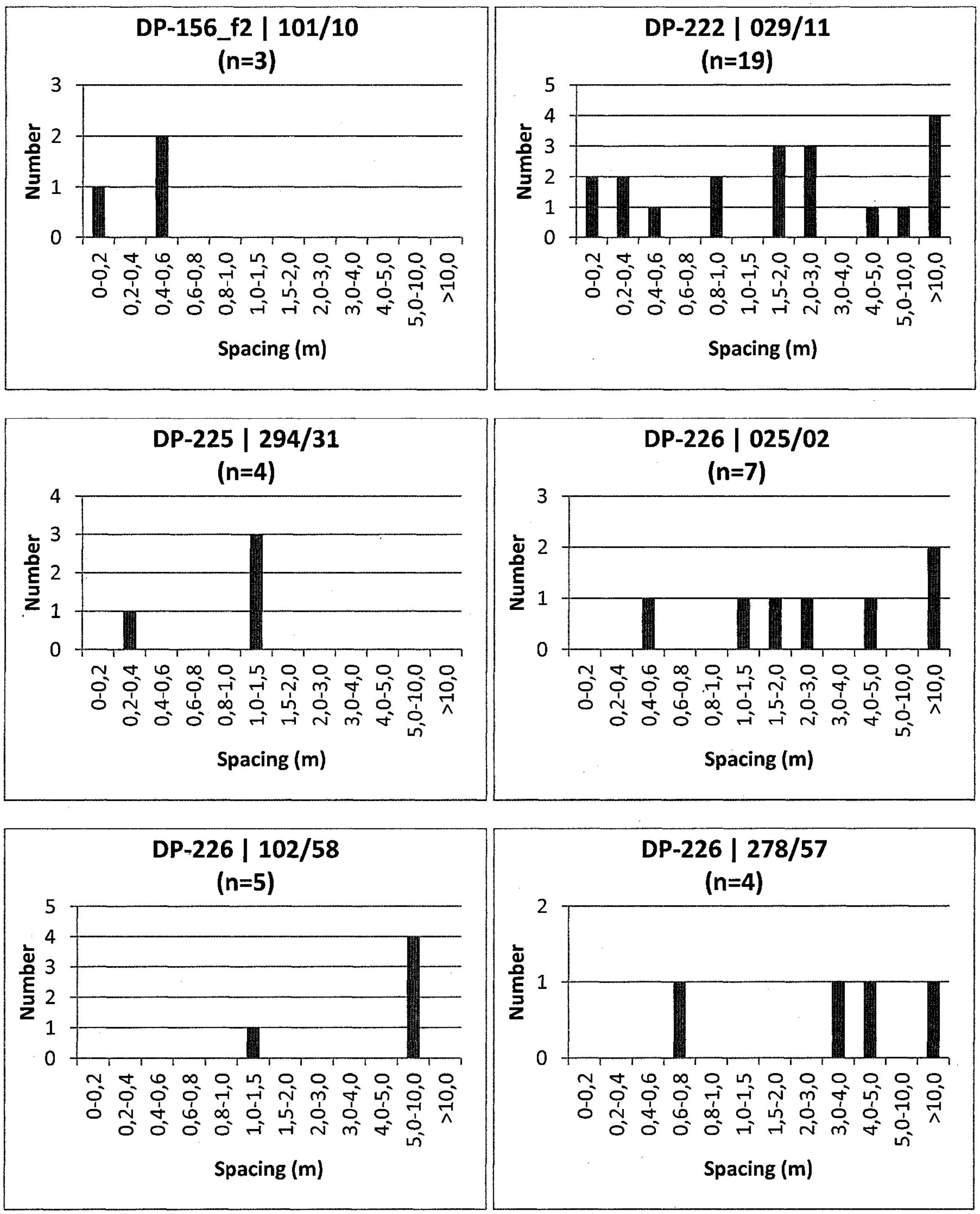

Fig. A8.5 (CONTINUATION)

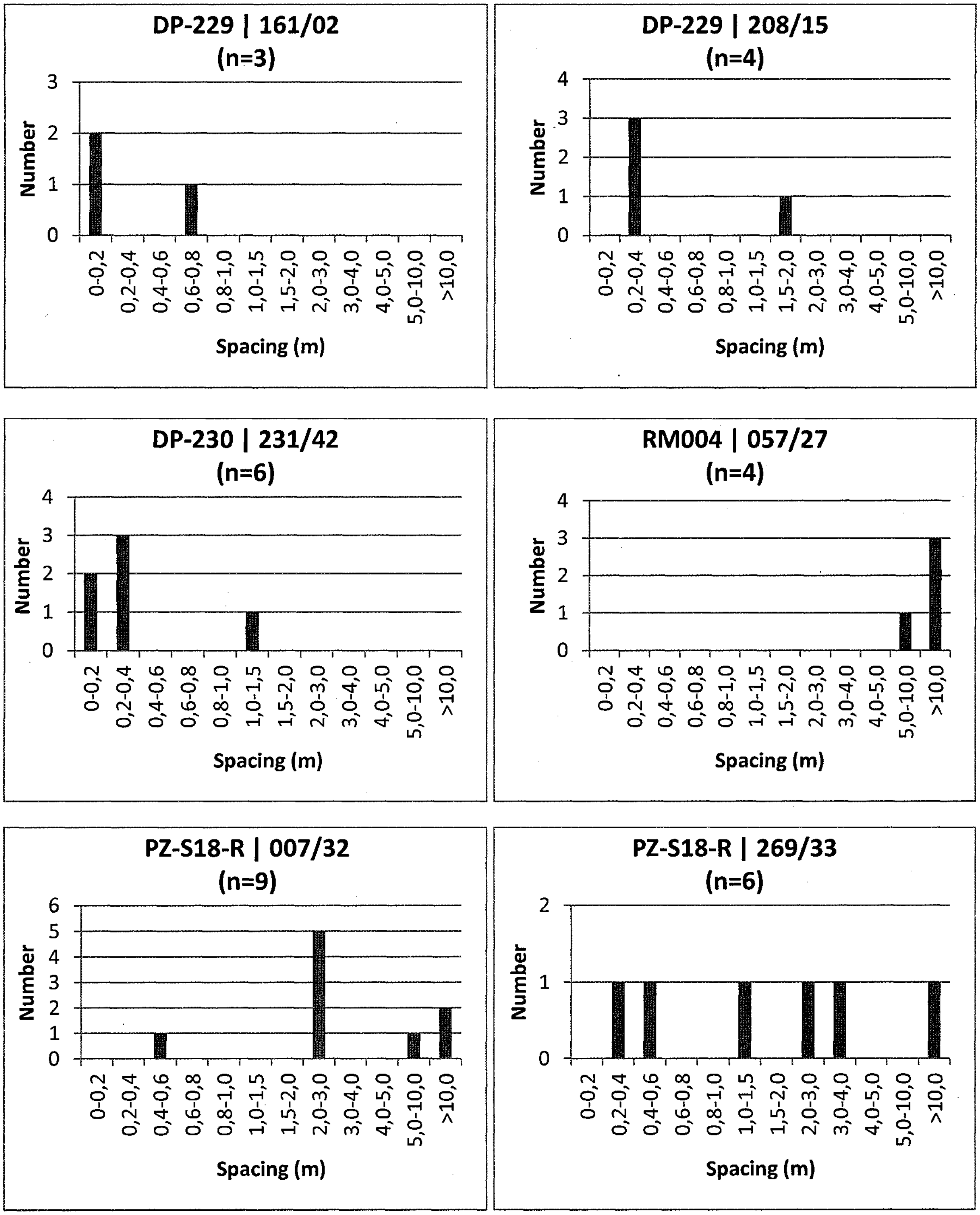

Fig. A8.5 (CONTINUATION)

APPENDIX 9

PHOTOS AND DRAWINGS REGARDING THE INTERPRETATION OF THE INTERACTION BETWEEN JOINTS AND THEIR RELATIVE AGES

This appendix brings an example of all steps of the study of the interactions between joint sets and their relative ages on an horizontal outcrop.

First, the drawing made at the site (Fig. A9.1) and respective photographs (Fig. A9.2). Notice the equivalence of markers position on both drawing and photograph.

Second, the sketch with the interpretations of joint sets (Fig. A9.3). It is possible to observe coeval joint sets (Fig. A9.3), as evidenced by the alternating cutting relationships between some joint sets (Fig. A9.3, sets in green and pink). An older set (Fig. A9.3, in blue) is also identified. This set is considered older because: (1) the two previously mentioned sets abut on it, but the contrary is not observed; (2) the same two sets are also observed crossing the main one, without interfering; (3) the portion where the set in red (Fig. A9.3) bends when approaching the main one (Fig. A9.3, in blue) suggests that this set was already present, conditioning the formation of the other one.

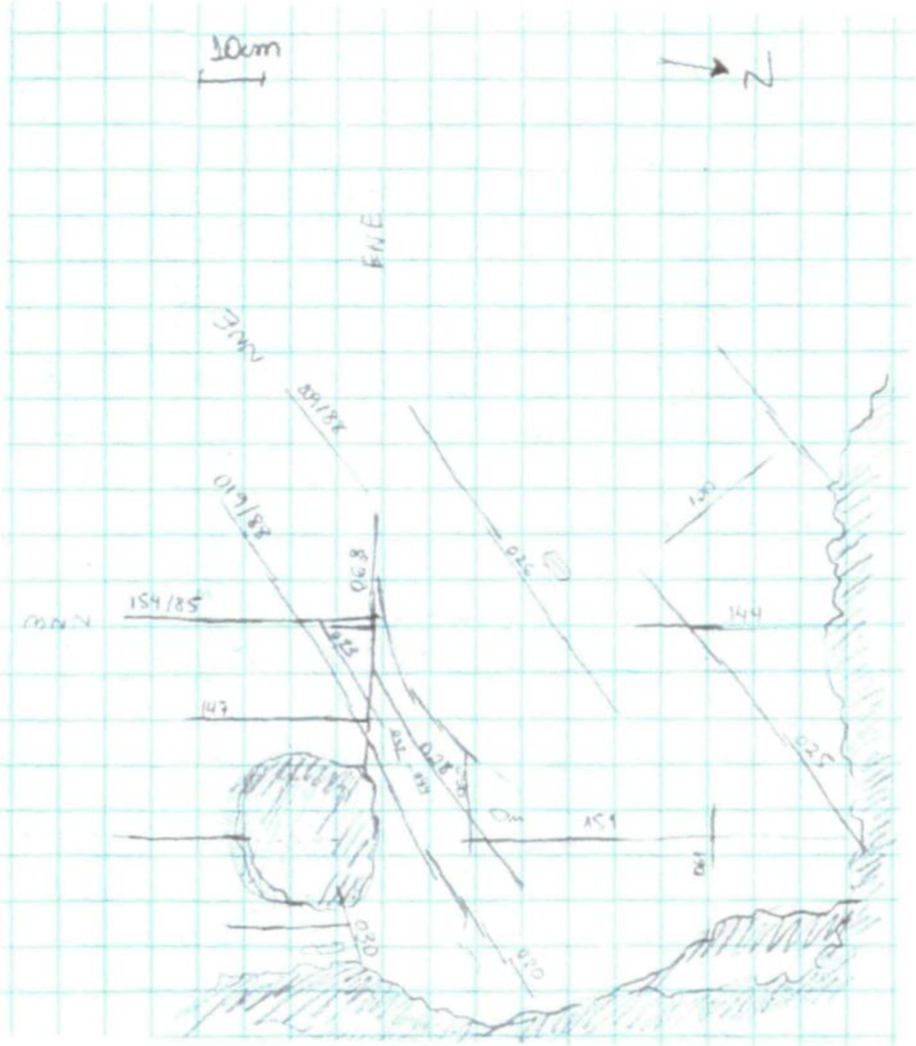

Fig. A9.1 Drawing of the joint sets on the horizontal outcrop DP-020.

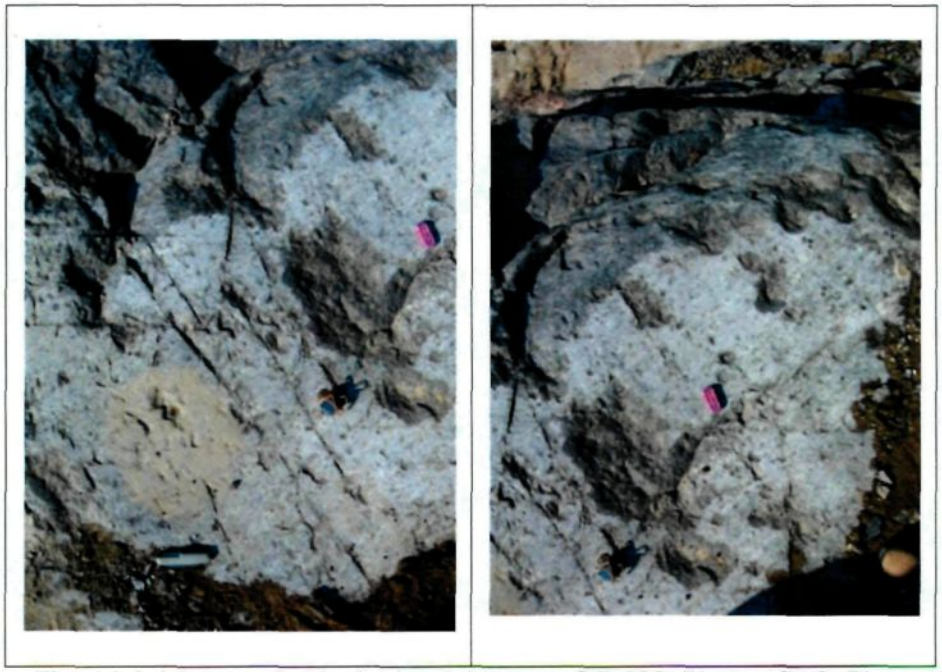

Fig. A9.2 Joint sets for the horizontal outcrop DP-020. Photos: D. S. Pino.

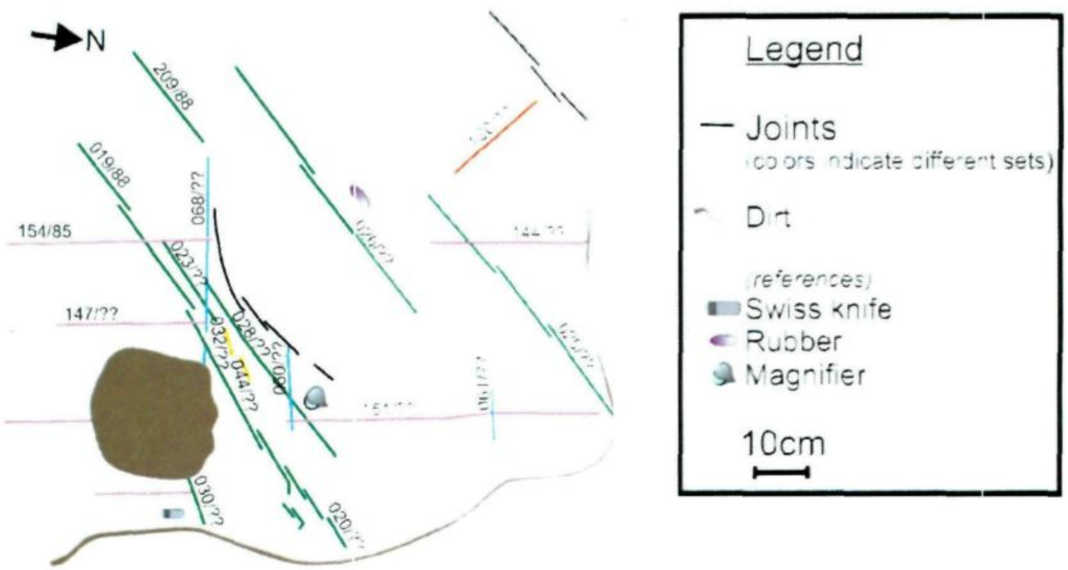

Fig. A9.3 Sketch of joint sets on the horizontal outcrop DP-020. Observe the alternating crosscutting relationship between the sets indicated in the colors pink and green. The blue set is the oldest one.

APPENDIX 10

RECENT STRESS FIELD IN EASTERN CANADA

The primary development of joint networks and their permeability are highly influenced by paleo-stress regimes during events of crustal deformation. Recent stress fields might superimpose a secondary influence on the pre-existing joint networks, altering joint apertures especially through relaxation at shallow to near-surface depths (Mortimer *et al.* 2011a, b). Other phenomena that may increase the spatial heterogeneity of a fracture network in shallow fractured aquifers (depths shallower than 200m) are the surface processes, e.g. weathering, erosion and unloading (Mortimer *et al.* 2011b).

The stress field may be considerably influent over the fluid control patterns, especially in fractured rocks with low matrix permeability (Mortimer *et al.* 2011b), as the regional stress state controls joint apertures and the potential reactivation of existing fractures (Henriksen & Braathen 2006). Therefore, the conductivity of a particular joint varies with its orientation in the in situ stress field (Henriksen & Braathen 2006): the flow occurs preferentially along joints that are normal to the minimum principal stress (σ_3) direction, due to low normal stress (Mortimer *et al.* 2011b), or inclined (around 30°) to the maximum principal stress (σ_1) direction, due to dilatation (Mortimer *et al.* 2011b). Moreover, joint permeability might be expected to be more stress-dependent at shallow depths (up to 200m), at which groundwater is usually extracted (Mortimer *et al.* 2011b).

In eastern Canada, the stress field components have a certain consistency regarding their directions, preferably NE-SW for the major compressional component (σ_1) (Arjang 1991; Hasegawa 1991; Zoback 1992, Assameur & Mareschal 1995) (Table 10.1). This relatively uniform regional stress field is believed to be related to plate-driving stresses (Zoback 1992). The dominant phenomenon, and that better explains this pattern, is the spreading at the mid-Atlantic Ridge (Hasegawa 1991, Assameur & Maréchal 1995). Those structures are reactivated under the present-day stress field as thrust or strike-slip faults (Mazzotti & Townend 2010).

Table A10.1 Information on *in situ* measurements of the stress field in eastern Canada.

Stress field component	Intensity (MPa)	Direction	Region	Reference
σ_1	21,055 [1]	N270-N280	Niobec Mine	Arjang (1986)
	8,18 ± 0,0422	E-W	Canadian Shield	Arjang (1991)
		N055-N065	Eastern Canada	Zoback (1992)
		N066	Saguenay (1988)	Zoback (1992)
		NNE-SSW	NE North America	Wallach *et al.* (1993)
	13,58 [1]	N019-N068	Sept-îles	Haimson *et al.* (1996)
	14,23 [1]	N093-N133	Eastern Canada	Haimson *et al.* (1996)
	17. 7 (± 3.1)	NE-SW	Sept-îles	Haimson *et al.* (1996)
	29,5	N45	Niobec Mine	Corthésy (2000)
	22,5		Niobec Mine	Lajoie (2010)
		N055-N104	Eastern Canada	Mazzotti & Townend (2010)
σ_2	3,64 ± 0,0276	N-S	Canadian Shield	Arjang (1991)
	8,70 [1]	NW	Niobec Mine	Arjang (1986)
	8,94 [1]	N19-N68	Sept-îles	Haimson *et al.* (1996)
	9,77	N93-N133	Sept-îles	Haimson *et al.* (1996)
	11.0 (± 1.4)	NE-SW	Sept-îles	Haimson *et al.* (1996)
	16,0	N318	Niobec Mine	Corthésy (2000)
	14,5		Niobec Mine	Lajoie (2010)
$\sigma3$	6,75 [1]		Sept-îles	Haimson *et al.* (1996)
	7,08 [1]	N-S	Niobec Mine	Arjang (1986)
	7.5 (± 0.4)		Sept-îles	Haimson *et al.* (1996)
	9,1	N130	Niobec Mine	Corthésy (2000)

[1] Average value regarding data presented in the respective reference.